Metals and Ceramics Division

Heavy Vehicle Propulsion Materials Program
Quarterly Progress Report for
October through December 2002

D. R. Johnson
Technical Project Manager

Prepared for
U.S. Department of Energy
Assistant Secretary for Energy Efficiency and Renewable Energy
Office of FreedomCAR and Vehicle Technologies Program
EE 07 01 00 0

Prepared by the
OAK RIDGE NATIONAL LABORATORY
Oak Ridge, Tennessee 37831-6066
Managed by
UT-Battelle, LLC
for the Department of Energy
Under contract DE-AC05-00OR22725

CONTENTS

Materials for Fuel Systems

Smart Materials for Diesel Fuel System Injector (Detroit Diesel Corporation)

Cost-Effective Smart Materials for Diesel Engine Applications (ORNL)

Low-Cost Manufacturing Processes for Ceramic and Cermet Diesel Engine Components (SIU-C)

Low Cost High Toughness Ceramics (ORNL)

Materials for Exhaust Aftertreatment

Materials for Exhaust Aftertreatment (Caterpillar Inc.)

Development of Materials Analysis Tools for Studying NO_x Sorber Catalysts (Cummins Engine Company and ORNL)

Development of NO_x Sensors for Heavy Vehicle Applications (ORNL, Ford Motor Company, and Visteon Automotive Systems)

Materials for Air Handling, Hot Section, and Structural Components

Lightweight Valve Train Materials (Caterpillar Inc.)

Thick Thermal Barrier Coatings (TTBCs) for Low Emission, High Efficiency Diesel Engine Components (Caterpillar Inc.)

Processing and Characterization of Structural and Functional Materials for Heavy Vehicle Applications (North Carolina A&T State University)

NDE/C Technology for Heavy Duty Diesel Engines: Fuel Delivery and Insulating Materials (Argonne National Laboratory)

NDE Development for Ceramic Valves for Diesel Engines (Argonne National Laboratory)

Durability of Diesel Engine Component Materials (ORNL)

Life Prediction of Diesel Engine Components (ORNL)

Low-Cost Manufacturing of Precision Diesel Engine Components (ORNL)

Diesel Exhaust Filter Temperature Measurement and Cost-Effective Machining of Titanium Alloys (North Carolina State University)

Advanced Cast Austenitic Stainless Steels for High-Temperature Components (ORNL and Caterpillar Inc.)

Development of TiAl/Ti_3Al Nanocomposite for Advanced Diesel Engine Applications (Lawrence Livermore National Laboratory)

Synthesis of Powders for Titanium Carbide/Nickel Aluminide Cermets (University of Colorado)

Laser Surface Texturing of Lubricated Ceramic Parts (ORNL)

High-Density Infrared Surface Treatment of Materials for Heavy-Duty Vehicles (ORNL)

Test and Materials Standards

Standards for Reliability Testing of Heavy Vehicle Propulsion Materials (NIST)

Implementing Agreement for a Programme of Research and Development on Advanced Materials for Transportation Applications (ORNL)

Mechanical Property Test Development (NIST)

Smart Materials for Diesel Fuel Injector

Yury Kalish, He Jiang, and Craig Savonen – Detroit Diesel Corporation
Naeim Henein – Wayne State University

Design of the hydraulic amplification device for the piezoelectric actuator development has been completed. The design process was guided by a finite element analysis of critical components, including membranes and pistons. Several key decisions have been made including geometric design and material selection for the O-rings and hydraulic fluid for the amplification chamber. Drawings of all components were completed and procurement activities have started.

Failure analysis of a piezoelectric stack was concluded. The cause of failure was insufficient preload applied to the stack. The inertia forces at high current levels exceeded the preload. Failure analysis involved both analytical calculations of dynamic forces acting on the stack as well as experimental investigation of the failure on the scanning electron microscope (SEM). Findings from the analysis fed into the design of the amplification device.

Several features of the piezo material bench fixture were upgraded in order to provide a larger range and more precise application and measurement of preloads and dynamic forces.

Requirements continue to be gathered for future fuel injector actuator performance, utilizing prototype fuel injectors under a range of engine and test rig operating conditions.

Cost-Effective Smart Materials for Diesel Engine Applications

J. O. Kiggans, Jr., F. C. Montgomery, and T. N. Tiegs
Oak Ridge National Laboratory

Objective / Scope

There are two objectives for this project. The first is to evaluate the cost-effectiveness and maturity of various "Smart Materials Technologies," which are under consideration for diesel engine applications, such as fuel injection systems. The second is to develop "Smart Materials" to be incorporated into working actuators and sensors.

Task 1 - Multilayer Electroded Laminates

The purpose of this study is to find satisfactory methods for the preparation of PZT laminates with internal electrodes from tape cast materials. There is no new data on this task to include in the present report.

Task 2 – Compositional Alteration of PZT-4

A major task of this project is to develop cost-effective PZT compositions and processing methods that will give PZT powders that will sinter to high density at a temperature below 960ºC. This goal is driven by the need to lower the cost of multilayer PZT actuators by reducing the cost of the interlayer electrodes. Commercial hard PZT powders require sintering at temperatures exceeding 1200ºC and, thus, multilayer devices must use costly Pd/Ag electrodes.

In earlier progress reports we provided data that supports our contention that small additions of bismuth oxide compounds can lower the PZT sintering temperature sufficiently that Ag or Ag/Pd alloy (70/30) can be used as internal electrodes. We showed that attrition milled PZT-840 powder containing a sintering aid consisting of 2 wt % Bi_2O_3 with an acceptor ion oxide resulted in a powder that sintered to greater than 99% of the theoretical density after 1 h at 900ºC. Additionally, the sintered PZT has piezoelectric properties which are as good as the properties of commercial PZT sintered at ~1275ºC and, because of the acceptor ion, the electromechanical Q is significantly higher than that of either the undoped powder or commercially sintered PZT-840.

Since piezoelectric ceramics based on PZT have poor mechanical properties that could cause actuators with a PZT element to have low reliability, we have studied the effect of adding a second phase in order to toughen and strengthen the sintered ceramic. We reported in the last quarterly that adding 0.5 vol % of silicon carbide (SiC), boron nitride (BN), Alumina (Al_2O_3) or alumina coated with 5 wt % Pt effects the physical and piezoelectric properties of PZT-840 containing the Bi_2O_3 sintering aid sintered for 3 h at temperatures below 960ºC. In the current quarterly we report the results of extending the sintering time to 24 h.

Experimental

The experimental techniques have been described in detail in the earlier progress reports. In this study, several milled powders were prepared. All of the powders were formulated with PZT-840 and a sintering aid containing 2 wt % of Bi_2O_3 and 0.33 wt % Mn_3O_4. One powder was prepared by ball milling for 24 h with ZrO_2 media. A second powder was attrition milled for 6 h also with ZrO_2 media. In addition, powders containing 0.5 vol % of SiC, BN, and Al_2O_3 were prepared by attrition milling.

Results and Discussion

In order to reduce sample preparation effort, initial experiments have been performed with die pressed powders containing sintering aids to determine the conditions required to produce fully

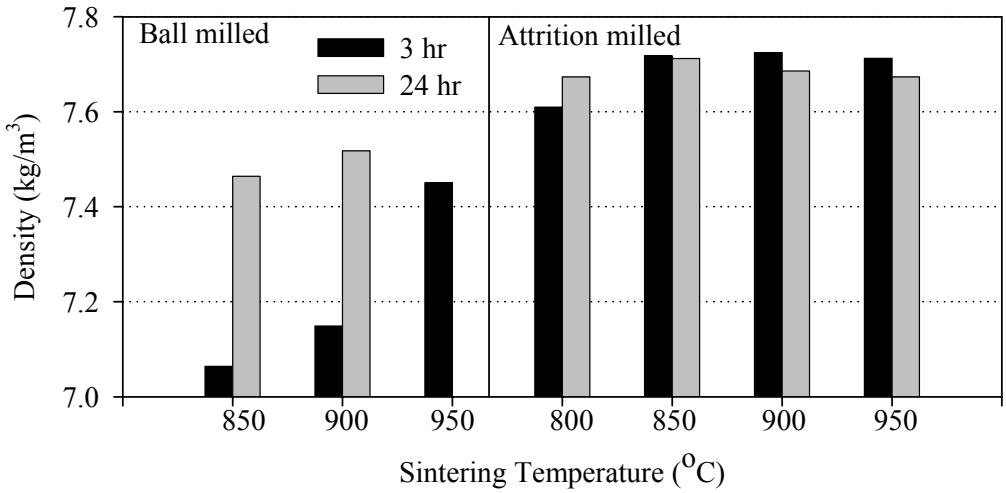

Figure 1. Densification of ball milled and attrition milled PZT-840 containing sintering aids.

dense PZT materials from powders without any strengthening additives. Figure 1 shows the sintered densities. The attrition milled powder samples reached higher densities than the ball milled powder samples when sintered between 800°C and 950°C for 3 and 24 h. The longer sintering time substantially increases the density for the ball-milled powder. The attrition milled powder containing the sintering aids reaches a fairly constant density after 3 h at 850°C but the longer sintering time results in a slightly lower density when the powder is sintered above 850°C. Attrition milled powder that did not have any sintering aids reached only 70% density after 3 h at 960°C and did not sinter to full density until heated for 3 h at 1125°C.

Figure 2 shows the piezoelectric properties of disks sintered at between 800°C and 950°C for 3 and 24 h which were fabricated from the ball-milled and attrition-milled powders containing the sintering aids. A horizontal line is drawn across each bar graph to show the values for

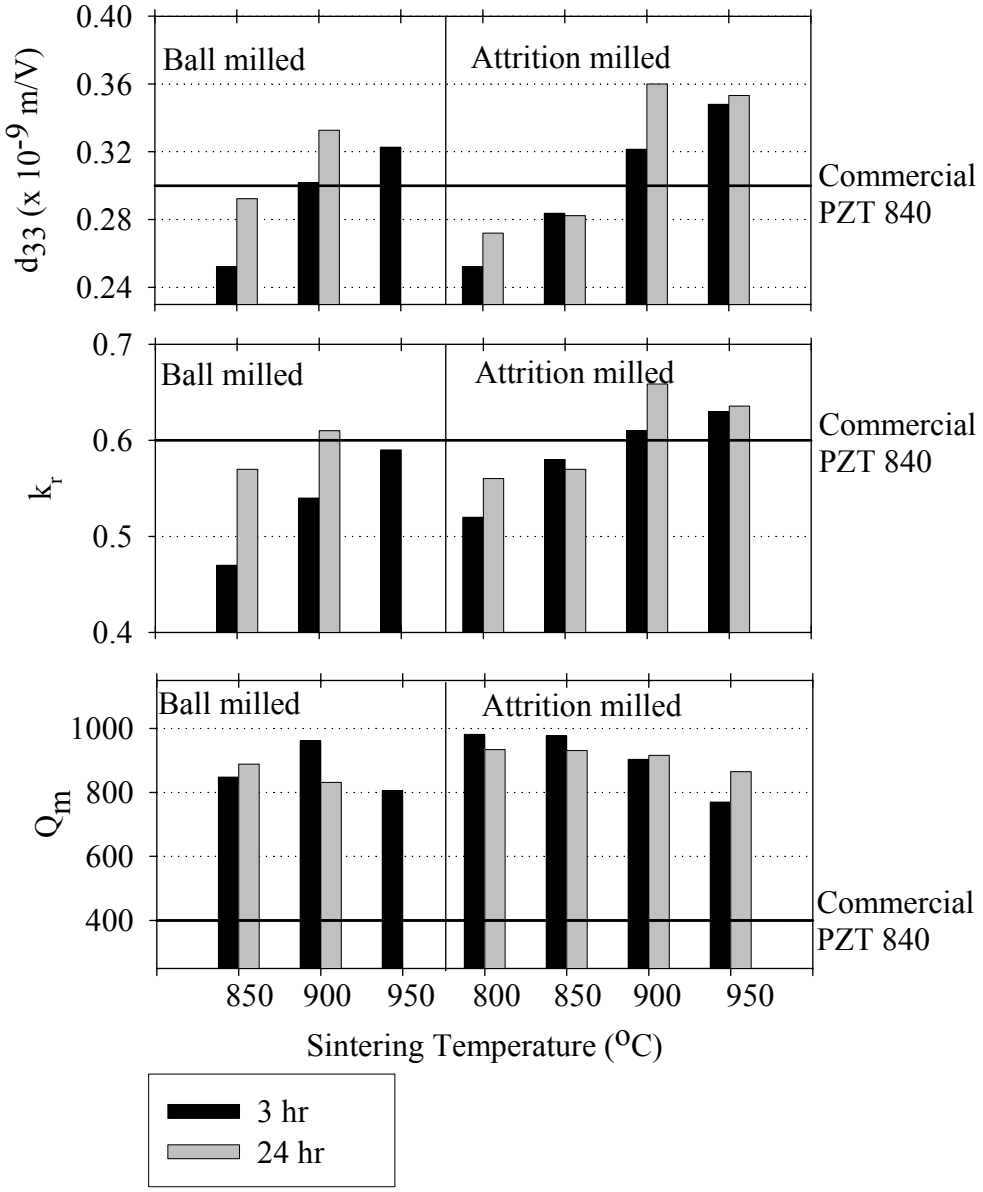

Figure 2. Electromechanical properties of sintered disks fabricated from the ball milled and attrition milled powders doped with ORNL sintering aids and sintered at between 800 and 950 °C for 3 and 24 h.

commercial PZT 840 sintered at >1250°C by the manufacturer. For both powder types sintering for 3 h results in the d_{33} and the k_r values increasing with increasing temperature but Q_m reaches a maximum at between 850°C and 900°C, and then declines as the sintering temperature is increased. Both milling techniques yielded powders that could be sintered and poled to meet the manufacturer's piezoelectric values. However, only the attrition milled powder could be sintered to full density in 3 h at temperatures <950°C.

The effects that the sintering time and temperature have on the density and on the piezoelectric properties of attrition milled PZT 840 containing 0.5 vol % of SiC, BN, or Al_2O_3 and the Bi_2O_3 sintering aid are shown in Figures 3 and 4, respectively. When sintered at 900°C the additional

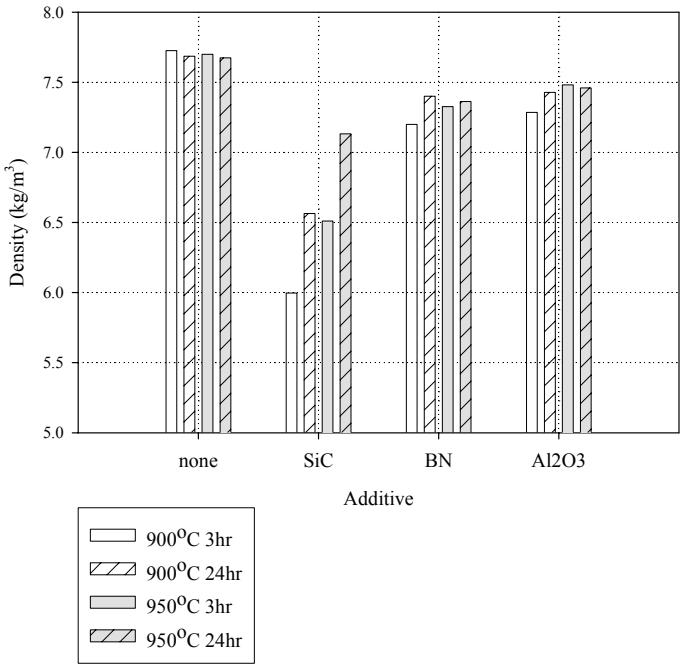

Figure 3. Density of PZT-840 containing sintering aids and doped with second phase additives.

time results in an increase in the density of the samples containing the second phase additives, but causes a small decrease in the density of the material without the additive. When the sintering temperature is 950°C the longer time causes a large increase in the density of the material containing SiC, but has little, if any, effect on the density of samples doped with BN or Al_2O_3.

The piezoelectric properties, d_{33} and k_r, are substantially increased when the sintering time is increased to 24 h. As shown in Figure 4, the relative increase in both properties is largest for the materials with the SiC and BN additives. Q_m also increases with the longer anneal time for materials with both the SiC and the BN additives. With Al_2O_3, however, the longer anneal time causes a decrease in Q_m when sintering at 950°C.

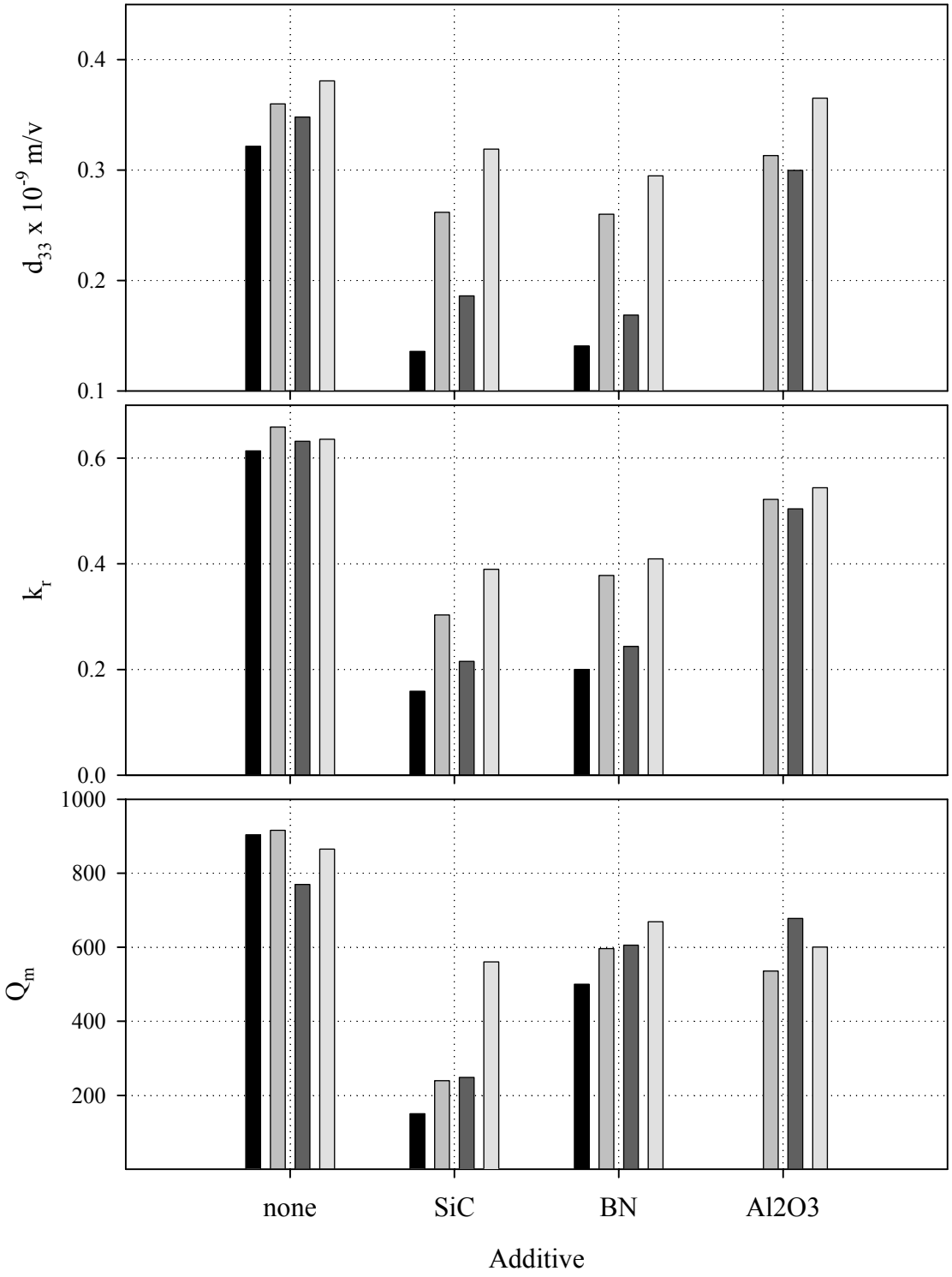

Figure 4. Piezoelectric properties of PZT-840 containing sintering aids and doped with second phase additives.

Task 3 - Fabricate a test fixture for stroking the multiplayer PZT parts.
Work for this task is in progress, and is being directed by Boyd Evans of ORNL. The first phase of this work is to build a fixture to stroke a commercial multilayer PZT stack (EDO E100P-4) manufactured by EDO Corp. Acoustic Products, Salt Lake City, Utah. Evaluation of the this first prototype fixture will be used to help refine the fabrication of the second generation fixture required to contain the multilayer stacks made from PZT materials with low temperature sintering aids.

Status of Milestones
1). Fabricate and characterize several multilayer PZT stacks using low temperature PZT materials.
Status: Additional tests are underway with sintering aids designed to increase strength or reduce grain size in low temperature PZT materials.
2). Fabricate a test fixture for stroking the multiplayer PZT parts.
Status: This task is underway with no results to report.
3). Make PZT powders with a nano-additive and characterize sintered discs for electromechanical and strength measurements.
Status: This task has not been started.

Low-Cost Manufacturing Processes for Ceramic and Cermet Diesel Engine Components

D. E. Wittmer
Southern Illinois University

Objective/Scope

The purpose of this work is to investigate the potential of low-cost manufacturing processes for ceramic and cermet diesel engine components. The primary task is to develop cost effective processing, forming and sintering methodologies for cermet and ceramic formulations, used by industrial diesel engine manufacturers.

Technical Highlights

Task 1. Collaboration with industrial partner(s).

This task involves the collaboration with industrial partners to assist them in processing and sintering of their diesel engine components. Our goal is provide assistance in processing and sintering which may result in a reduction in surface reactions and part warping. Moreover, this may also provide an alternative sintering process that will allow improved throughput efficiency and manufacturing economy. Due to the proprietary nature of this task, any research data generated from this task is normally controlled by the terms of each specific confidentiality agreement. The reporting of this data and any results are the responsibility of the industrial partner(s).

Task 2. Cost Effective Processing and Sintering

This task was completed and reported in previous quarterly report.

Task 3. Economic Comparison of Materials and Processing of Cermets for Use as Diesel Engine Components

This task involves the development of an economic model for comparing both materials and processing methods for cermets targeted for use as diesel engine components. The cermet is a combination of an intermetallic and TiC, where the intermetallic can be nickel aluminide, chrome aluminide, nickel chromium. Modification of these intermetallics may be necessary to obtain the properties desired.

During this reporting period, the cost associated with the various processes associated with these intermetallic bonded cermets was compiled and input into an economic model. These processes included injection molding, debinding, isopressing and sintering. Both the continuous sintering process and a commercial process based on a vacuum/pressure cycle were explored. In previous work, continuous sintering was found to afford up to a 50% reduction in the cost of sintering over conventional methods. In the sintering of cermets, higher sintering rates and more rapid through-put is possible with continuous sinter. However, the properties required or acceptable for cermets for diesel engine applications have not been identified.

A proposal will be made during the next reporting period to investigate powders prepared by Alan Weimer at CSM and to more fully investigate the influence of high heating rates on the microstructure and properties of continuously sintered cermets. In addition, wear specimens for tribological studies will be submitted to Peter Blau at ORNL.

Status of Milestones

1.	Collaboration with Industrial Partners	On Schedule
2.	Cost Effective Processing and Sintering of Diesel Engine Components	Completed
3.	Economic Comparison	On Schedule

Communications/Visits/Travel

D. E. Wittmer to ORNL to meet with Terry Tiegs for discussions.

Problems Encountered

None

Publications and Presentations

"Low Pressure Injection Molding of Intermetallic-TiC Cermets," Dale E. Wittmer and Jeffrey Hazelwood, SIUC, and Terry N. Tiegs, ORNL, abstract submitted to MPIF for presentation at PM2TEC 2003, Las Vegas, NV, June 8-12, 2003.

Low Cost-High Toughness Ceramics

T. N. Tiegs, F. C. Montgomery, and P. A. Menchhofer
Oak Ridge National Laboratory

Objective/Scope

Significant improvement in the reliability of structural ceramics for advanced diesel engine applications could be attained if the critical fracture toughness (K_{Ic}) were increased without strength degradation. Currently, the project is examining toughening of ceramics by incorporation of ductile intermetallic phases.

Technical Highlights

Previous studies have shown that the properties of the aluminide-bonded ceramics are attractive for diesel engine applications and consequently, development of these materials was started. At the present time, TiC-based composites with 40-60 vol % Ni_3Al are being developed because they have expansion characteristics very close to those for steel. Previously, the general property envelope has been studied and the compositions refined. Further processing studies are needed to examine lot-to-lot variation using statistically designed experiments, determine compaction behavior, assess dimensional control during sintering, identify suitable binders which will not add carbon ash during sintering, and develop a viable and cost-effective source of NiAl powder. The development effort is being done in collaboration with CoorsTek, Inc.

Large Batch Processing of TiC-Ni_3Al Composites – As reported previously, a series of large batches (≥2 kg) was processed and the properties measured. In the past reporting period, additional sintered materials were machined at a second facility for subsequent testing. Qualitatively, the machined surface finish was better on the MOR bars from the second facility. A comparison of the measured fracture strengths is shown in Table 1. As shown, the strength was higher for the cermet materials machined at the second facility. Apparently, the quality of the finishing has a considerable effect on the properties. This type of behavior is commonly observed with ceramics having low fracture toughness. However, these high toughness cermet materials are also affected by the condition of the machined surface. Further work in this area is definitely warranted.

Alternate Precursors for Ni_3Al Formation - All previous work used a combination of Ni and NiAl for an in-situ reaction to form the Ni_3Al. Because the costs of the starting raw materials can be a significant fraction of the total cost of a component, alternative materials for fabricating the cermets is of interest. Compositions have been mixed and pressed that use an Al-Ni product produced by a catalyst manufacturer in large quantities. These samples have been fired using the same vacuum/low-pressure hot-isostatic-press cycle as previous samples to determine their densification behavior and the densities achieved were >99.5 % T. D.

The sample utilizing the Al-Ni catalyst product was machined into mechanical property specimens. Those results are summarized in Table 2. As shown, the strength measurements for the first two cermet samples are in the range of the large-scale batches shown above. However, the sample (#2002-5) made by the reaction of NiAl (catalyst precursor) and Ni showed very poor strength in comparison. X-ray diffraction showed no other phases besides the TiC and Ni_3Al

typically observed in these materials. Examination of the microstructure revealed no unusual features (Fig. 1). A comparison with a prior cermet material (Fig. 2) showed the TiC grains were larger than other high strength. However, the sizes of the grains in the sample (#2002-5) were not sufficiently large to be the main factor for the low observed strength. Further examination of the samples is in progress.

Status of Milestones

On schedule.

Communications/Visits/Travel

Travel by T. N. Tiegs to Las Vegas, NV, Dec. 9-11 to attend the 2003 Powder Metallurgy Conference planning meeting.

Problems Encountered

None.

Publications

None.

Table 1. Summary of large batch properties for different TiC- Ni_3Al composites machined at two different facilities.

Batch No.	Ni_3Al Content (vol %)	Grain Growth Inhibitor (wt %)	Total Milling Time (min)	Flexural Strength (MPa) Facility #1	Flexural Strength (MPa) Facility #2
#C-9A	50	1% Mo*	120	1199±169	1353±34
#C-10	50	2% Mo*	120	1247±104	1443±149
#C-11	60	2% Mo*	120	N. D.	1092±404
#C-12	50	2% Mo*	20	1001±178	1155±32
#C-13	50	2% Mo*	120	1164±95	1398±52
#C-14	50	4% TaC	120	798±310	1248±206
#C-15	50	1% Mo*, 2% TaC*, 0.1% $B_4C^{\dagger}$, 1% Fe†	120	790±255	924±512

* Percent based on TiC content.
† Percent based on Ni_3Al content.

Table 2. Summary of processing variables for different TiC- Ni_3Al composites that will examine the effects of multiple additives.

Batch No.	Ni_3Al Content (vol %)	Grain Growth Inhibitor (wt %)	TiC Milling Time (min)	Metal Milling Time (min)	Flexural Strength (MPa)
2002-1	50	2 Mo*, 2 TaC*	60	20	1276±12
2002-2	50	2 Mo*, 2 TaC*, 2 Fe*	60	20	1457±118
2002-5†	50	2 Mo*, 2 TaC*	60	20	593±152

* Percent based on TiC content.
† Ni_3Al derived from reaction of NiAl and Ni precursors.

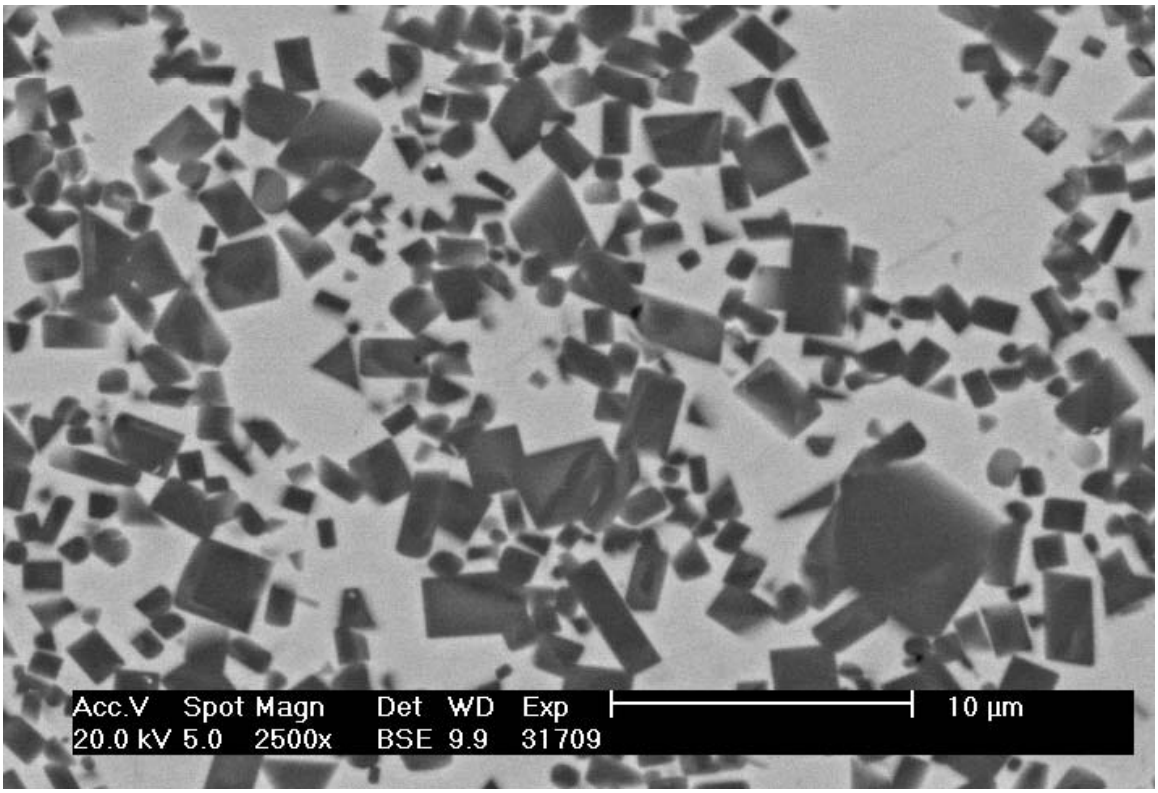

Fig. 1. Microstructure of sample #2002-5 showing large TiC grains in Ni_3Al matrix.

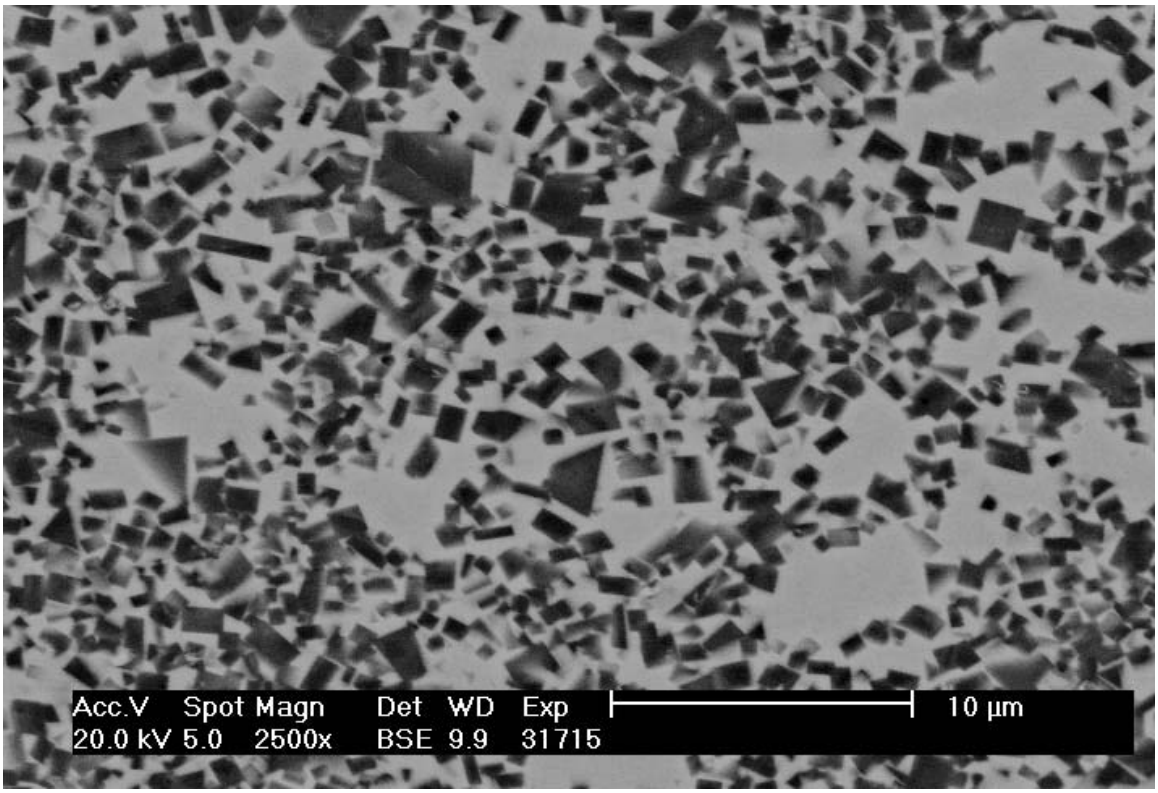

Fig. 2. Microstructure of sample #C-10 showing fine TiC grains in Ni_3Al matrix.

Materials for Exhaust Aftertreatment

Paul W. Park, Alexander G. Panov, Gerald A. Gegel, and Craig F. Habeger
Caterpillar Inc.

Objective/Scope

The objective of this effort is to develop and evaluate materials that will be utilized in aftertreatment systems for diesel engines. These materials include catalyst for NO_x abatement, filtration media for particulate abatement, and materials to improve NO_x sensing capabilities in the exhaust system. This project is part of a Caterpillar strategy to meet EPA requirements for regulated emissions in 2007 and out. This years focus is on the durability of NO_x catalysts developed for lean burn applications in the presence of sulfur, evaluation of filtration properties of sintered metal media for application in diesel particulate filters (DPF), and evaluation of current NO_x sensor technologies while developing materials to improve sensing capabilities.

Technical Highlights

Lean NO_x Catalysis. A series of silver doped alumina catalysts were prepared using different silver precursors, silver nitrate and silver sulfate. Evaluation determined that the activity of the catalyst increased due to the formation of silver sulfate. These results confirmed the hypothesis that silver sulfate is more active than metallic silver or silver oxide for NO reduction to N_2.

After the N_2 yield stabilized in the presence of SO_2, the recovery of the NO reduction was examined by discontinuing SO_2 injection in the gas stream, as shown in Figure 1. The filled symbols represent when SO_2 was added and the open symbols represent when SO_2 was removed from the feed stream. The N_2 yield over a 2 wt %Ag/Al_2O_3 catalyst (Ag2) increased from 44% to 48% for the first 60 min when 30 ppm SO_2 was introduced to the feed stream. After 60 minutes, the N_2 yield sharply decreased to 31% then stabilized from 500-2000 min. The catalytic performance of Ag2 recovered up to the initial activity (44%) when SO_2 was removed from the feed stream. For 8 wt %Ag/Al_2O_3 catalyst (Ag8), the initial activity was less than 1% but the N_2 yield increased up to 28% in 400 min then leveled off in the presence of SO_2. Surprisingly, the performance of Ag8 decreased when SO_2 was removed from the feed stream.

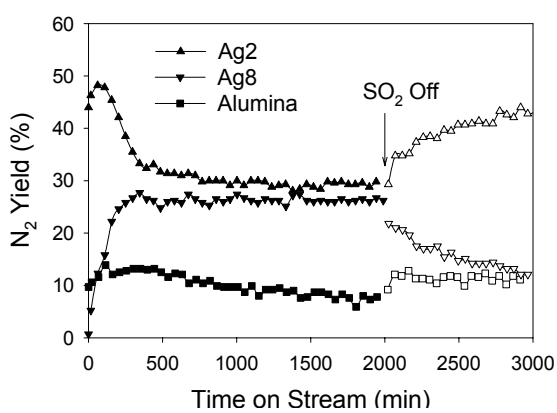

Figure 1. The change in NO reduction performance as a function of time when 30ppm SO_2 was introduced into the reaction feed stream over fresh catalysts.(Ag/Al_2O_3 catalysts, 0.1% NO, 0.1% propene, 9% O_2, 30ppm SO_2, 7% H_2O, 30,000h^{-1}, 500°C)

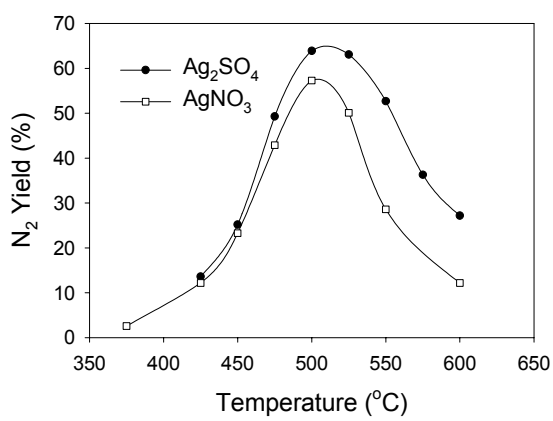

Figure 2. Effect of silver precursors on NO reduction over 2 wt.% Ag/Al2O3 catalysts (0.1% NO, 0.1% propene, 9% O2, 7% H2O, 30,000h-1)

The results indicate that SO_2 does not permanently poison silver catalysts. On the contrary SO_2 may promotes the NO reduction performance under certain conditions. The improvement in the catalytic performance of Ag8 for the first 400min can be attributed to the suppression of propene oxidation. Silver metal in Ag8 favors propene oxidation over NO_x reduction. After exposure to SO_2 a substantial amount of silver sulfate that suppressed propene oxidation was formed on the Ag8 catalyst. The initial increase in N_2 yield for Ag2 suggests that silver sulfate is active for NO reduction. The decrease in activity after 60 minutes of exposure is due to the sulfation of the alumina support. Figure 2 shows the comparison of NO reduction over 2 wt % silver catalysts prepared with sulfate and nitrate precursors. The silver catalyst prepared with silver sulfate compound contained 0.22 wt % S in the sample; however, it showed higher catalytic performance for NO reduction than the sample prepared with silver nitrate. The catalyst performance and characterization results indicate that the silver sulfate phase has similar or higher catalytic activity than silver oxide species for NO_x reduction. The order of catalytic activity for NO_x reduction for silver species is proposed as follows; $Ag_2SO_4 \geq Ag_2O >> Ag$.

Diesel Particulate Trap. Materials of four different pore structures were prepared from 430SS. The materials were formed into sheets of various thicknesses. Five of the filtration media samples were characterized with mercury porosimetry, and evaluated for filtration efficiency and pressure drop. Figure 3 shows the Mercury porosimetry results. The pore size distribution was adjusted by changing the metal powder properties.

These samples were evaluated for filtration efficiency and pressure drop using the diesel fuel burner. Efficiencies of the filters varied from 40 to 90%. Filtration properties of the materials can be improved either by increasing the thickness of the filter or by decreasing the pore size. For materials with similar filtration efficiency, thicker filter exhibited slower pressure drop increase during soot accumulation.

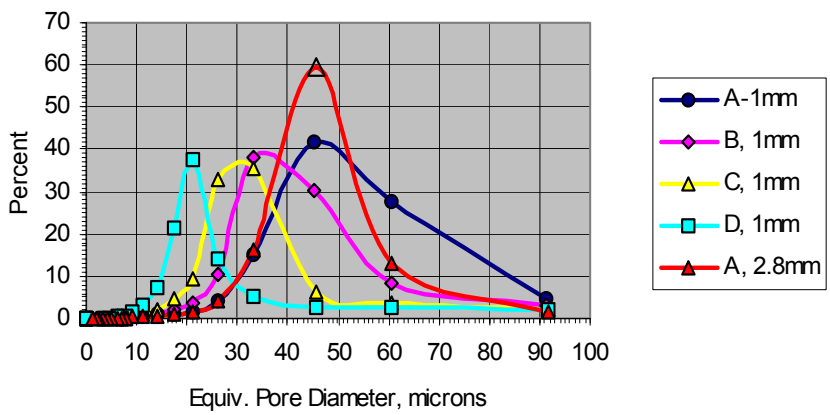

Figure 3. Mercury porosimetry results of filtration media samples.

NO_x Sensor. The NO_x sensor testing bench was completed this past quarter. Software to control the bench is currently being written. The bench will be entirely controlled from the computer to allow for ease of use. The bench was designed to test up to flow rates of 0.5 L/min and to evaluate sensitivity, response times, cross sensitivity, and deleterious contamination resistance of sensors. The versatile configuration allows testing of both commercial production and experimental sensors.

Figure 4. A picture of the NO_x sensor test bench.

A number of sensors have been fabricated or

acquired and are ready to be evaluated. Experimental electrochemical sensors have been fabricated and are being prepared for evaluation. Three types of electrochemical sensors have been fabricated: amperometric, mixed potential, and conductometric.

Future Plans

(1) Optimize layered catalyst formulation.
(2) Continue to characterize silver catalyst.
(3) Improve catalyst durability.
(4) Complete testing of the prepared 430SS sintered metal materials.
(5) Sinter and test high temperature alloy sintered metal filters.
(6) Develop a model correlating materials' properties to filtration efficiency and pressure drop.
(7) Write control program for NO_x sensor bench.
(8) Begin sensor evaluation.

Travel

None.

Status of FY 2003 Milestones

1) *Catalyst Formulation:* Improve catalyst deNO_x performance via dual function mechanism concept identified in the previous study (under progress)
2) *Catalyst Durability:* Improve catalyst durability for sulfur poisoning (under progress)
3) *Washcoat Technology:* Develop a controlled catalyst coating technique in order to fully demonstrate selected catalyst chemistries on a full size honeycomb monolith (under progress)
4) *NO_x Sensor:* Complete NO_x sensor bench fabrication. (complete)

Publications

Paul W. Park, Carrie L. Boyer "SO_2 Effect on deNO_x Performance of Ag/Al_2O_3 Catalysts in Lean Condition" abstract submitted to North American Catalysis Society, 18th North American Catalysis Society Meeting, Cancun, Mexico, June 1-6, 2003

Development of Materials Analysis Tools for Studying NO_x Sorber Catalysts

Roger England, Cummins Engine Company
and Thomas Watkins, Oak Ridge National Laboratory

Objective/Scope

The objective of this cooperative effort is to participate in development of NO_X control for diesel engine exhaust, with the aim of answering fundamental questions about the micro-scale and meso-scale dynamics of the NO_X conversion process. The expected result is that this improved description of mechanisms will enable industry to improve NO_X catalyst performance and durability. As the state-of-the-art evolved during the course of the CRADA, the study focused more on NO_X adsorber materials and processes. A Cummins catalyst supplier provided new materials, which are being examined with diagnostic tools developed under the CRADA. Investigations of these candidate-production materials are being implemented on both the bench and engine research scale. These investigations include the examination of unused and engine-aged catalyst samples. Investigative tools included transmission electron microscopy (TEM), X-ray diffraction (XRD), Raman Spectroscopy and infrared spectroscopy (IR).

Technical Highlights

Transmission Electron Microscopy. TEM data were obtained from unused and aged catalyst samples. These samples had been aged on an engine using 150-ppm sulfur fuel. Temperatures exceeded 500°C for 1000 hours during the test. During this first set of studies, the effects of the

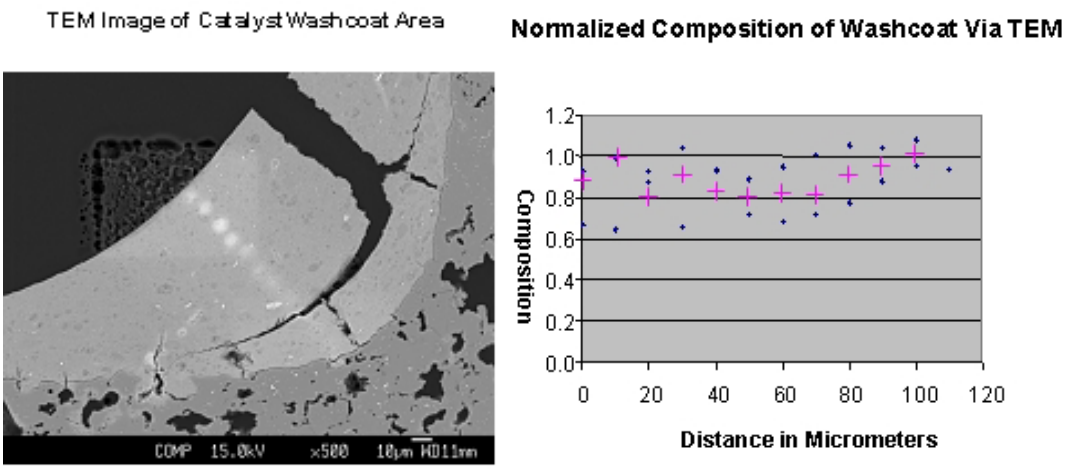

Figure 1. TEM data detailing the Pt composition of the catalyst washcoat as a function of washcoat depth. Blue diamonds represent the data obtained from the unused sample, the pink crosses from the sample aged for 1000 hours at >500°C.

aging on the Pt dispersion and size was monitored (samples were removed from the engine after 150, 500 and 1000 hours of high-temperature operation). One of the key findings is the apparent immobility of the Pt as a function of washcoat depth. The left side of Figure 1 shows a low-resolution image of the sample washcoat area. The "light spots" seen in the image are where Pt composition data was taken. The right side of Figure 1 shows example data that was obtained

from the unused and aged samples. It is apparent that during the on-engine tests the Pt did not migrate toward or away from the cordierite substrate. No preferential mobility was observed with respect to catalyst depth. Furthermore, the Pt is well dispersed as a function of catalyst depth as well.

Raman and Infrared Spectroscopy. Efforts were made in using Raman Spectroscopy (RS) to monitor the growth of Pt particles as a function of aging. The data indicated that RS could indeed monitor particle size and lead to dispersion data. These results have been correlated with chemisorption measurements for verification. Using RS to evaluate PT particle size is more rapid than the conventional chemisorption techniques.

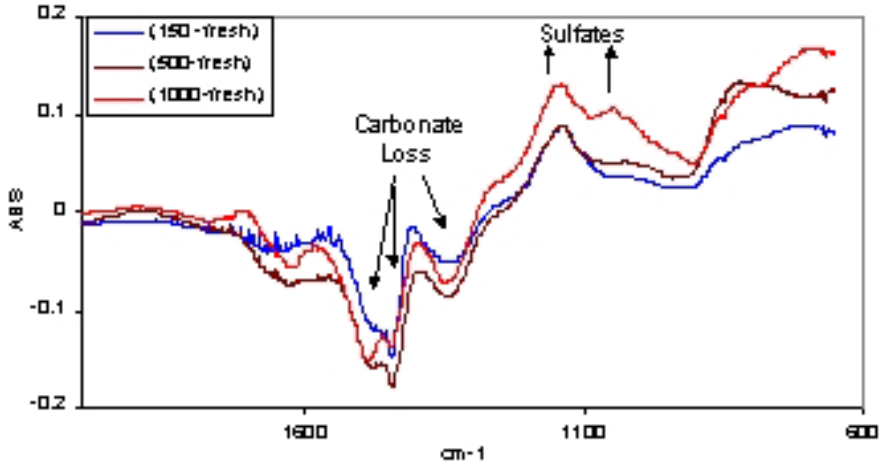

Figure 2. Normalized regional IR data obtained from the 3 aged samples.

IR spectroscopy was used to evaluate and monitor sulfur and carbonate species at the catalyst surface. The data shown in Figure 2 indicate that sulfur species, specifically sulfates, are present and their concentration on/in the catalyst build with time. It is also apparent that catalyst carbonate species decrease with aging. These studies have been expanded to include individual sulfur exposures and sulfur removal techniques from catalyst samples. IR has proven to be quite useful in monitoring these phenomena.

X-Ray Diffraction. XRD data were taken at Brookhaven National Laboratory.

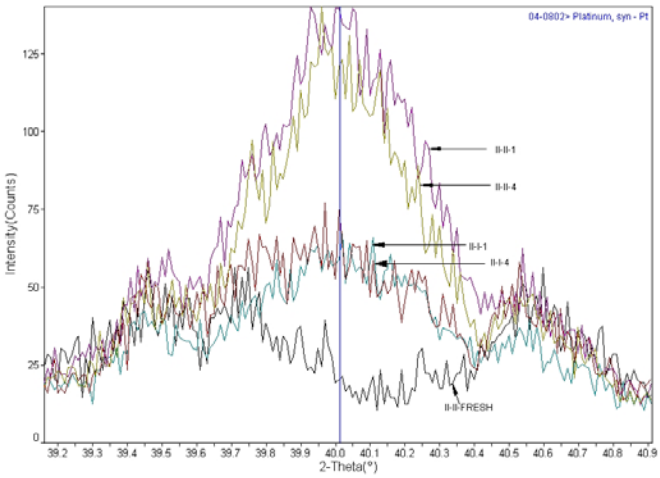

Figure 3. XRD Crystal size measurements

This technique was also used to monitor precious metal changes that might occur with catalyst aging. The XRD data did show that changes in Pt crystallite size occurred over the test period. The data obtained from the unused catalyst show no Pt features, indicating the crystallite size is below the "detection" limit of the technique (no crystalline structure due to small particle sizes). Pt features did appear upon examination of the aged samples. These XRD results are being compared to the TEM and chemisorption measurements to determine the limitations of the XRD for crystallite size evaluation.

Development of NO_x Sensors for Heavy Vehicle Applications

Timothy R. Armstrong
Oak Ridge National Laboratory

CRADA No. ORNL 01-0627
with Ford Motor Company

Objective

The proposed project seeks to develop technologies and materials that will facilitate the development of NO_x and ammonia sensors. The development of low-cost, simple NO_x will facilitate the development of ultra-low NO_x emission engines, directly supporting the OHVT goals.

Technical Highlights

1. The sensor test stand was completed in December and is fully operational. The test cell design and stand performance were evaluated on a known catalyst whose composition we found in the literature.
2. A new test has been designed to determine the ability of the catalyst to adsorb NO and NO_2. This test is based on infrared adsorption. A test stand has been designed with a quartz window through which an IR camera will focus on the catalysts deposited on an insulating body. The change in temperature of the catalyst when exposed can be measured with the IR camera. The greater the change in temperature, the greater the ability of the catalyst to adsorb NO and NO_2. This method is being developed as a quick screen of new catalyst materials and will be applied to NH_3 as well.
3. Our testing has found that the mixed potential sensors are sensitive to the oxygen concentration in the exhaust gas. ORNL has been able to describe this phenomenon mathematically and will demonstrate this and the experimental verification to Ford in February. While we will continue to develop and test catalysts, sensor redesign may be warranted. We will also work with Ford to evaluate this data and its impact on all the similar sensors under development at all the other labs.

Status of Milestones

Although this project had a late kick-off, we are ahead of schedule of most of the milestones:

1. Modify current sensor test stand for operation at 800°C (delayed at request of Ford)
2. Test NGK sensor in modified test stand (delayed at request of Ford)
3. Deliver NO_x catalyst assessment and program plan to Ford (completed 6/2002)
4. Construct NO_x electrode test stand. (8/2002)
   The test stand was completed (12/2002) and is fully operational.
5. Deliver report on initial rest results (9/2002).
   The report is to be delivered to Ford in February 12, 2003.
6. Design and procure screens for simplified NO_x sensor design. (9/2003
   This task was completed in December 2002.
7. Produce first simplified NO_x sensors for testing (delayed until December 2002).

The completion of this task will be delayed while we continue with development and testing of NO catalysts. The sensor is designed to operate at 700°C and measure the NO content in the

exhaust gas stream. However, all the catalysts listed in the literature work well in a lab environment but not in real exhaust environments. We are developing and testing new catalysts daily; however, none have given us a large signal for NO. In addition, we have determined through rigorous electrochemical calculations that all the mixed potential designs may be limited by the oxygen in the exhaust gas stream. This data will be presented to Ford and may be used to evaluate sensor design as we develop and test catalysts.

Communications/Visits/Travel

1. We have planned a meeting at Ford for February 2003 to discuss our progress.
2. Members from DuPont's development staff visited us and indicated they are in negotiation with Ford to become a development partner in their sensor program. DuPont has indicated that they wish to partner with us in the future on electrochemical sensors for exhaust gas environments.

Problems Encountered

None to date.

Publications

None to date.

Lightweight Valve Train Materials

Mark J. Andrews
Caterpillar Inc.

Introduction

Valve train components in heavy-duty engines operate under high stresses and temperatures, and in severe corrosive environments. The light-duty engine market requires cost-effective reliable materials that are wear resistant and lightweight in order to achieve high power density. For both engine classes, better valve train materials need to be identified to meet market demand for high reliability and improved performance while providing the consumer lower operating costs.

Advanced ceramics and emerging intermetallic materials are highly corrosion and oxidation resistant, and possess high strength and hardness at elevated temperatures. These properties are expected to allow higher engine operating temperatures, lower wear, and enhanced reliability. In addition, the lighter weight of these materials (about 1/3 of production alloys) will lead to lower reciprocating valve train mass that could improve fuel efficiency. This research and development program is an in-depth investigation of the potential for use of these materials in aggressive engine environments.

The overall valve train effort will provide the materials, design, manufacturing, and economic information necessary to bring these new materials and technologies to commercial realization. With this information, component designs will be optimized using computer-based lifetime prediction models, and validated in rig bench tests and short- and long-term engine tests.

Program Overview:

The results presented in this report are based on previous proprietary research conducted under Cooperative Agreement DE-FC05-97OR22579.

Ceramic Materials:

Silicon nitride materials have been targeted for valve train materials in automotive and diesel industries since early 1980's. Silicon nitride material grades have now reached maturity, and few new material grades are being introduced. Commercial successes have been reported in both automotive and diesel valve trains, with large-scale production underway. The reported valve train applications exploit the high contact damage and wear resistance of the ceramic material.

The reported strength, toughness and limited dynamic fatigue data available for certain grades of silicon nitride are impressive, and the corrosion resistance are also exceptional. Hence, the focus of the present valve train effort is on realizing the commercial potential of silicon nitride materials to solve corrosion problems in the short term, and improving engine performance in the longer term.

Intermetallic Materials:

Titanium aluminide based intermetallics retain their strength to elevated temperature and are highly corrosion-resistant. They are lightweight, and posses high fracture toughness. These alloys are actively being investigated for several aerospace and automotive applications.

Fourth Quarter Summary

Valve Test Rig:

Investigations using the SEM further examined three of the metallic seat inserts from previous 100-hour valve bench tests. The purpose of these investigations was to identify particles that were found imbedded in the contact area of the seat insert. Figures 1-5 show the SEM and EDS results of specified regions on the seat inserts, and indicate that the embedded particles are chipped pieces of the Si_3N_4 valve. Figure 6 is a SEM backscatter image of one of the regions containing embedded particles. This region has a darker tone that is representative of elements with low atomic numbers, such as oxygen, nitrogen, silica, and alumina, the elements that make Si_3N_4.

During the current reporting period, two 100-hour ambient temperature valve bench tests were completed. The first test examined the impact and wear patterns that a 30 ° valve contact angle has with an eccentrically machined 30 ° valve seat insert. Eccentric machined seat inserts were obtained from Caterpillar Engine Research for using on the test rig. A schematic showing the top view of these eccentric seats is depicted in Figure 7.

The second test examined the modifications made to the test rig during the past reporting period. The installed pressure regulator maintained a constant oil pressure as the rig warmed up from ambient conditions to the steady-state operating temperature. The attached metal plate remained on the valve face and did not appear to influence the impact wear test results. The fracture detection system was able shut down the test rig when it the sensor was moved away from the valve face, simulating a valve failure. The failure detection system did not falter due to the adverse oil environment and continuous mechanical vibration.

Figures 8-11 illustrate the wear patterns of the eccentric seat inserts and corresponding Si_3N_4 valves from the completed 100-hour test. There are several locations on the seat inserts (Figures 8 and 10) where embedded particles appear that are likely Si_3N_4. Contact damage and wear to the Si_3N_4 valves (Figures 9 and 11) was minimal, in like fashion to previous 100-hour bench test results. However, there are roughened surface areas in the Si_3N_4 contact region, indicating perhaps where the imbedded seat insert particles came from.

Valve blanks fabricated by Kyocera Industrial Ceramics using SN235P un-hipped were received in two shipments during the current reporting period. The dimensions of the valve blanks were designed to accommodate the final dimensions of the intake and exhaust valves from the 3406 gas and the 3401 diesel engines. The first shipment contained 10 valve blanks and these blanks were made in accordance with the Caterpillar print specifications. The second shipment contained 40 valve blanks that were further optimized by Kyocera by removing 1 mm of material from the Caterpillar print specifications. These valve blanks are closer to the net shape of the finished valve dimensions.

Intermetallic Materials Research:

A series of friction welding experiments were conducted with the objective of increasing the joint strength to levels higher than the room temperature strength of the base TiAl material (~400MPa).

Cylindrical TiAl bars were welded either to Ti-6Al-4V or to titanium matrix composites (CermeTi). Friction welding parameters were varied to study their effect on optimizing the joint in terms of tensile strength of the weld. The selected process conditions included a range of patented [1] parameters that reportedly produced weld strengths with Ti-6Al-4V higher than the strength of the base TiAl material. The friction welding experiments were conducted at Manufacturing Technology Inc. (MTI) at South Bend, IN.

Figure 12a shows the glowing bars being welded within the first 4 seconds of the friction welding operation. A completed weld bar is illustrated in Figure 12b, with the flash material rolled out towards the Ti side. After the weld was completed, the flash was removed by a grinding operation to eliminate the notches that would act as stress concentrators during tensile testing.

The results from different combinations of rotational speed and forge pressure were recorded. To date the highest tensile strength was obtained with Ti-6Al-4V is 273MPa. The results for the welding trials of TiAl to CermeTi give in the highest tensile strength of 173 MPa. Fractography analyses showed a protrusion in the center of the TiAl bar, and a dimple in the mating Ti-6Al-4V. Further friction welding experiments will be conducted based on these results.

Life Prediction of Valves Made from Advanced Materials:

Finite element modeling of the Si_3N_4 valve continued in the current reporting period, examining the valve seating event against the seat insert. Discussions with CTO staff members indicate that in addition to the combustion pressure loads that the seating of the valve against the seat insert is another critical event that should be examined for life prediction. The finite element model should examine the stresses as a result of the valve impacting the seat insert. In addition, the model should also include an eccentric seat insert contact region.

A conservative approach was used for this series of finite element models; a terminal velocity was applied followed by a combustion load. The proposed Si_3N_4 valve design indicates a reduction of the maximum principle tensile stress by approximately 40% when compared to the baseline model. However, the finite element model of the proposed Si_3N_4 valve design shows higher stresses in other valve locations. Presented in Figure 13 are these higher stress regions.

During the seating event and subsequent pressure load, a stress wave passes through the valve. As the wave propagates, the same stress magnitude is found in the valve stem (fig. 13b), while higher stresses are estimated near the stem-fillet radius juncture (fig. 13c) and within the keeper notch (fig. 13d). The greatest maximum principle tensile stress in baseline metallic finite element model was estimated in the fillet radius region.

Another finite element model developed in the current reporting period is shown in Figure 14. This 3D, one-quarter-symmetry model is of the baseline metallic valve model and includes an eccentric seat insert. Comparing fig. 14a with fig. 14c illustrates the eccentric seat insert; a small gap can be seen between the valve and the seat insert.

The stress field results from this model are presented in Figure 15. The eccentric seat insert increases the maximum principle tensile stress by nearly a factor of 4, and this stress is in a localized part of the fillet radius.

ANL:

Dr. J. G. Sun at ANL has provided NDE of two Si_3N_4 valves that completed a 100-hour bench test. The results of Dr. Sun's work indicate that the valve did not exhibit any surface or subsurface microcracks in the contact and the fillet radius regions. The NDE scans did indicate regions where subsurface damage may exist as a result of material processing. Dr. Sun plans to scan additional Si_3N_4 valves that have completed the 100-hour bench test and compare these results with prior NDE scans.

Presentations:

None

Future Work:

Additional finite element modeling will be made and will focus on optimizing the valve keeper notch, and with establishing a complete valve load cycle for fatigue analyses. Life prediction codes will then estimate the probability of failure for many of the finite element models developed. A final design will be agreed upon that includes members from LEC, CTO, MEC and Engine Research.

Solicitations for machining the Si_3N_4 valves will be sent out and a vendor(s) will be chosen. Valves that have been tested in the bench test will be sent to ANL for NDE. Flexure specimens will be ordered from the same SN235P powder lot and their strengths will be obtained under several experimental parameters.

References:

1 Kokai patent application No. HEI 2[1990]-160188

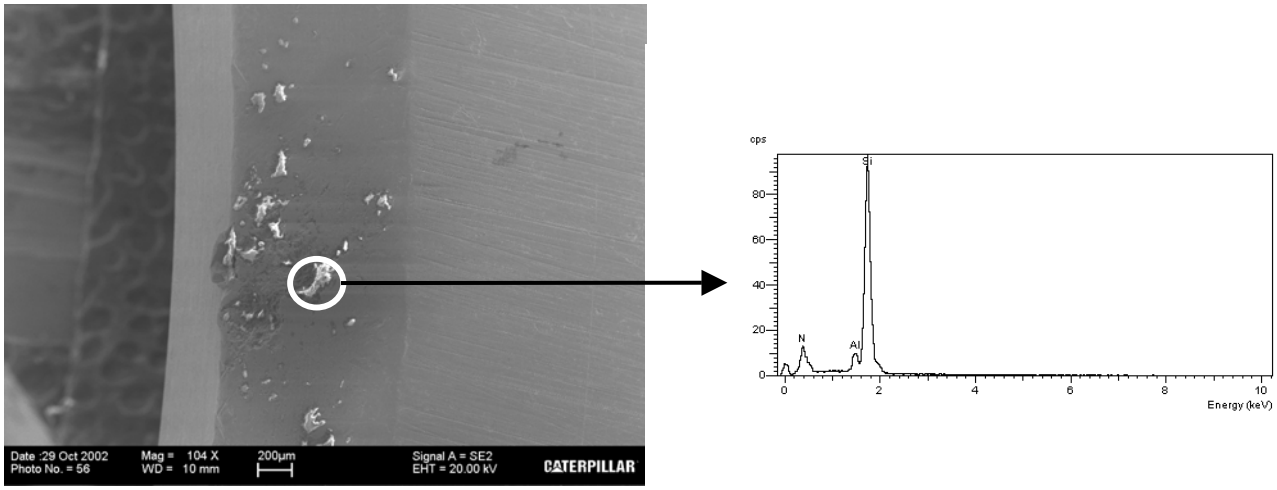

(a) (b)

Figure 1. SEM image and corresponding EDS scan of CV-12 metallic seat insert after 100-hour bench test. The EDS in (b) represents the lighter region within the circle (a). This shows the presence of silicon nitride (silica and nitrogen elements detected) embedded in the seat insert.

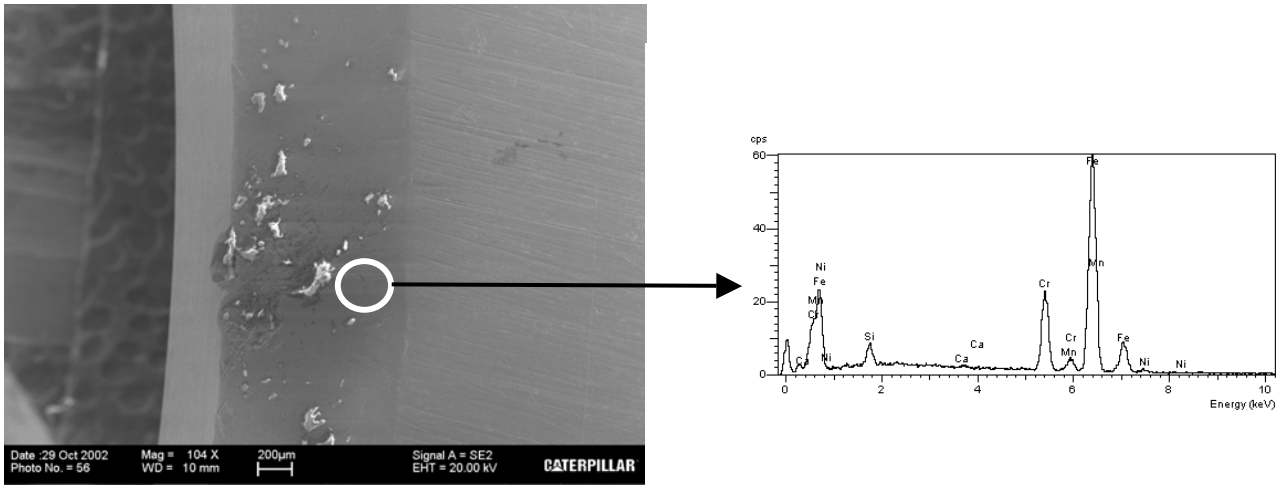

(a) (b)

Figure 2. The same SEM image (CV-12) as in Figure 1 (a) but with a different EDS scanned region. The EDS in (b) represents the circled region in (a) that indicates the base metal of the seat insert.

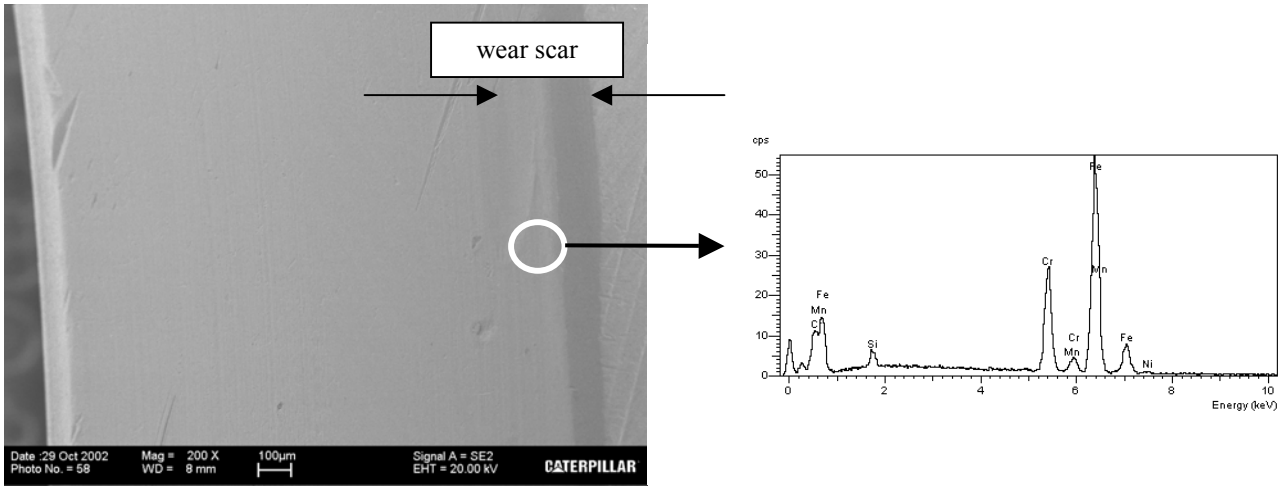

(a) (b)

Figure 3. SEM image of wear scar on CV-20 metallic seat insert (a) with corresponding EDS scan (b). The scan indicates that the plastically deformed region consists mainly of the base metal seat insert material.

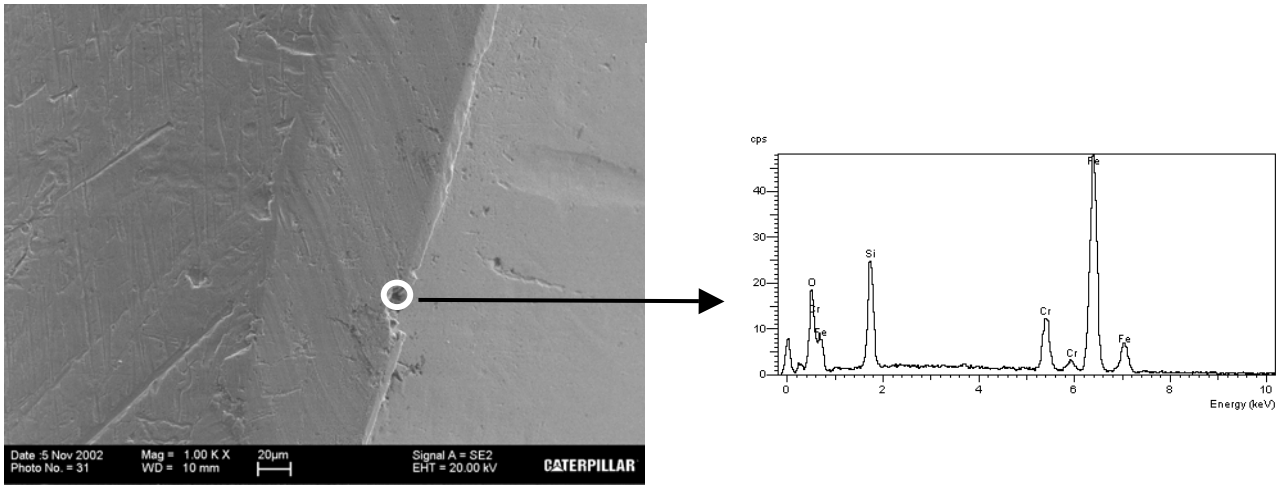

(a) (b)

Figure 4. SEM image of seat insert CV-14 contact area (a) with corresponding EDS scan (b). Along with identifying the base metal, there is the presence of silica and oxygen imbedded region, indicating particles from the valve are embedded in the seat insert.

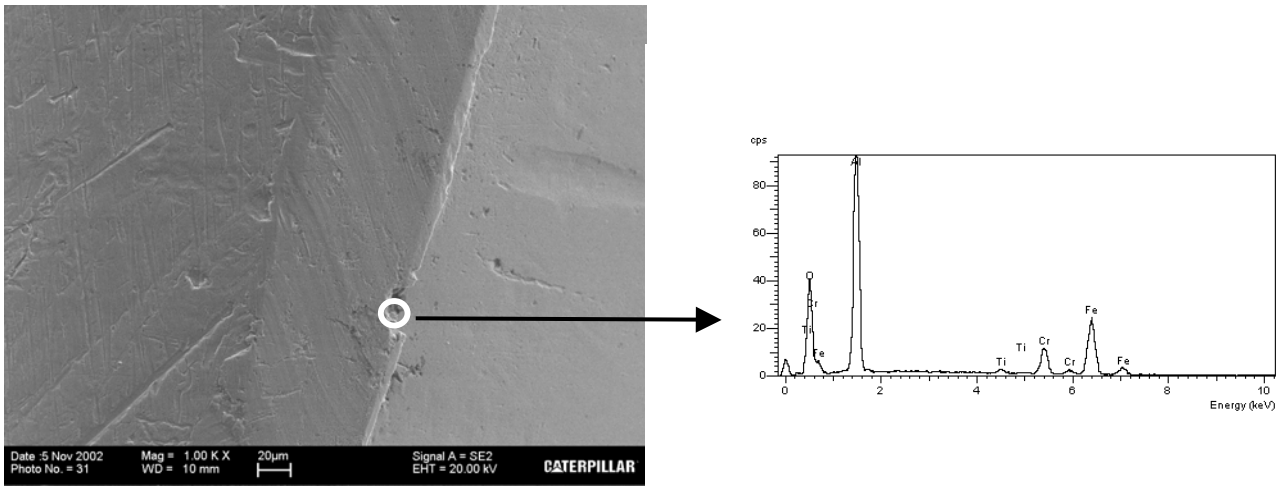

(a) (b)

Figure 5. Same SEM image as in Figure 4 (a) (CV-14) but with a different EDS scan (b). The EDS indicates the presence of alumina and oxygen in the area of embedded particles from impact with the Si_3N_4 valve.

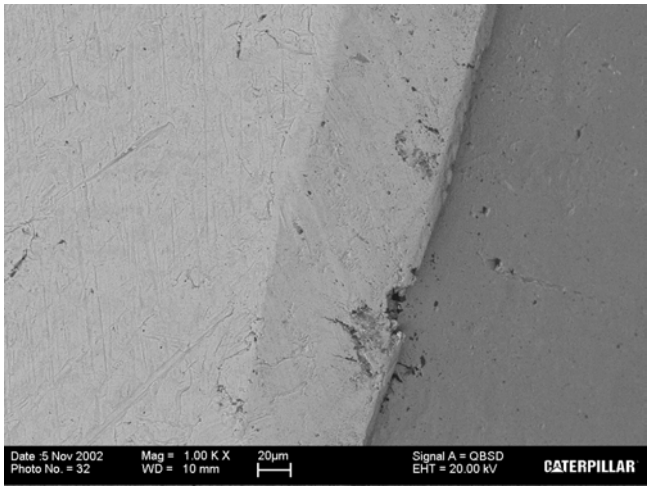

Figure 6. SEM Backscatter image of Figures 4 and 5 (a). Imbedded particles appear as the darker regions and indicate the presence of elements with small atomic numbers (e.g. silica, nitrogen, oxygen, and alumina).

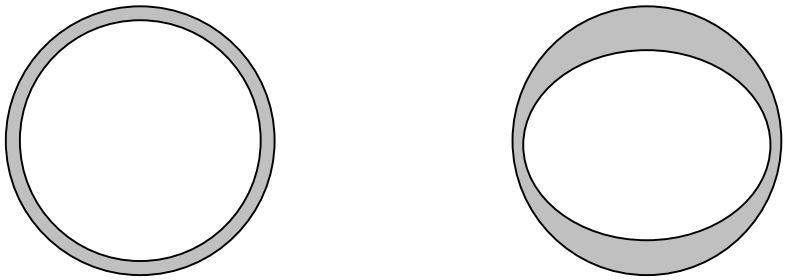

(a) (b)

Figure 7. Schematic top views of valve seat insert contact region: (a) normal, (b) eccentric shape.

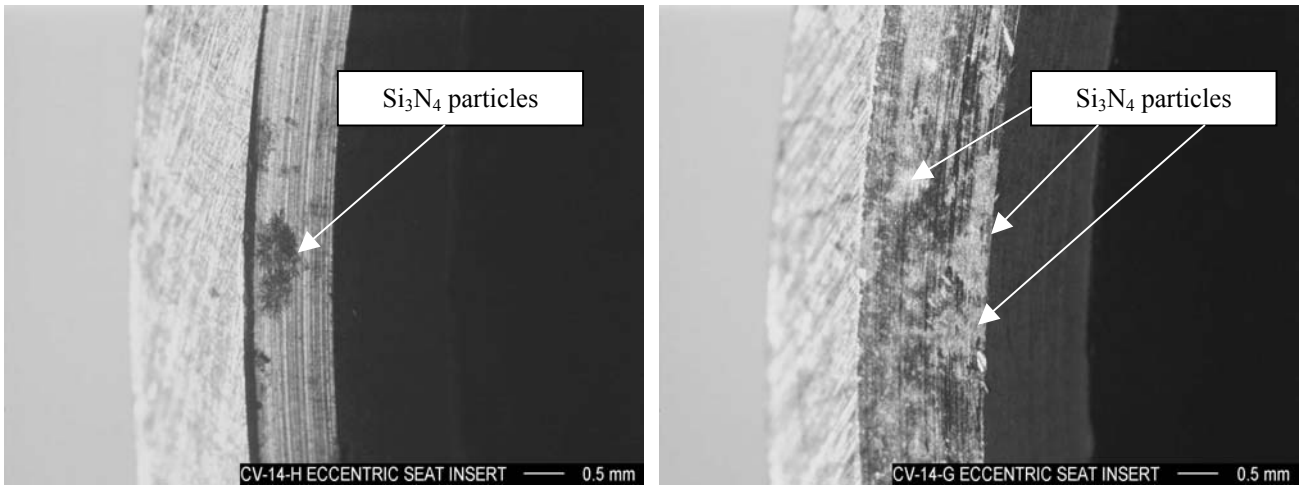

(a) (b)

Figure 8. Eccentric machined seat inserts, CV-14, after the 100-hour bench test. In (a) a distinct region appears as Si_3N_4 embedded particles and in (b) there are several regions of embedded Si_3N_4 particles.

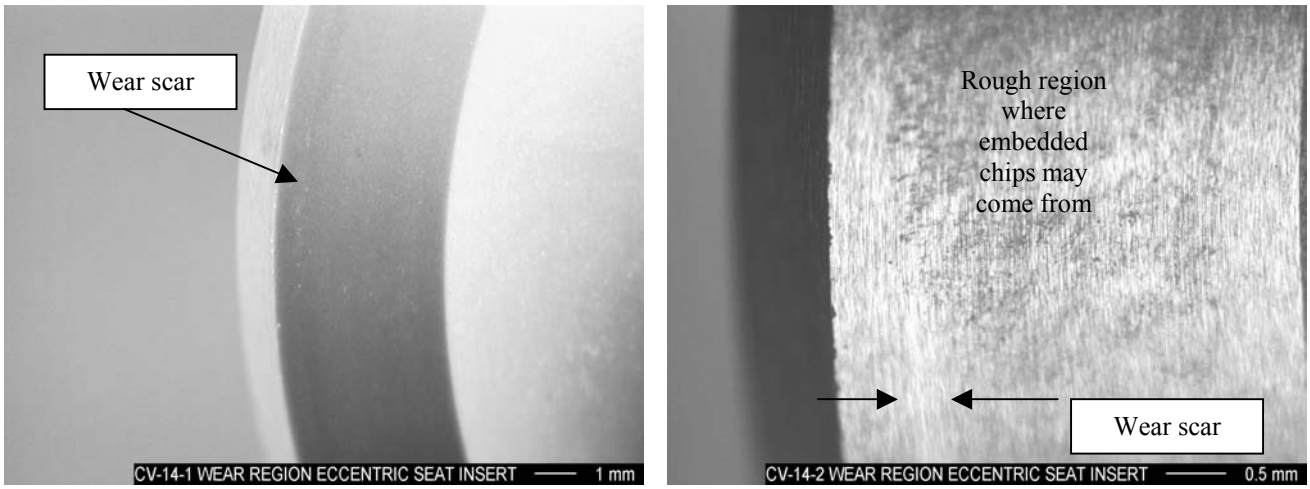

(a) (b)

Figure 9. Si_3N_4 valves after the 100-hour bench test (CV-14). A small wear scar is shown in (a) while in (b) the wear scar is pointed out along with rough regions where the embedded Si_3N_4 particles in the seat insert came from.

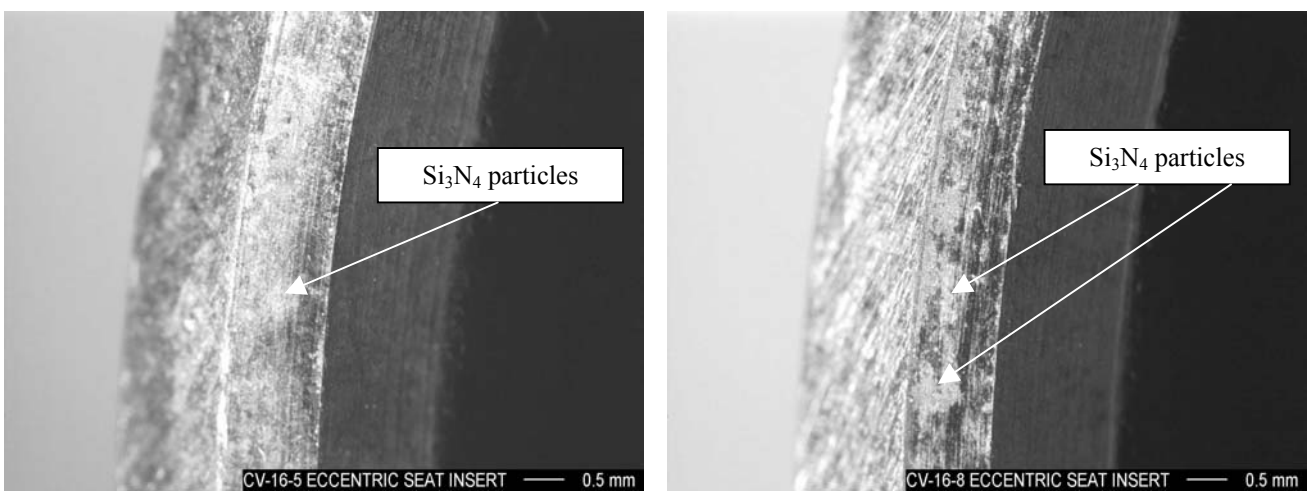

(a) (b)

Figure 10. Eccentric machined seat inserts, CV-16 after the 100-hour bench test. The lighter regions in (a) and (b) appear to be Si_3N_4 particles.

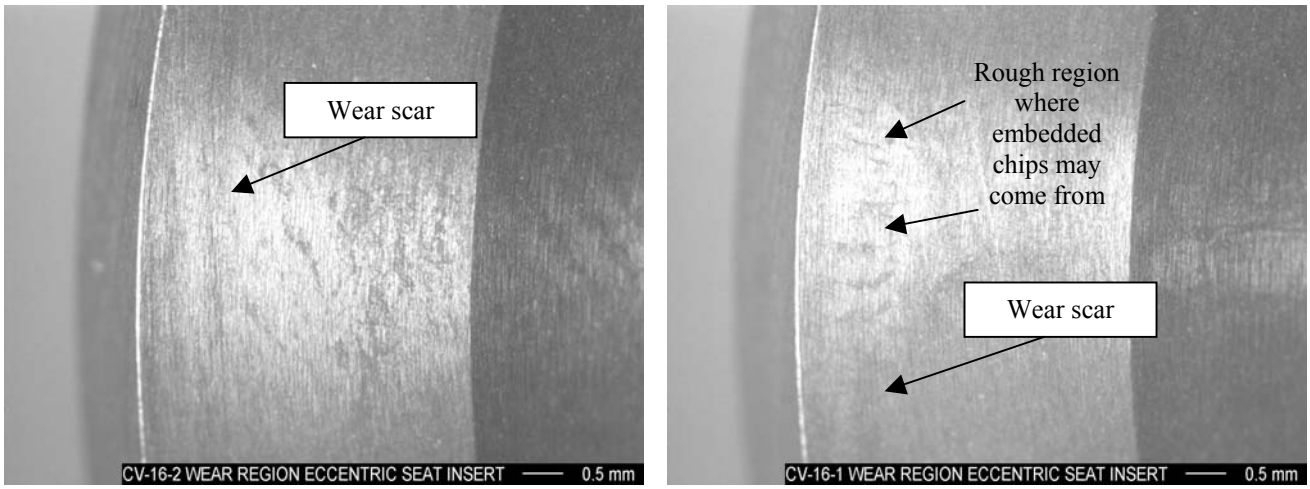

(a) (b)

Figure 11. Si_3N_4 CV-16 valve contact region showing wear scars (a) and regions where embedded particles found in the seat inserts came from (b).

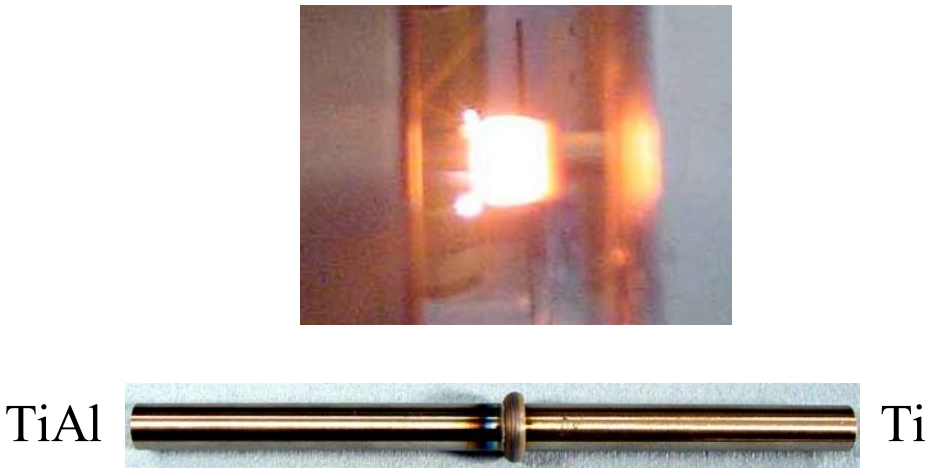

(a)

(b)

Figure 12. (a) Incandescent Ti-6-4 and TiAl during the friction welding operation. (b) Friction welded TiAl/Ti-6-4 bar.

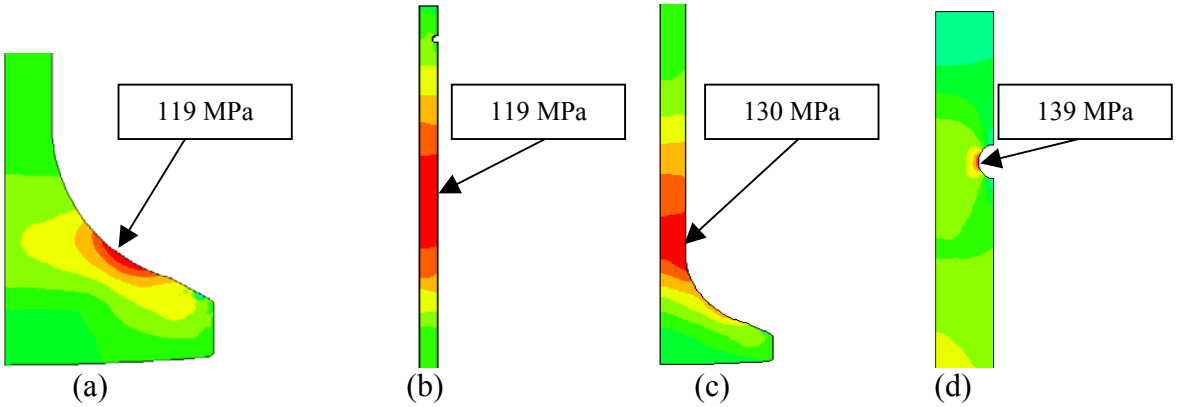

Figure 13. Si_3N_4 valve design during the seating event along with pressure load. Maximum principle tensile stresses propagate through the valve body beginning with (a) and ending with (d). The new design has higher stresses in regions other than the fillet radius.

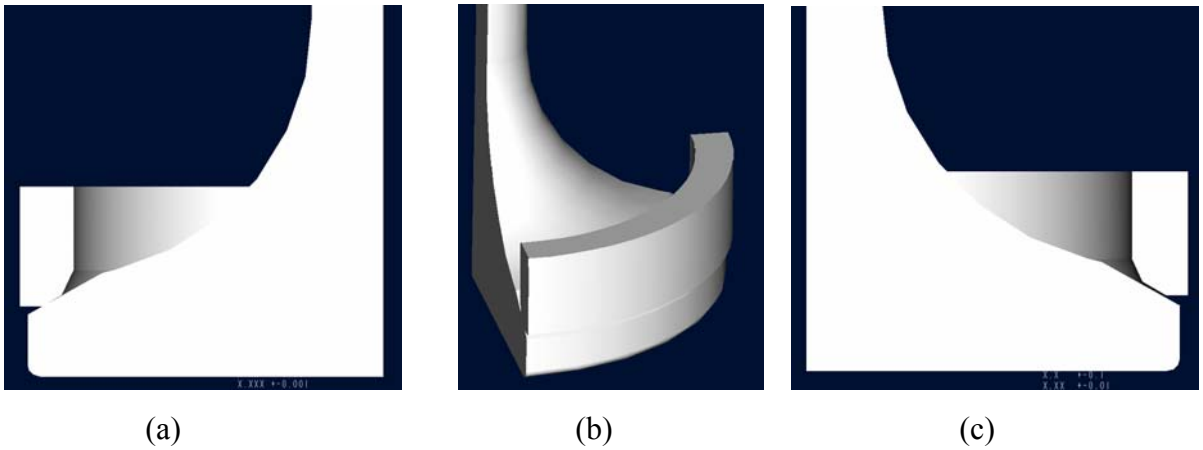

Figure 14. Solid one-quarter-symmetry finite element model of the baseline metallic valve and seat insert. The seat insert makes contact in (a) but there is a gap between the valve and seat insert in (c).

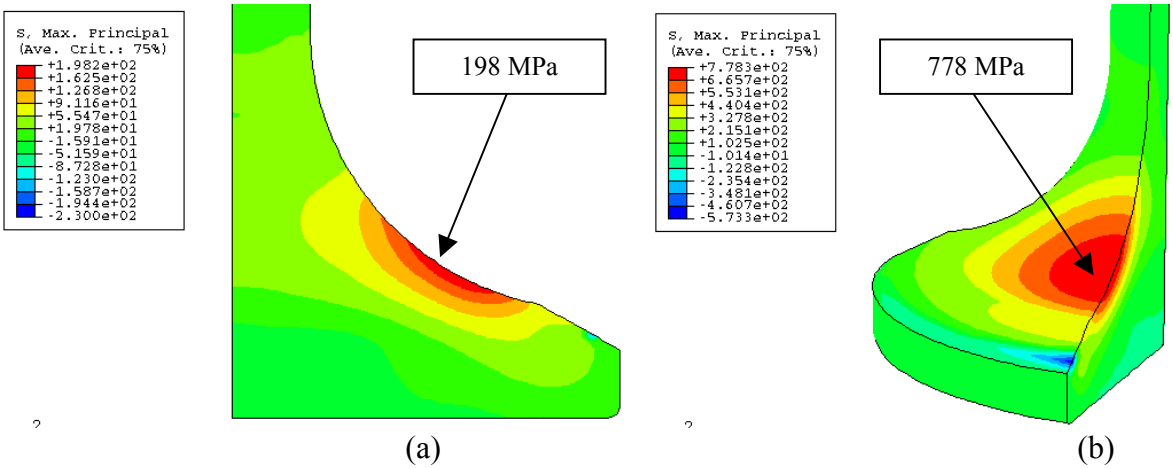

(a) (b)

Figure 15. Results from the valve seating event presented using 2D and 3D finite element models. In the 2D model, (a) the corresponding valve seat insert is not warped while in (b) the seat insert is warped. The stress increases by nearly a factor of 4 when the eccentric seat insert is included in the modeling.

Thick Thermal Barrier Coatings (TTBCs) for Low Emission, High Efficiency Diesel Engine Components

M. Brad Beardsley and Jesus G. Chapa-Cabrera
Caterpillar Inc.

Objective/Scope

Engine testing of thermal sprayed coatings has demonstrated their use as thermal barriers and wear coatings can reduce fuel consumption, reduce wear and reduce component temperatures. The durability of thermal sprayed coatings, particularly thermal barrier coatings, remains as the major technical challenge to their implementation in new engine designs. New approaches to coating design and fabrication will be developed to aid in overcoming this technical hurdle. New laser technology of surface dimpling, cleaning and laser assisted spraying will be applied to enhance adherence and increase coating strength. Refinements of current seal coating technologies will be developed to further enhance the durability of the coating structure. New quasicrystalline materials will be evaluated as thermal barrier coatings as well as wear coatings for ring and liner applications and as low friction coatings for camshafts and crankshafts. Plasma spraying, D-Gun and HVOF processing will be used to develop these new coatings.

Technical Highlights

Work has been conducted aimed on developing a thermal insulating coating that can be applied at room temperature, cured at temperatures in the order of 250°C and resist application temperatures in excess of 1200°C. Thin films of amorphous, metal phosphates, originally developed at Caterpillar are being modified for application as thick thermal insulation coatings. Composites consisting of an amorphous aluminum phosphate matrix and various filler materials have been produced. Aluminosilicate hollow microspheres, illustrated in Figure 1, were used as filler in these composites, introducing controlled porosity and reducing the thermal conductivity. Two additional formulations were prepared with glass hollow microspheres and Al_2O_3. Figure 2 shows thermal conductivity data for the three formulations calculated from laser flash thermal diffusivity and heat capacity measurements. A conductivity of 1.1 W/m-K was obtained for the composite formulated with aluminosilicate microspheres, which makes this material a good candidate for thermal barrier applications in terms of thermal conductivity.

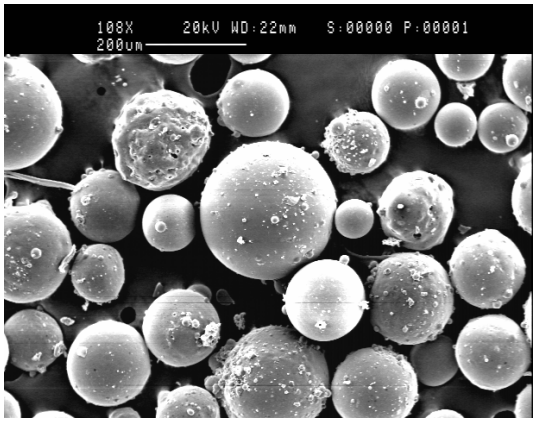

Figure 1 Aluminosilicate microspheres.

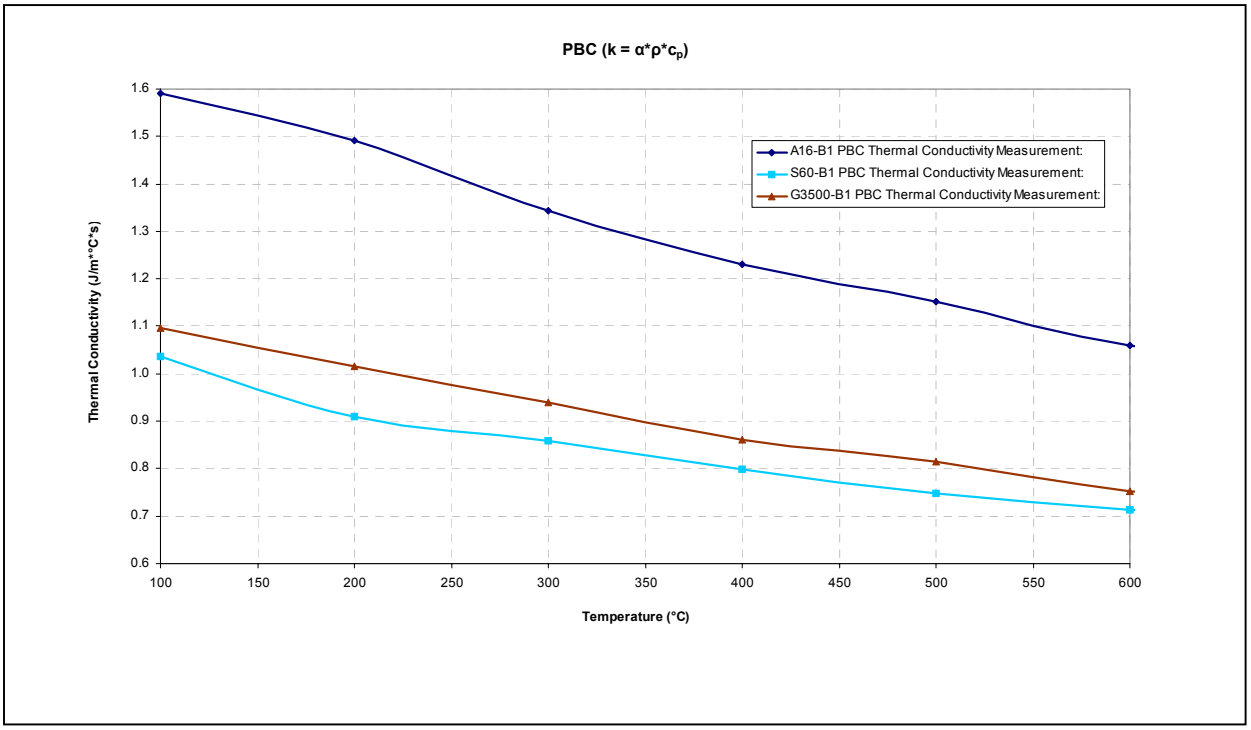

Figure 2. Thermal conductivities for three different aluminum phosphate composite formulations.

Future Plans

Primary focus in the next quarter will be on the measurement of the phosphate composite strengths and thermal physical properties of quasicrystal materials.

Travel

None.

Status of FY 2003 Milestones

Milestones:

321. Determine the effect on TTBC bond strength due to laser micro-dimpling of the substrate surface prior to coating. (July 31, 2003)

Work has been completed to evaluate initial laser parameters for microdimpling of the substrate. Further work to evaluate the bond strength with the microdimpled surfaces is planned for April of 2003.

322. Determine the effect on TTBC coating strength and permeability due to laser shock peening after coating application. (July 31, 2003)

No progress to report.

323. Determine the effect on the hardness and microstructure of the TTBC due to laser assisted plasma deposition. (July 1, 2003)

Subcontract issues with Fraunhofer Germany have not been fully resolved delaying the start of this work. If agreement is not reached by Feb. 15, 2003, an alternate subcontractor will be sought.

324. Incorporate torsional fatigue testing results into life models. (Completed May 29, 2002)

Shear properties of the coating were determined in multiaxial fatigue and the influence of the biaxial stress state on facture behavior was determined.

325. Develop FEA models to aid in the design of life prediction tools for the TTBC system. (December 1, 2003)

No progress to report.

325. Evaluate the microstructure of the ceramic TTBC material using varying laser power.

No progress to report.

Publications

None this period.

Processing and Characterization of Structural and Functional Materials for Heavy Vehicle Applications

J. Sankar, D. Kumar, N. Sudhir, and S. Yarmolenko
North Carolina A & T State University

Objective/Scope

The objective of this work is synthesis and characterization of metal-ceramic thin film composites with improved mechanical properties processed through the pulsed laser deposition (PLD) technique. This work presents the study of effect of processing parameters on structure of nickel single domain particles embedded in alumina matrix. The report gives an update on the task "magnetic properties of self-assembled single-domain nickel and iron nanomagnets." The research work was carried out in collaboration with J. Narayan (Center for Advanced Materials and Smart Structures, Department of Materials Science and Engineering North Carolina State University, Raleigh, NC 27695) and S. J. Pennycook and A. Lupini (Solid State Division, Oak Ridge National Laboratory, Oak Ridge, TN 37831).

Technical Highlights

Synthesis of thin film metal-ceramic composites with nickel nanocrystallites embedded in alumina matrix

Nanocrystalline nickel crystallites were embedded in alumina matrix using a KrF excimer laser (252 nm, 30 ns full width at half maximum) focused alternately onto high-purity targets of nickel and alumina. The depositions were carried out on silicon substrates in a high vacuum environment (~5 X 10^{-7} Torr). The substrate temperature was approximately 500 ºC. The energy density and repetition rate of the laser beam used were 2 J/cm^2 and 10 Hz, respectively. The size of Ni particles was controlled by selecting the deposition time of magnetic materials and insulating matrix and the deposition temperatures. The deposition times were 40-60 sec for magnetic materials and 120 sec for insulating material (Al_2O_3). The number of alternating layers (Ni - Al_2O_3) was five from which we can get enough signal during magnetic measurements. Schematic of thin film nickel-alumina composite is presented on Figure 1.

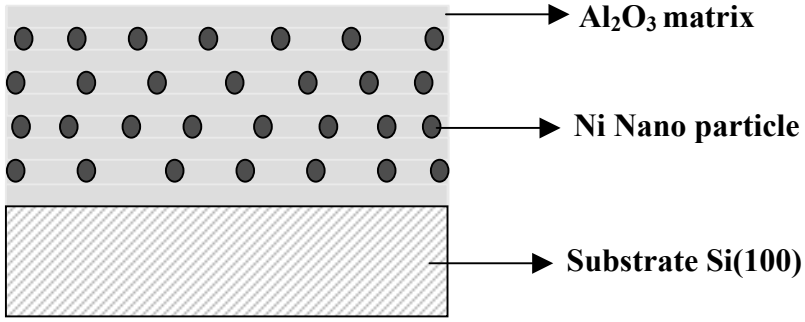

Figure 1. Schematic of Ni-alumina nanocomposite.

Characterization of nano-engineered Ni/Al_2O_3 composites

The size distribution of metallic particles (Figure 2) and the crystalline quality of both the matrix and metallic particles were investigated by cross-sectional scanning transmission electron microscopy with atomic number (Z) contrast (STEM-Z).

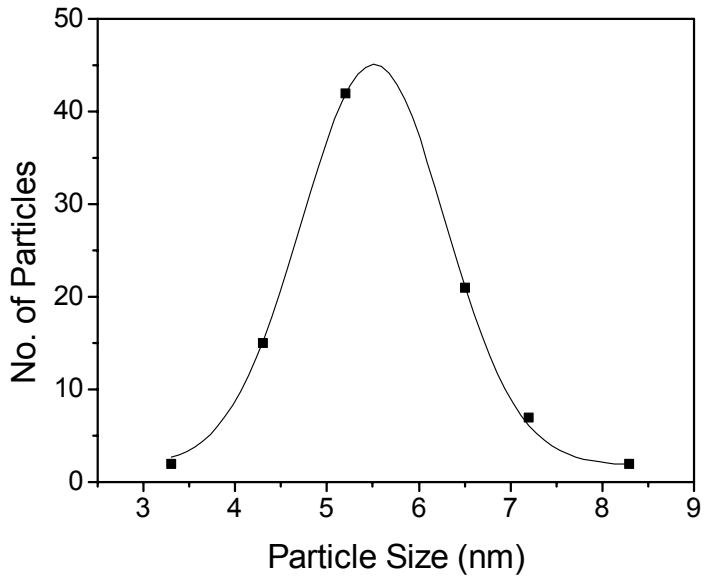

Figure 2. Size distribution of Ni particles in alumina matrix. The solid line is a log-normal fit to the data points.

Shown in Figure 3 is the cross sectional STEM-Z micrograph of Ni nanocrystallites embedded in alumina matrix. Z-contrast in the STEM provides an incoherent image in which changes in atomic structure and composition across an interface can be interpreted directly without the need for preconceived atomic structure models. This is true provided the incident electron probe is smaller than the lattice spacing (for sample oriented along a major axis) or atomic columns. Since the probe is scanned, the resultant image is a map of the column, scattering power of which in turn depends upon the atomic number, Z^2 of each column. The spatial resolution is limited primarily by the probe size which is 1.2 Å in our field emission instrument.

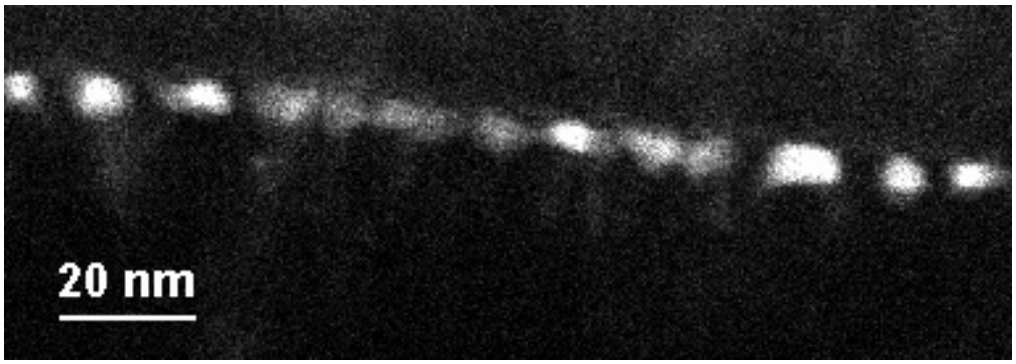

Figure 3. Cross sectional STEM-Z micrograph of Ni nanocrystallites embedded in alumina matrix

The Z-contrast image in the STEM is formed by electron scattered through high angles. The average size of the Ni nanocrystals was determined to be ~5 nm. It is clear from the cross sectional images that the Ni nanoparticles are mostly uniform in size and are well separated from each other. The average intralayer separation between the particles is estimated to be ~2-5 nm.

In order to evaluate the crystalline quality of the metal particles and the alumina matrix, a high resolution STEM-Z was recorded (Figure 4) from a single metal particles and alumina matrix in its immediate vicinity. It is clear from this figure that the Ni nanoparticle is crystalline and the alumina matrix is amorphous in nature. Such a biphase system is formed as both materials are immiscible (i.e., they display thermodynamically driven segregation during deposition) and the cohesive energy at the interface between the both phases is high.

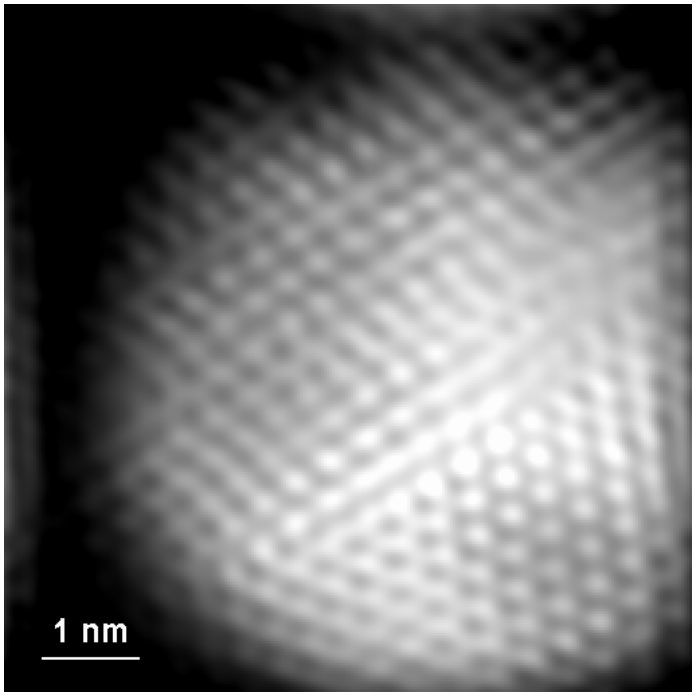

Figure 4. A high resolution STEM-Z recorded from a single Ni particles and alumina matrix in its immediate vicinity.

The amorphous phase of the matrix can provide high structural flexibility in order to accommodate the coherency strain without forming dangling bonds, voids or other flaw as observed in Figure 4. In this case the nanostructure would be stable and the grain boundary sliding is greatly avoided.

Future Plans

1. Continue to study effect of processing parameters (temperature of substrate and deposition time) on properties of thin film metal-ceramic composites.
2. Study mechanical properties of thin film metal-ceramic composites processed by PLD technique.

Status of Milestones

On Schedule

Communications/Visitors/Travel
Presentation of the work at 2002 ASME International Mechanical Engineering Congress and Exposition (November 19, 2002, New Orleans, LA).

Problems Encountered
None

Publications
D. Kumar, N. Sudhir, S. Yarmolenko, Q. Wei, J. Sankar, J. Narayan, and S. J. Pennycook, "Synthesis and Characterization of Metal-Ceramic Thin Film Nanocomposites with Improved Mechanical Properties," 2002 ASME International Mechanical Engineering Congress and Exposition, New Orleans, LA, 2002, CD-ROM, Paper #IMECE2002-39370.

NDE/C Technology for Heavy Duty Diesel Engines: Fuel Delivery and Insulating Materials

W. A. Ellingson, C. Deemer, J. Christensen
Argonne National Laboratory

Objective/Scope

The objective of the work in this task, part of the Testing and Characterization research area of the Heavy Vehicle Propulsion System Materials Program, is to develop enabling nondestructive evaluation/characterization (NDE/C) technology for lower cost and high performance materials. Specifically, this project addresses development of advanced NDE/C technology for; a)-advanced fuel delivery systems (including injector nozzles) and b)-insulating materials for reducing heat losses in the combustion zone. Fuel delivery systems for heavy-duty diesel engines are complex, very expensive and represent a significant portion of the cost of a heavy vehicle diesel engine. High pressures inside these fuel delivery systems contribute to poor fuel delivery and hence poor emissions. Materials development is part of Goal 3 of the heavy vehicle propulsion materials program. Insulating materials are also a significant materials development area because of the improvement in engine efficiency if reduced heat losses can be obtained. NDE/C technology that can provide information for reliable cost production and engine component surveillance would be of benefit to reaching the goals.

Technical Highlights

The technical highlight this period is that the ABB robot arm has been more fully developed now and 360-degree rotation has been achieved. Further, we have established that normal incidence of the laser is far better for detection of subsurface features so have discontinued the work on angle scattering.

Technical progress

The efforts this period have been on modifying the scanning set on the robot arm for better data acquisition as well as better defining the optimum set up for the laser back scatter to acquire subsurface features in the plungers. We have obtained data on new test specimens

Robot arm back-scatter laser scans

This period we again modified the laser scatter data acquisition parameters for the 6-axis articulated arm robot. As a part of this effort, we used a new machined Si3N4 specimen machined from GS44. A diagram of the new specimens is shown in Figure 1. The "blind" side region scanned is shown schematically in Figure 2. In order to establish the effect of the angle of incidence of the laser beam, hence angle of reflection, a series of tests were conducted using 10, 15 and 20 degrees angle of incidence. The results of these scans are shown in Figures 3 through 5 respectively. It is to be noted that visual observation of the back-scatter data suggests that the detected signal is not uniform across the width of the test samples. Indeed in discussions with the machinists, it was noted that the machining had a variable depth most likely. In order to establish sensitivity in a quantitative sense, a line plot was made along the long axis of the specimens. Shown below in Figure 6 is one such line plot that clearly shows the effect of the depth of the notch on the detected back-scatter data.

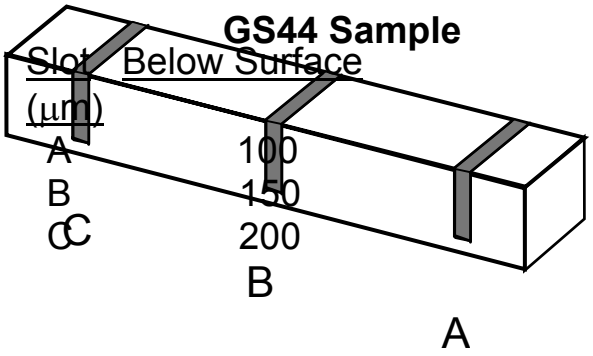

Fig.1. Schematic diagram of new silicon nitride GS-44 test specimen used for laser back-scatter experiments

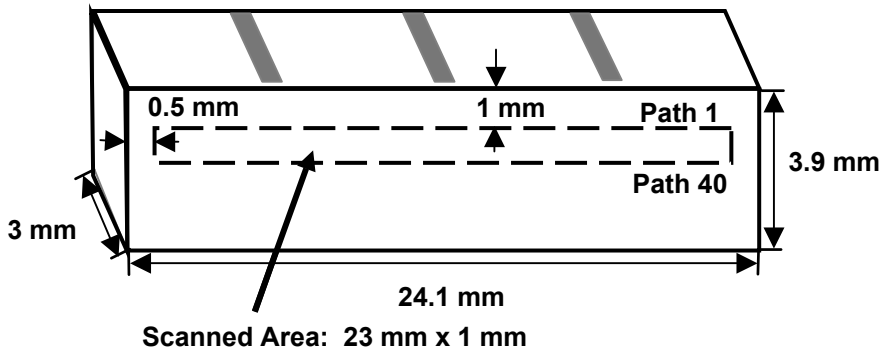

Fig. 2. Schematic diagram showing the laser back-scatter region

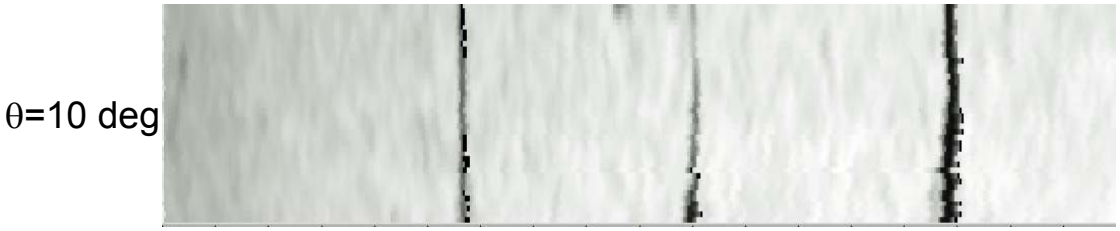

Fig. 3. Laser back-scatter "image" data for 10-degree angle of incidence for test sample of Fig. 1

θ=15 deg

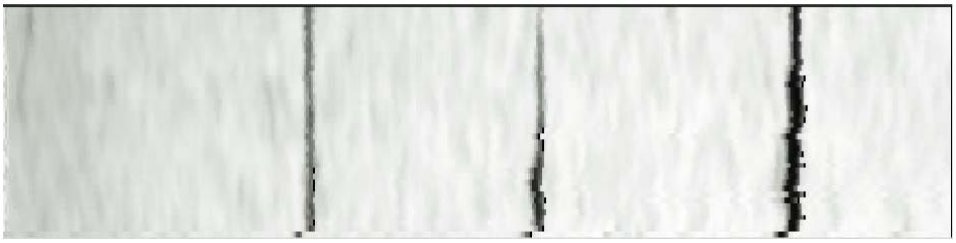

Fig. 4. Laser back-scatter "image" data for 15-degree angle of incidence for test sample of Fig. 1

θ=20 deg

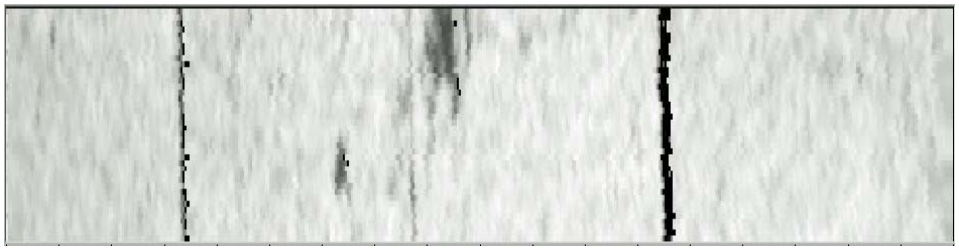

Fig. 5. Laser back-scatter "image" data for 20-degree angle of incidence for test sample of Fig. 1

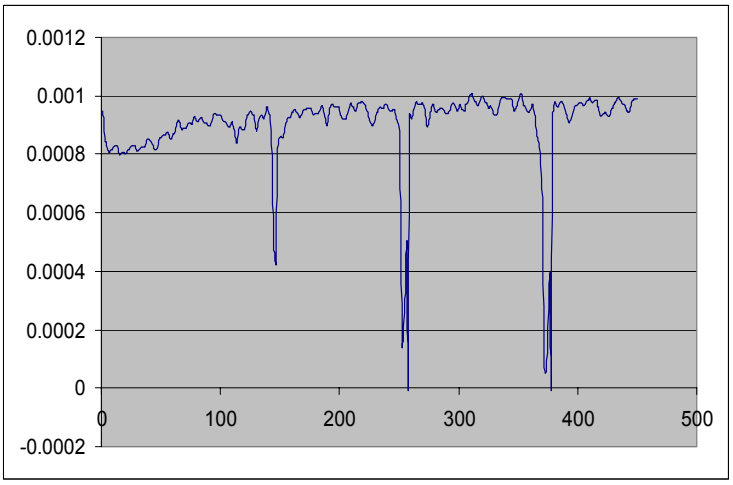

Fig. 6. Line plot of the back-scatter image data of Fig. 4: 15-degree incidence angle

Future Plans

Travel

Taken: None

Planned: W.A. Ellingson plans to participate in the 27th annual Cocoa Beach meeting sponsored by the American Ceramic Society, to be held January 20-24, 2003 in Cocoa Beach, FL.

Status of FY 2003 Milestones

On schedule

Publications

None this period.

NDE Development for Ceramic Valves for Diesel Engines

J. G. Sun, J. Zhang, W. A. Ellingson,
and M. J. Andrews *
Argonne National Laboratory
***Caterpillar, Inc.**

Objective/Scope

Emission reduction in diesel engines designated to burn fuels from several sources has lead to the need to assess ceramic valves to reduce corrosion and emission. The objective of this work is to evaluate several nondestructive evaluation (NDE) methods to detect defect/damage in structural ceramic valves for diesel engines. One primary NDE method to be addressed is elastic optical scattering. The end target is to demonstrate that NDE data can be correlated to material damage as well as used to predict material microstructural and mechanical properties. There are three tasks to be carried out: (1) Characterize subsurface defects and machining damage in flexure-bar specimens of NT551 and SN235 silicon nitrides to be used as valve materials. Laser-scattering studies will be conducted at various wavelengths using a He-Ne laser and a tunable-wavelength solid-state laser to optimize detection sensitivity. NDE studies will be coupled with examination of surface/subsurface microstructure and fracture surface to determine defect/damage depth and fracture origin. NDE data will also be correlated with mechanical properties. (2) Assess and evaluate subsurface damage in ceramic valves to be run in bench test and in a single-cylinder-engine test. All valves will be examined at ANL prior to test, during periodic scheduled shut downs, and at the end of the planned test runs. (3) Evaluate healing of subsurface damage by laser glazing on machined surfaces of GS44 ceramics. ANL will perform laser-scattering characterization on machining surfaces at before and after glazing treatment. NDE data will be correlated with glazing parameters and mechanical properties.

Technical Highlights

Work during this period (October-December 2002) focused on examining the laser-glazing effect on machining damage in Si_3N_4 ceramics and on developing a laser-scatter system for full-valve scans.

1. Elastic Optical Scattering NDE for Machining Damage

We conducted laser-scattering tests on the laser-glazing treated Si_3N_4 flexure-bar specimens received from Caterpillar during last period. Figure 1 shows photos of these specimens. Each set contains 5 treated bars and the rests were untreated. Laser scattering sum images for all specimens are shown in Fig. 2. The scanned length for all bars was 45 mm, and the spatial resolution was 10 μm/pixel in both directions. It is apparent that the scatter intensity (grayscale) is related with the color of the material, i.e., darker material produced lower scatter intensity. The subsurface scattering is very low in regions with surface gold coating (specimens no. 6 and 9 of the transversely ground GS44) which was applied for surface SEM (not performed at ANL).

The laser-scattering data in Fig. 2 do not show apparent effect of the laser-glazing treatment. This is understandable because it was estimated that the glazing treatment only affected the top surface layer of a few microns while the detected scattering signal comes from a much thicker subsurface layer. For GS44, this subsurface-scattering layer is deeper than 400 μm and for

SN235P, deeper than 100 μm, although the scattering near the surface contributes more than that comes from deeper layers.

Figure 3 shows detailed comparison of laser-scattering images of glazing-treated and untreated GS44 and SN235P specimens. It is evident from the images that, for both materials, the distribution and intensity of the machining damage marks (brighter lines) are essentially same for treated and untreated surfaces. This is again due to the shallow glazing effect compared with the deeper machining damage. The hardness of the surfaces was measured with micro indentations. Two of the indents within the Fig. 3 images are indicated; they caused additional subsurface damage. Typical sizes and shapes of the indents are shown in Fig. 4.

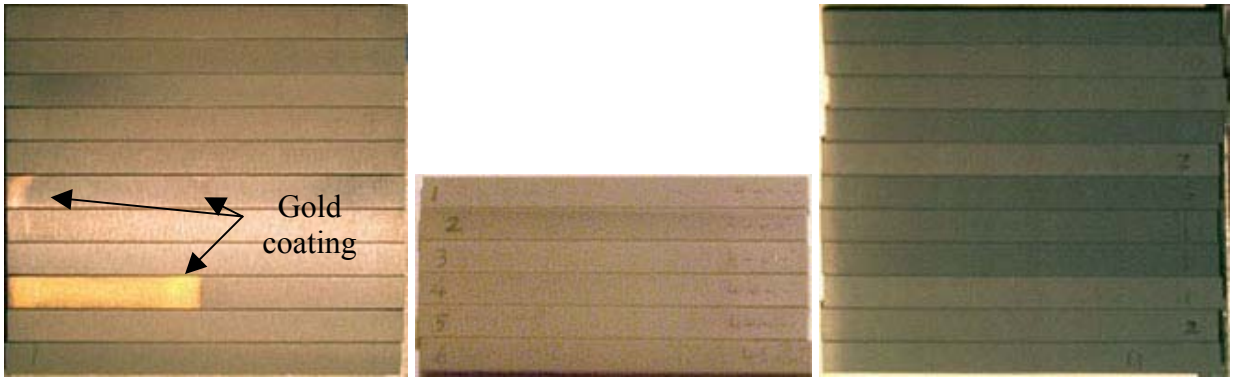

transversely ground GS44 longitudinally ground GS44 longitudinally ground SN235P

Fig. 1. Photos of flexure-bar specimens with 5 in each set treated by laser glazing.

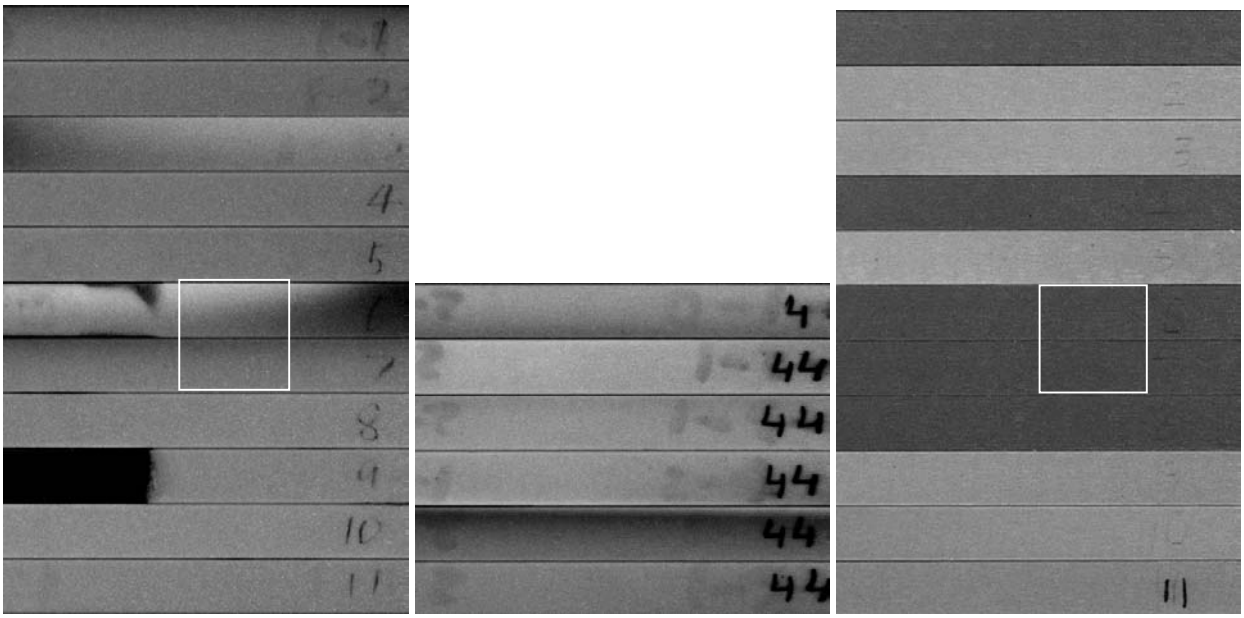

transversely ground GS44 longitudinally ground GS44 longitudinally ground SN235P

Fig. 2. Laser-scattering sum images of flexure-bar specimens (the 5 bars at bottom in each set were laser-glazing treated). Detailed images within the white frames are shown in Fig. 3.

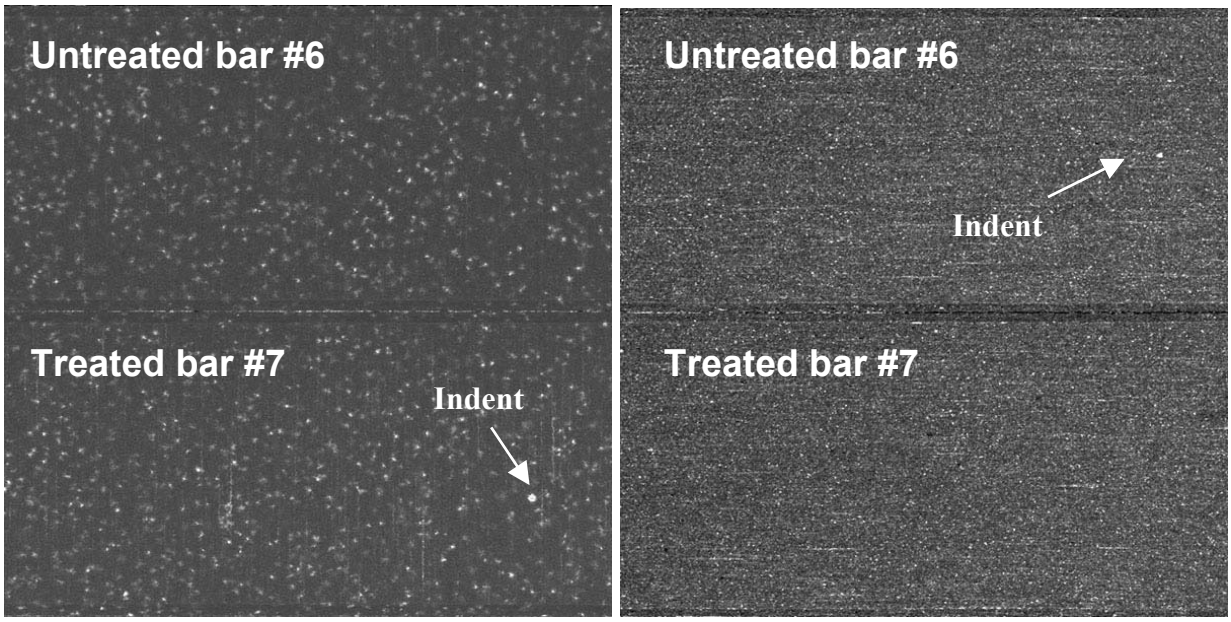

(a) (b)

Fig. 3. Detailed laser-scattering images of flexure-bar specimens: (a) transversely ground GS44, (b) longitudinally ground SN235P. Image size is 8mm x 8mm.

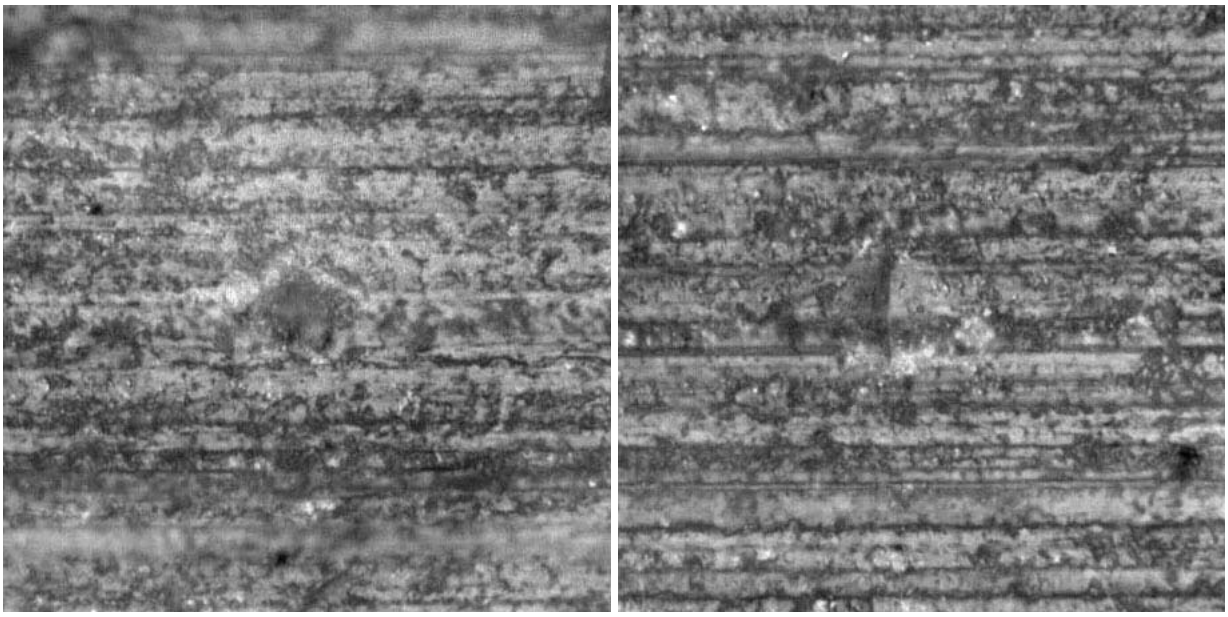

untreated laser-glazing treated

Fig. 4. Photomicrographs (1000X) of indents on untreated and treated longitudinally-ground GS44 specimens. Image size is 0.1mm x 0.1mm.

2. Laser-Scattering System Development for Si_3N_4 Valves

During this period we finished developing a prototype laser-scattering system suitable for scanning an entire valve. Figure 5 is a photograph of the experimental setup. It has been used to scan the entire valve-head section for several valves. The cylindrical shaft was not scanned because the axial-movement distance is limited by the current 100-mm-range translation stage; a translation stage with 200-mm range is needed. It should be pointed out that, with appropriate input of the axial-profile data, this system is capable of scanning any part of axially-symmetrical geometry.

Figure 6 shows typical laser-scattering scan data of a NT551 valve. The scanned region (valve head) is illustrated in Fig. 6a. The scan resolution along the axial-length direction was 20 μm, and the resolution along the circumferential direction was 22 μm at "top" and 4 μm at "bottom" because of the change of diameter. The scan image of the entire valve-head section is shown in Fig. 6b, and a small area with a flaw is enlarged in Fig. 6c. The laser-scattering images in Fig. 6 are typical of those for the NT551 material. The darker lines/regions in Fig. 6b image are due to surface marking/contamination.

We are continuing optimizing the system setup and software. New results will be reported in the next period.

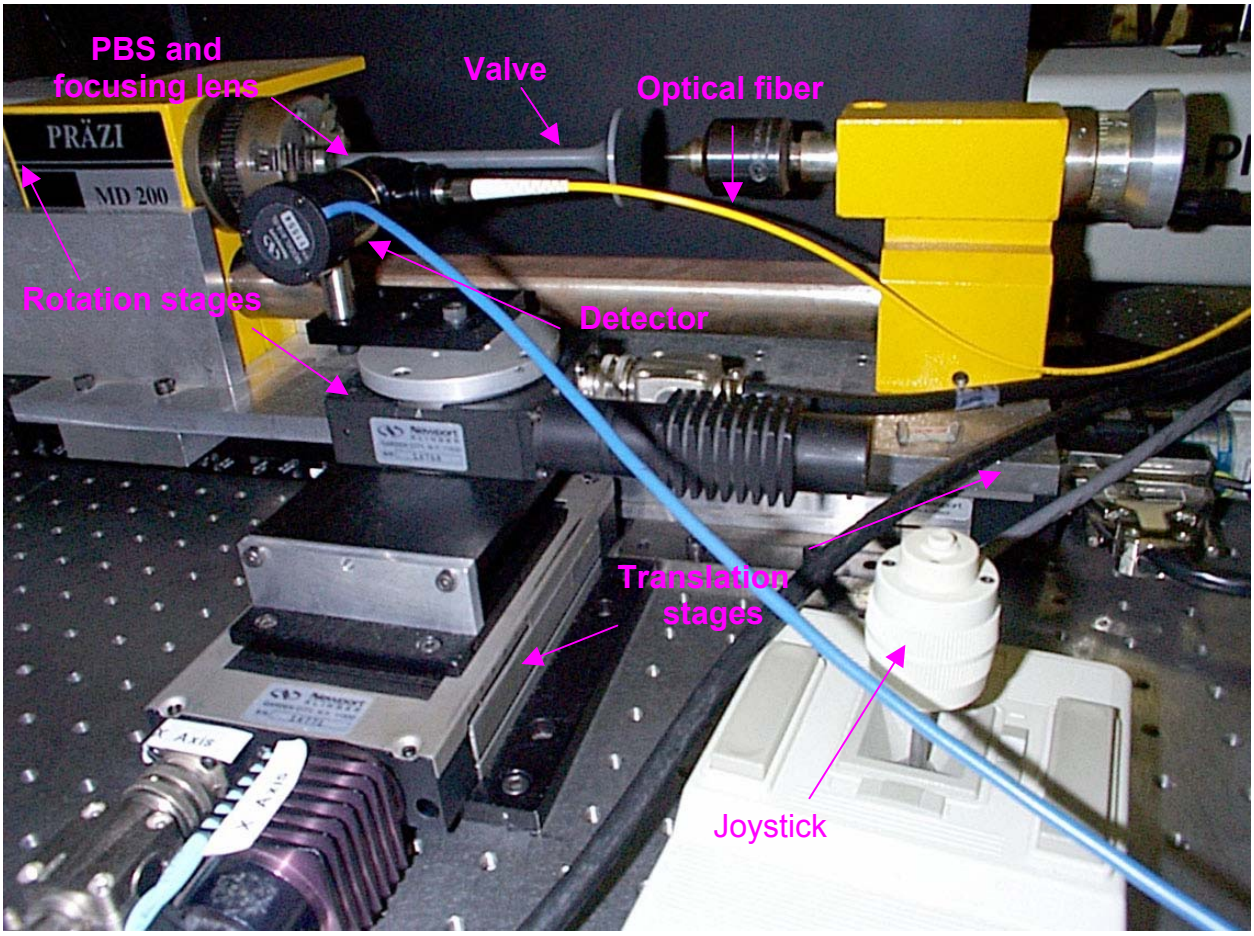

Fig. 5. Photograph of the laser-scattering system for scanning an entire valve.

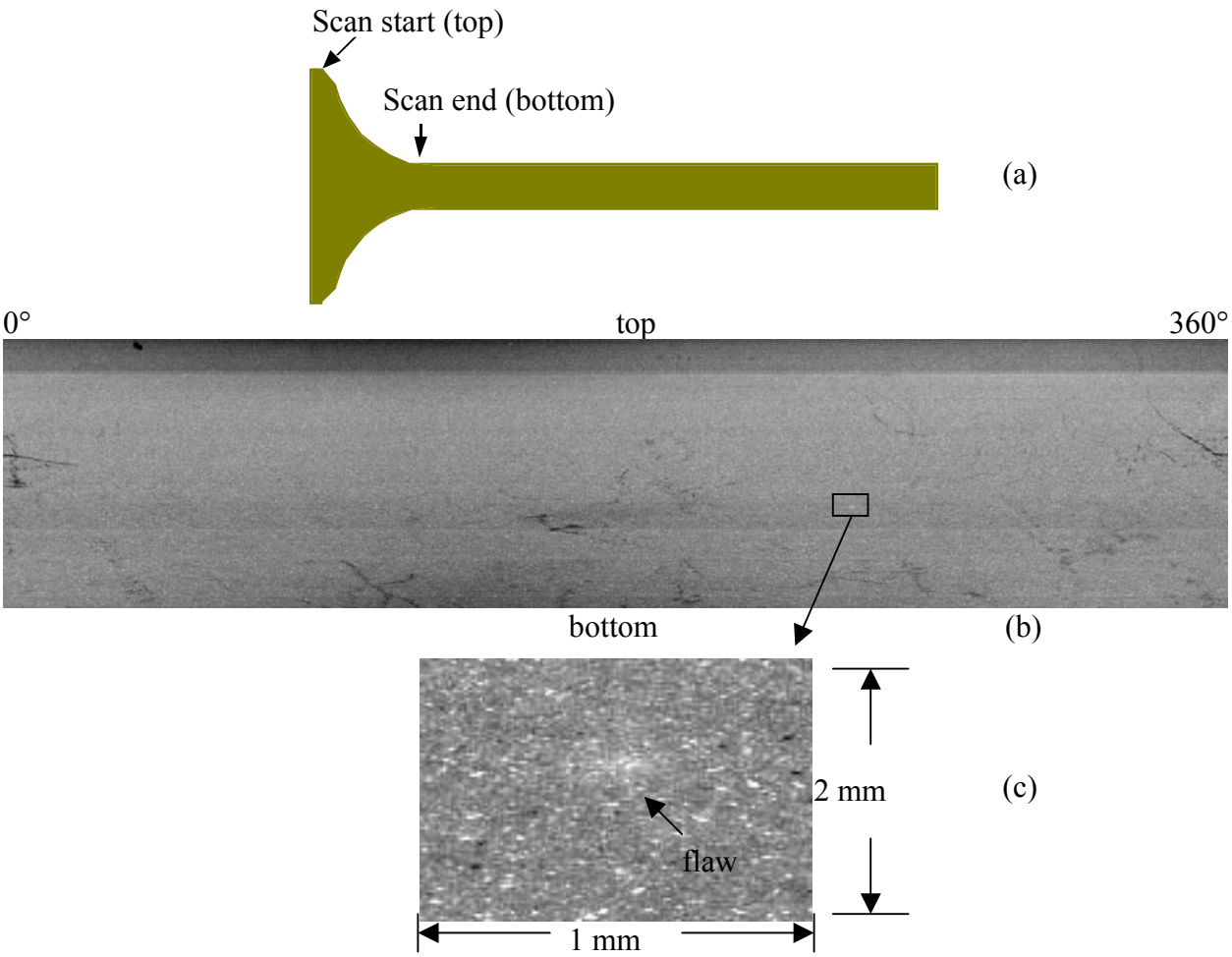

Fig. 6. (a) Illustration of scanned valve-head region (between top and bottom), (b) laser-scattering image of a NT551 valve and, (c) an enlarged area from (b).

Status of Milestones

Current ANL milestones are on or ahead of schedule.

Communications/Visits/Travel
None this period.

Problems Encountered
None this period.

Publications
None this period.

Durability of Diesel Engine Component Materials

Peter J. Blau
Oak Ridge National Laboratory

John Truhan
University of Tennessee, Knoxville, TN

Jun Qu
ORISE Post-Doctoral Fellow

Objective/Scope

The objective of this effort is to enable the development of more durable, low-friction moving parts in diesel engines for heavy vehicle propulsion systems by conducting friction, lubrication, and wear analyses of advanced materials, surface treatments, and coatings. The scope of materials and coatings is broad and includes any metallic alloy, intermetallic compound, ceramic, or composite material which is likely to be best-suited for the given application. Parts of current interest include scuffing-critical components, like fuel injector plungers and EGR waste gate components. Bench-scale simulations of the rubbing conditions in diesel engine environments are used to study the accumulation of surface damage, and to correlate this behavior with the properties and compositions of the surface species. The effects of mechanical, thermal, and chemical factors on scuffing and reciprocating sliding wear are being determined. Results will be used to develop wear maps and models for selecting materials for durability-critical engine components.

Technical Highlights

Fuel Injector Plunger Scuffing. As previously reported, the pin-on-twin configuration was established as a reasonable testing protocol, and reciprocating friction and wear experiments were performed on annealed AISI 52100 steel under lubrication by Jet A fuel and on-highway #2 diesel fuel. Observations of time-dependent changes in the wear scar morphology verified that the friction force could be used to provide a reliable real-time monitor of the onset of scuffing.

During this quarter, pin-on-twin tests were conducted on hardened (heat-treated) 52100 steel and transformation-toughened zirconia, which are representative of fuel injector plunger materials in current diesel engines. The reciprocating frequency and stroke length were set to 10 Hz and 10 mm, respectively, the same as those used in the tests of annealed 52100 steel reported last time. The hardened 52100 steel cylindrical pins, with a 9 mm diameter, were polished with 600 grit SiC paper to get a consistent surface finish, about 0.08 μm in R_a. The zirconia pins were tested as received, 9.5 mm in diameter and 0.04 μm in R_a.

Short-duration, 5-minute pin-on-twin tests with 100 N constant load were conducted on self-mated annealed 52100 steel, self-mated hardened 52100 steel, and zirconia against hardened 52100 steel. These combinations were lubricated by both Jet A and #2 diesel fuel.
The wear scars for the Jet A fuel-lubricated condition are shown in Fig. 1. Compared with annealed 52100 steel, there was a significant reduction in the degree of surface damage observed for tests using the hardened 52100 steel, both self-mated and against zirconia. The worn

surfaces of the hardened 52100 steel pins were fairly smooth and material removal and transfer were only seen at a few small areas, as shown in Figs. 1 (b) and (c). In the annealed 52100 steel tests, the material removal and transfer accumulated quite fast to become the predominant features on the wear scar as soon as scuffing started. The hardened 52100 steel on steel and zirconia on hardened 52100 steel showed much higher wear resistance. It took hours to propagate scuffing damage to encompass the full length of the wear scar.

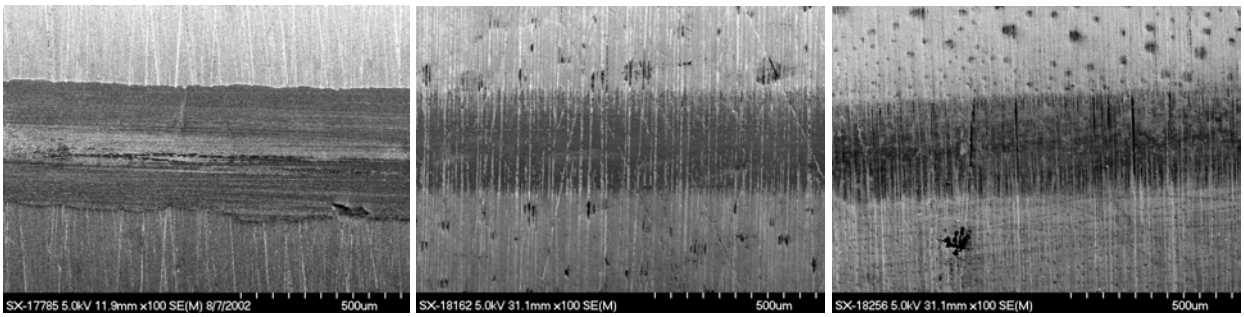

(a) (b) (c)

Figure 1. Wear scars of different material combination lubricated by Jet A fuel under 100 N load for 5 minutes. (a) Annealed 52100 steel on steel. (c) Hardened 52100 steel on steel. (d) Zirconia on hardened 52100 steel.

The coefficients of friction before and after the on-set of scuffing are listed in Table 1. The values of friction coefficient before scuffing were in the same level for all three material combinations. The onset of scuffing was detected by a significant transition of the friction force trace in the annealed 52100 steel tests, as reported before. However, there was no noticeable transition on the friction force traces in the tests of the hardened 52100 steel and zirconia. That is because the measured friction force was the average value along each full stroke and did not reflect the local surface damage before the wear scar became well-scuffed. A more delicate friction measurement in finer time scale is proposed to be able to catch the onset of local scuffing. Interrupted tests will be performed to verify the transition through examination of the worn surface morphology.

In addition to friction force versus time records, the wear scar width and surface roughness were considered as a possible means to detect the onset of scuffing, but they did not prove as useful. However, their general characteristics changed in such a manner as to reflect the dependency of wear severity on the material, lubricant, applied load, and time of sliding contact.

Table 1.

Friction coefficients for three different material combinations under fuel lubrication
(100 N load, 10 Hz, 10 mm stroke)

Coefficient of friction		Jet A		Diesel	
Top pin material	Bottom pin material	Before scuffing	After scuffing	Before scuffing	After scuffing
Annealed 52100	Annealed 52100	0.11	0.25	0.10	0.15
Hardened 52100	Hardened 52100	0.10	0.11	0.10	0.10
Zirconia	Hardened 52100	0.11	0.11	0.10	0.11

Future Plans

1. Continue pin-on-twin testing of hardened 52100 steel and zirconia. More detailed friction measurements, with higher data sampling rates, are planned in order to catch the onset of local scuffing events.
2. Tests of other candidate plunger materials are planned. These include AISI 440C stainless steel and Stellite 6B. Commercial TiN-coated fuel injector plungers will also be tested.
3. Conduct tests using a new contact configuration, flat-on-flat, which may better simulate the lower stresses and types of damage seen in actual plunger components.

Progress Review Meeting

A progress review with Sid Diamond, DOE, was held on 11/22/02 at ORNL. Results to date were presented and future directions were discussed.

Travel

No project travel was undertaken during this quarter.

Status of FY 2002 Milestones

3) Complete tests of candidate ceramic materials and cermets for fuel injector applications. Submit report. (September 30, 2002 – the pin-on-twin test configuration under Jet A and Diesel fuel-lubricated conditions are established and systematic tests have been conducted on both annealed and hardened AISI 52100 steel and zirconia to detect onset of scuffing. Tests on other candidate materials and new configuration will be conducted in next quarter.)

Publications

J. Qu, P.J. Blau, R. Ott, and J. Truhan "The Development of a Pin-on-Twin Scuffing Test to Evaluate Materials for Heavy Duty Diesel Fuel Injectors," poster accepted for presentation at the *2003 International Conference on Wear of Materials*, Washington, DC.

Life Prediction of Diesel Engine Components

H. T. Lin, T. P. Kirkland, A. A. Wereszczak, and M. K. Ferber
Oak Ridge National Laboratory

and
M. J. Andrews
Caterpillar Inc.

Objective/Scope

The valid prediction of mechanical reliability and service life is a prerequisite for the successful implementation of structural ceramics and advanced intermetallic alloys as internal combustion engine components. There are three primary goals of this research project which contribute toward that implementation: the generation of mechanical engineering data from ambient to high temperatures of candidate structural ceramics and intermetallic alloys; the microstructural characterization of failure phenomena in these ceramics and alloys and components fabricated from them; and the application and verification of probabilistic life prediction methods using diesel engine components as test cases. For all three stages, results are provided to both the material suppliers and component end-users.

The systematic study of candidate structural ceramics (primarily silicon nitride) for internal combustion engine components is undertaken as a function of temperature (< 1200°C), environment, time, and machining conditions. Properties such as strength and fatigue will be characterized via flexure and rotary bend testing.

The second goal of the program is to characterize the evolution and role of damage mechanisms, and changes in microstructure linked to the ceramic's mechanical performance, at representative engine component service conditions. These will be examined using several analytical techniques including optical and scanning electron microscopy. Specifically, several microstructural aspects of failure will be characterized:

(1) strength-limiting flaw-type identification;
(2) edge, surface, and volume effects on strength and fatigue size-scaling
(3) changes in failure mechanism as a function of temperature;
(4) the nature of slow crack growth; and
(5) what role residual stresses may have in these processes.

Lastly, numerical probabilistic models (i.e., life prediction codes) will be used in conjunction with the generated strength and fatigue data to predict the failure probability and reliability of complex-shaped components subjected to mechanical loading, such as a silicon nitride diesel engine valve. The predicted results will then be compared to actual component performance measured experimentally or from field service data. As a consequence of these efforts, the data generated in this program will not only provide a critically needed base for component utilization in internal combustion engines, but will also facilitate the maturation of candidate ceramic materials and a design algorithm for ceramic components subjected to mechanical loading in general.

Technical Highlights

At present there are limited material suppliers that could provide consistent and reliable material resources and efforts to the end users. The lack of committed materials suppliers could then hamper the smooth implementation of silicon nitride ceramic components for advanced diesel engine applications. Thus, it is important to extend the database generation efforts to other potential candidate silicon nitride ceramics especially manufactured by the domestic material suppliers. Studies of dynamic fatigue behavior in four-point bending for a commercial grade silicon nitride (SN147-31N, Ceradyne Advanced Ceramic Operation, Inc., CA) were carried out during this reporting period. The database generated will be used for life prediction for exhaust valve components and be compared to those previously generated for Kyocera SN235 and SN235P silicon nitride. The SN147-31N silicon nitride bend bars were longitudinally machined based per ASTM C116 standard. The dynamic fatigue tests were carried out at 20 and 850°C and at stressing rate of 30 and 0.003 MPa/s in air.

Dynamic fatigue test results at 20 and 850°C showed that the SN147-31N exhibited an inert characteristic strength value between SN235 and SN235P (as shown in Table 1, and Fig. 1and 2.). Also, the SN147-31N exhibited Weibull moduli, which were comparable to those obtained for SN235 and SN235P under the same test conditions. The strength versus stressing rate curves showed that the SN147-31N exhibited a fatigue exponent of 47 and 131 at 20 and 850°C, respectively (Fig. 3). The increase in fatigue exponent with increased test temperature could be attributed the onset of creep deformation process, evident by the permanent curvature observed for those SN147-31N bend bars after testing at 850°C and 0.003 MPa/s. Electron microscopy analysis of fracture surface for specimens tested at 850°C and at 0.003 MPa/s will be carried out to provide insight into the possible change in microstructure or chemistry of secondary phase at test temperature. In addition, measurement of thermal expansion as a function of temperature up to 1000°C will be carried out to correlate the softening point of secondary phased to the onset of creep deformation process.

SEM examination of polished cross section of TiAl intermetallic alloy after 48h oil immersion test at 850°C in air was carried out to evaluate the effect of environment on the microstructure as well as the corrosion resistance. Figure 3 shows the microstructure taken from the exposed surface region, which exhibits an oxide scale (2 µm thick) formed during the oil immersion exposure. The EDAX analysis of material underneath the oxide scale did not detect any elements from the oil ash, indicating excellent corrosion resistance. A longer exposure time up to 1000h needs to be followed to ensure the long-term stability and thus mechanical reliability of the material.

Status of Milestones

Milestone: "Complete testing and analysis of prototype silicon nitride valves after bench rig testing" was on schedule.

Communications / Visitors / Travel

Update of the status of modification of rotary bending fatigue test rig for testing TiAl alloy was held with Juses Chapa-Cabrera at Caterpillar

Update of the bench test on Norton NT551 exhaust valves was held with M. J. Andrews at Caterpillar.

Problems Encountered

None.

Publications

None.

References

[1] H. T. Lin, T. P. Kirkland, M. K. Ferber, and M. J. Andrews, "Life Prediction of Diesel Engine Components," Heavy Vehicle Propulsion System Materials Program Bimonthly Technical Progress Report to DOE Office of Transportation Technologies, Jan. – March 2001.

Table 1. Summary of uncensored Weibull and strength distributions for Ceradyne SN147-31N silicon nitride specimens longitudinally machined per ASTM C1161. Data of Kyocera SN235 and SN235P are used for reference.

Material	# of Spmns. Tested	Stressing Rate (MPa/s)	Temp. (°C)	Uncens. Weibull Modulus	± 95% Uncens. Weibull Modulus	Uncens. Chrctstic Strength (MPa)	± 95% Uncens. Chrctstic Strength (MPa)
SN235	9	30	20	12.8	6.8, 21.2	999	937, 1061
SN235P	9	30	20	32.6	18.8 49.6	792	773, 810
SN147-31N	15	30	20	21.73	14.07. 31.09	836	814, 858
SN147-31N	15	0.003	20	20.70	13.38, 29.67	694	675, 713
SN235	9	30	850	17.0	9.2, 27.5	866	826, 906
SN235P	8	30	850	30.3	16.5, 48.1	673	643, 691
SN147-31N	15	30	850	20.35	13.58, 28.20	777	755, 799
SN235P	9	0.003	850	23.6	12.7, 38.8	641	662, 641
SN147-31N	15	0.003	850	16.19	10.57, 23.02	732	706, 757

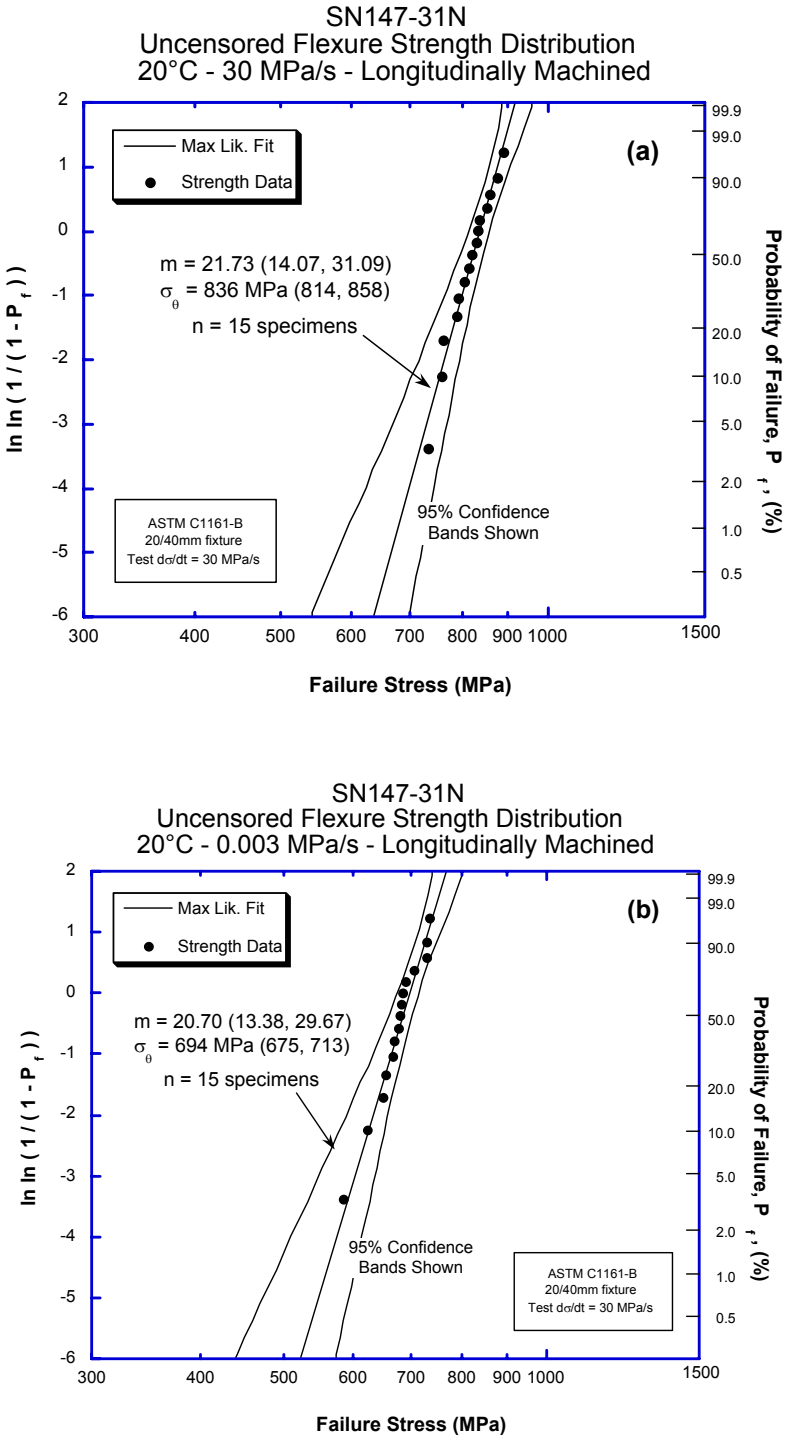

Figure 1. Strength distribution of Ceradyne SN147-31N longitudinally machined and tested at 20°C and at (a) 30 MPa/s and (b) 0.003 MPa/s.

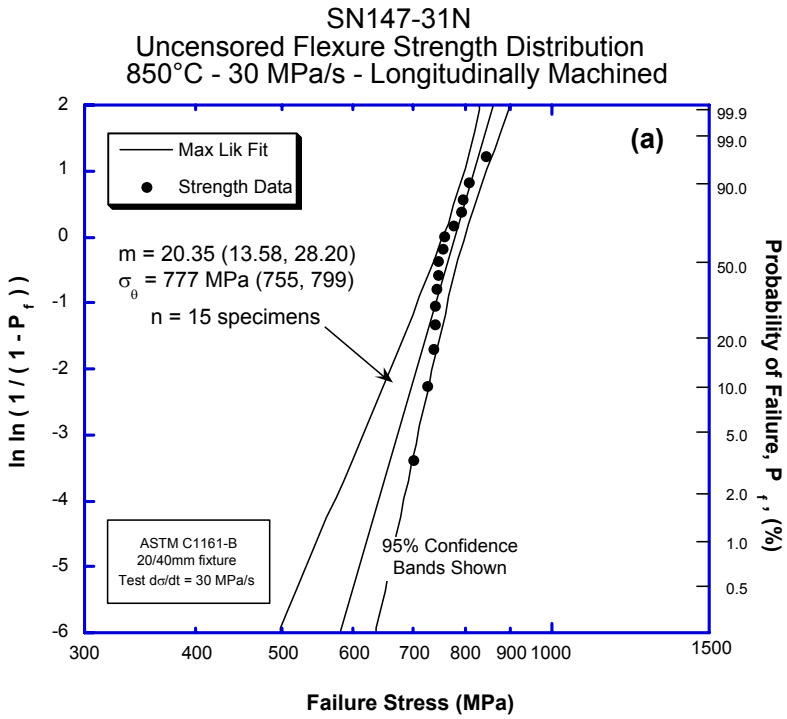

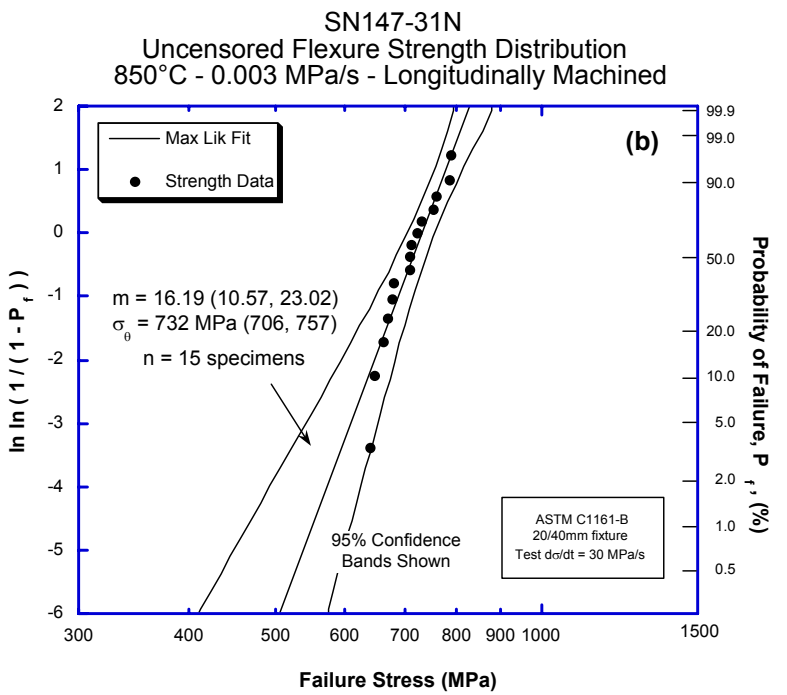

Figure 2. Strength distribution of Ceradyne SN147-31N longitudinally machined and tested at 850°C and at (a) 30 MPa/s and (b) 0.003 MPa/s.

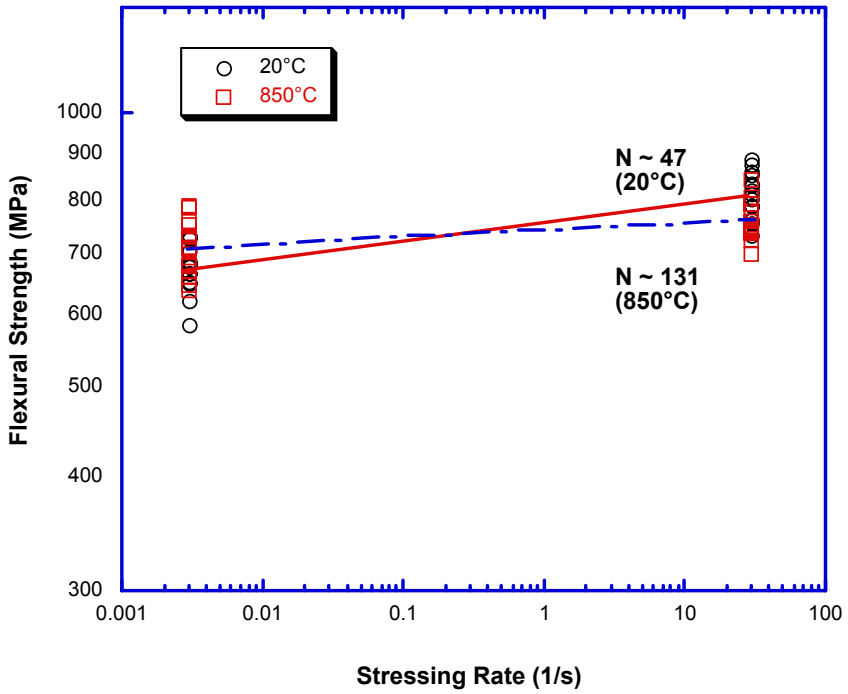

Figure 3. Strength versus stressing rate curves of SN147-31N which was longitudinal machined.

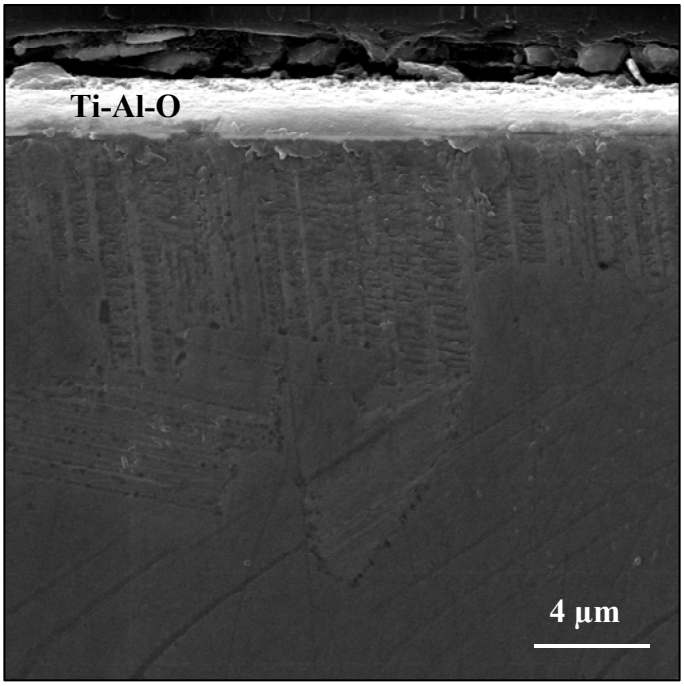

Figure 4. SEM micrograph of polished cross section of TiAl alloy after 48h oil immersion test at 850°C in air.

Low-Cost Manufacturing of Precision Diesel Engine Components

S.B. McSpadden, Jr.
Oak Ridge National Laboratory

Objective/Scope

- To develop and demonstrate optimized, cost-effective fabrication processes for producing precision components for use in diesel engines.
- To develop and demonstrate optimized, cost-effective, non-destructive testing methods for detecting and preventing machining-induced damage in engine components.

Technical Highlights

Tabletop Turning and Machining Centers Provide New Machining Capabilities – Machining capabilities at the Machining, Inspection, and Tribology User Center were recently expanded to include turning and milling with the purchase of two tabletop machines. The Prolight 3000™ computer-controlled lathe and the Benchman 4000™ vertical machining center (Figure 1) have

Figure 1. The Benchman 400 Tabletop Vertical Machining Center will be used to test the performance of industrial drills.

just been installed and will be modified to include dynamometer and other instrumentation in the near future. A dynamometer and related instrumentation have been ordered for the Benchman 4000 machining center, and custom-written data collection software is being procured.

KSI 2000 Scanning Acoustic Microscope Used to Study Subsurface Damage Caused by Machining – Specimens have been prepared for instrumented grinding on the K.O. Lee creep feed grinder. Grinding will be performed under controlled conditions to vary material removal rates and depths-of-grind in a systematic fashion. These conditions will range from very conservative to aggressive so that some specimens should have easily detectable machining damage and others should have no damage. The acoustic microscope will then be used to

determine conditions at which damage begins. Images generated on the microscope should provide insight into the nature and extent of machining damage and should help to minimize such damage in a production environment.

Future Plans

In our first practical application for the Benchman 4000 tabletop vertical machining center, performance tests will be performed on two groups of industrial drills such as those used in the automotive industry. Group one will contain a friction-reducing coating, and group two will comprise the baseline drills. Performance comparisons will be based on by measurement of drilling forces, torques, and drill life.

Our first application for the ProLight 3000 tabletop lathe will be a study on the machinability of metallic glass materials. Mustafa Bakkal, a graduate student from North Carolina State University, will begin this work in early 2003.

Communications/Visits/Travel

Sam McSpadden attended a workshop on *Smart Machine Tools* at N.I.S.T. in Gaithersburg Maryland. This workshop focused on the need for better integration of instrumentation and improved controls technology for machine tools of the future. Among the more "leading edge" ideas discussed was a suggestion that "smart tags" could be used on machine tools as well as the materials being machined. For example, using a standardized format, the machine tool would be able to automatically communicate all its capabilities to the process planner so that he/she could determine whether it is appropriate for a specific machining task. In a similar fashion, a workpiece material would be "tagged" with information about its mechanical properties, present dimensions, and prior processing history to assist in planning the most appropriate machining process.

Sam McSpadden communicated with Messrs. Darryl Gust and Mike Bowling at Cummins Engine regarding upcoming collaborations to optimize a grinding process used in the manufacture of fuel systems components.

Status of FY 2002 Milestones

Milestone 1 *(A scanning acoustic microscope will be used to detect and minimize machining damage in ceramic materials such as zirconia silicon nitride.)* Specimens have been prepared and the acoustic imaging should be complete by 2/28/2003.

Publications

None.

Diesel Exhaust Filter Temperature Measurement and Cost-Effective Machining of Titanium Alloys

Albert Shih
University of North Carolina

Objective/Scope

The objective of this research is to develop infrared-based techniques for temperature measurement in diesel exhaust after-treatment filters and to investigate cost-effective machining methods for titanium alloys.

Technical Highlights

In this quarter, significant research results were obtained in the goniometric characteristics of optical fibers for temperature measurement in diesel engine exhaust aftertreatment filters. The accurate in-situ, non-contact measurement of the temperature distribution within diesel after-treatment filters requires the employment of optical fibers with special tip geometry. The goniometric characteristics of optical fibers with flat, 45° angled, and bent and polished tip are studied such that the specific radiation acceptance region can be determined. One 2 mm diameter fused silica and two 0.425 mm diameter sapphire optical fibers are examined.

The use of optical fibers for infrared temperature measurement has evolved with the development of diesel engine exhaust after-treatment filter technologies. Diesel exhaust after-treatment filters are designed to capture and periodically remove the NO_x and particulates. These filters are typically made of porous ceramic material with deep cavities to increase the specific surface area. The temperature at filter surfaces, due to microwave, post combustion burning, or various other means of heating, controls the chemical kinetics of the storage and regeneration processes. A uniform temperature distribution is critical to controlling the chemical reactions as well as avoiding thermal stress fatigue and overheating of the filter. Accurate temperature measurements of a small and specific region on the filter wall provide important information to chemical engineers for the catalytic development and mechanical engineers for the design of the filter heating process.

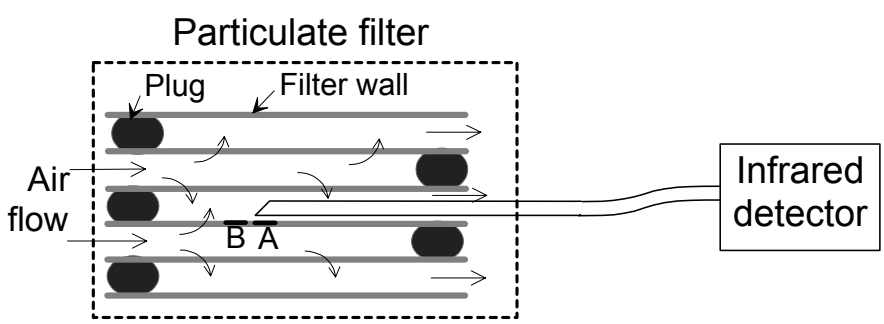

Fig. 1. Application of an angled tip optical fiber to transmit infrared signal to a detector.

Attaching traditional thermocouples to the porous ceramic wall at locations deep within the diesel exhaust after-treatment filter cavity has proven difficult due to space constraints. The filter also operates in a harsh environment; high temperature airflow from the engine combustion process as well as thermal cycling as a consequence of periodical regeneration. Furthermore, the

ceramic filter responds rapidly to microwave heating, precluding the use of traditional thermocouples due to their inherently metallic composition. As an alternative to using a thermocouple, an optical fiber is employed to transmit emitted surface radiation to an infrared detector for temperature measurement, illustrated in Fig. 1. The optical materials chosen, sapphire (Al_2O_3) and fused silica (SiO_2), are transparent to microwave radiation allowing for in-situ, non-contact temperature measurements during heating and filter regeneration.

Precise thermal mapping of the filter is achieved by measuring the surface temperature at various locations within the filter. The goal of this research is to investigate the goniometric characteristics of optical fibers with various tip geometries. The results of this study identify areas along the filter wall from which the optical fiber tip accepts incident radiation.

Systematic research regarding the acceptance of radiation from an external source is not readily available and is therefore studied in this research. Three tip geometries are investigated in this study. The flat, 45° beveled, and bent and polished tip geometries are shown in Fig. 2(a)-(e). In this study, the fiber with the bent and polished tip geometry is made of fused silica while the other two fibers are made of sapphire.

The numerical aperture (NA) of an optical fiber is an important characteristic in understanding the acceptance of incident radiation by the fiber tip. Nubling and Harrington [1] have studied the optical properties of single crystal sapphire optical fibers. With a refractive index of 1.75, an unclad flat tip sapphire fiber in air has a theoretical NA > 1 suggesting that the sapphire fiber will transmit all rays incident upon the input face regardless of the angle. In practice, this is not the case since bulk and surface defects originating from the manufacturing process scatter the light into modes that do not transmit through the length of the optical fiber. Using the angular scan method as dictated by the International Electrotechnical Commission (IEC) [2], the effective (versus theoretical) numerical aperture, NA_{eff}, of each fiber is therefore defined and investigated in this study.

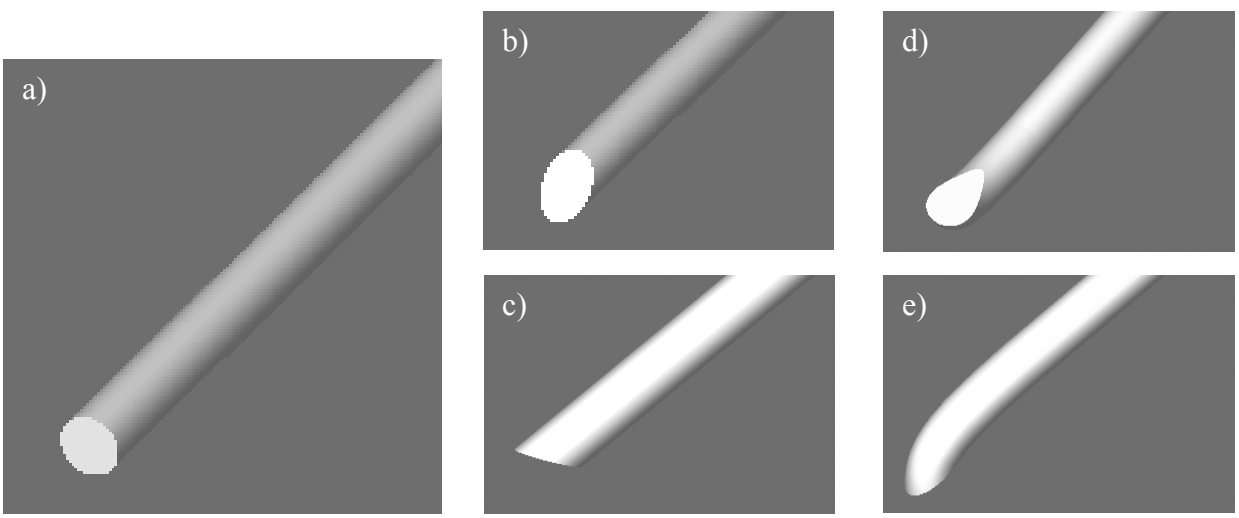

Fig. 2. Illustration of the various tip geometries of the optical fibers examined for this study; a) flat tip, b) and c) 45º angled tip, and d) and e) bent and polished tip.

Experiment Setup

Figure 3 shows the overall experimental setup used to measure the effective numerical aperture of the different fiber tip geometries. The experimental procedure employed to measure the numerical aperture of the optical fibers was the far-field pattern (FFP) method. This is a widely used method for measuring the acceptance angle of optical fibers. The experiments conducted in this research were based on instructions defined by the International Electrotechnical Commission (IEC) standard CEI/IEC 60793-1-43 [2]. A rotary table, as illustrated in Fig. 3, is used to rotate the radiation source around the tip of the fiber, which is aligned at the center of rotary table. The fiber is held fixed by a fiber clamp mounted to a post isolated from the rotary table.

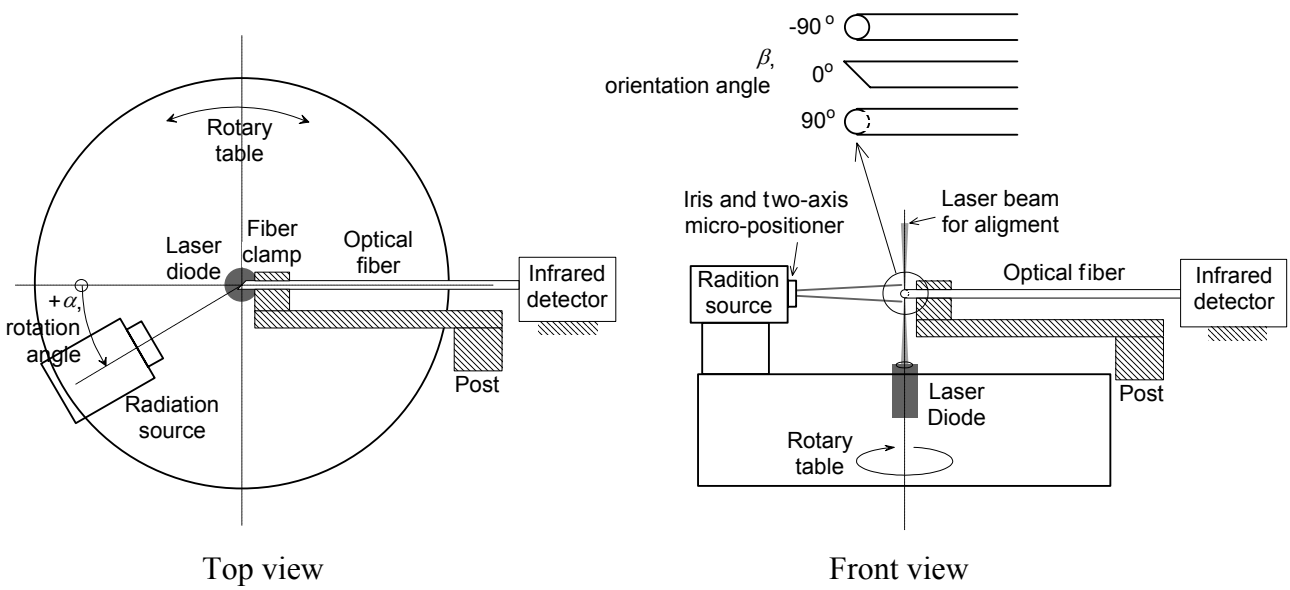

Fig. 3. Experimental setup and definition of rotation angle (α) and orientation angle (β).

Two angles are used to define the rotation and orientation between the fiber and radiation source. The rotation angle, α, defines the angular position of the radiation source relative to the central axis of the fiber. As shown in the top view in Fig. 3, $\alpha = 0°$ is defined by the radiation source positioned along the extended axis of the optical fiber. The angle α is positive when the rotary table rotates in the *ccw* direction off the 0º angle and negative otherwise. The orientation angle, β, is applied to characterize the angular position of the polished face of the angled and bent tip optical fibers. As shown in the fiber tip close-up in the front view of Fig. 3, $\beta = 0°$ is defined by the cut face of the fiber tip pointed downward. The orientation shown in the top view of Fig. 3 is $\beta = 90°$. A procedure for alignment was developed and documented in [3].

Experiment Results

1. Flat tip fiber

Figure 4 shows the relative intensity profile of the flat tip sapphire optical fiber at high temperature with the aperture diameter set to 1 mm. Each experimental run was conducted at increments of 0.5º over a range of ±14º. The two profiles essentially overlap validating the

repeatability of the experimental setup. Angular scan experiments were also conducted using a 3 mm aperture diameter at high temperature. The IEC standard [2] defines the fiber acceptance angle as the angle where 5% of the peak relative intensity exists. Consequently, the effective numerical aperture, NA_{eff}, is computed by taking the sine of that 5% angle. Based on the standard and the results from Figure 4, the flat tip sapphire fiber examined in this study has an effective acceptance angle, θ_{eff}, of 9° corresponding to an effective numerical aperture of 0.156. This is much smaller than the theoretical 90° acceptance angle. Similar observations for unclad sapphire fibers are reported in previous research [1].

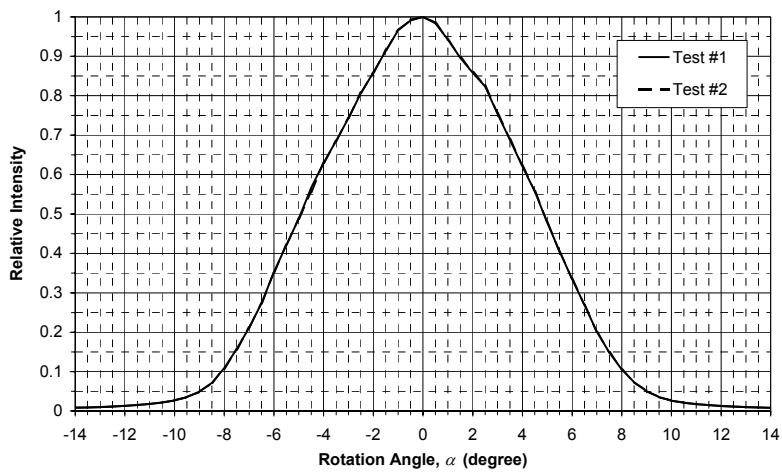

Figure 4. Relative intensity profile for the flat tip sapphire fiber at high temperature with a 1 mm diameter iris.

2. 45° angled tip fiber

Figure 5 shows the relative intensity profiles of the 45° angled tip sapphire fiber at 0° and 90° orientation angles (β). At $\beta = 90°$, the relative intensity peaks at a rotation angle (α) of 93.6°. A small hump, reaching to about 8.7% of the maximum relatively intensity, can be seen at roughly 18°. A local minima, or valley, between the peak and hump is located at $\alpha = 43°$. At $\beta = 0°$ and $\alpha = 0°$, the relative intensity compared to the peak at $\beta = 90°$ and $\alpha = 93.6°$ is very low, only about 6.5%. This indicates that principal amount of radiation received by the angled tip optical fiber is in the $\beta = 90°$ plane, particularly concentrated in the direction perpendicular to axis of the optical fiber. Using the IEC 5% relative intensity guideline, the effective acceptance region is between $0° < \alpha < 30°$ and $65° < \alpha < 125°$ for $\beta = 90°$ and between $-15° < \alpha < 15°$ for $\beta = 0°$.

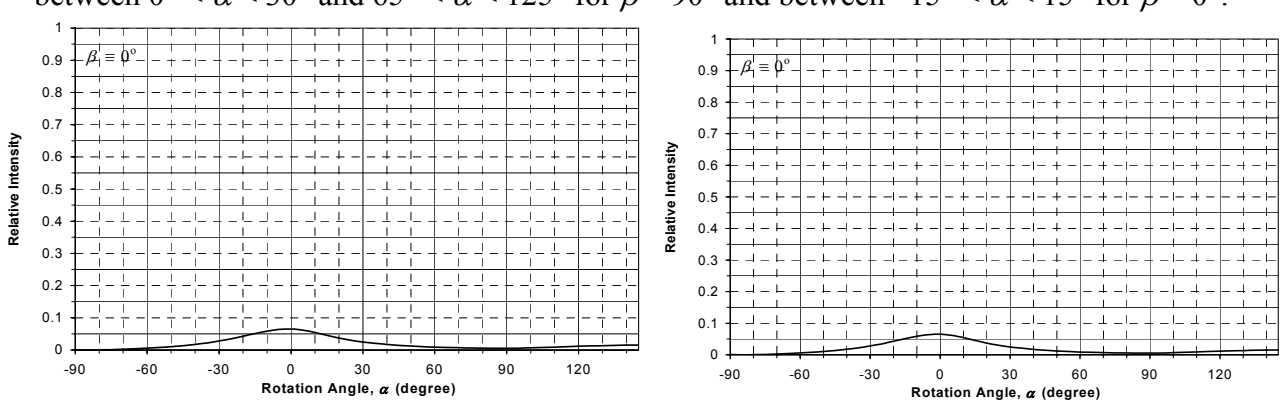

Figure 5. Relative intensity profile for the 45º angled tip sapphire fiber at high temperature.

3. Fiber with bent and polished tip

Figure 6 shows the two angular scan results of the bent and polished tip fiber at $\beta = 0°$ and 90° superimposed on the same graph. The relative peak is located at $\alpha = 80°$, close to the peak location observed for the angled tip fiber. However, this fiber is capable of receiving radiation across a wider range of α. Based on the IEC standard of 5% relative intensity, the effective acceptance angle covers the broad region between $-90° < \alpha < 117°$ for $\beta = 90°$ and $-30° < \alpha < 30°$ for $\beta = 0°$.

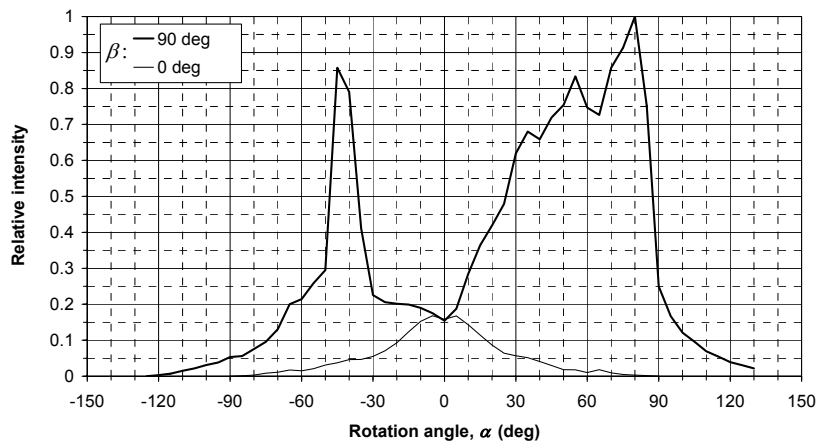

Figure 6. Relative intensity profile for the fiber with bent and polished tip at high temperature.

Application for the diesel exhaust filter temperature measurement

The ideal optical fiber tip geometry for temperature measurement applications in diesel exhaust after-treatment will have only one peak at $\alpha = 90°$, perpendicular to the fiber axis. This physically translates to an optical fiber looking at a precise location along the wall of the filter. Among the three fiber tips examined in this study, the 45° angled tip fiber is the closest to meeting such a requirement. As shown in Fig. 1, with the 45° angled tip fiber inside the filter cavity, a small distance is maintained between the fiber tip and the filter wall. Due to gravity, the fiber will bend slightly. The high elastic modulus of the sapphire is helpful in reducing the deflection of the fiber due to weight-induced bending. Using the orientation of angled tip shown in Fig. 1, the majority of the radiation emission received by the detector is from the area A underneath the fiber tip. The light emission from area B in front of the fiber tip has some, though relatively insignificant, contribution to the intensity of the signal received by the detector. Areas A and B correspond to the intensity peak and hump in Fig. 4 at $\alpha = 90°$ and 15°, respectively.

<u>Status of Milestones</u>

Milestone 1: Develop a temperature measurement system using sapphire fiber and infrared sensors for diesel exhaust filter.

Status: Extensive study was conducted to quantify the goniometric characteristics of optical fiber tips for temperature measurement in diesel engine exhaust aftertreatment filters has been developed.

Milestone 2: Establish calibration methods for the infrared temperature measurement system.
Status: New calibration data with the filter placing inside and outside the furnace has been gathered and analysis is underway. Preliminary results indicated that the PbS/PbSe two-color sensor is capable to measure temperature between 100 to 300 °C.

Milestone 3: Identify the sensitivity and external noise in infrared temperature measurement.
Status: Nothing to report in this quarter.

Milestone 4: Investigate the cylindrical abrasive waterjet machining of titanium alloys.
Status: Nothing to report in this quarter.

Milestone 5: FEM modeling and setup cutting experiments to evaluate new cutting tools and coatings for machining of titanium alloys
Status: The FEM cutting simulation software by Third Wave has been evaluated for machining of Ti alloys.

Brian Boothe, supported under this project, received the MS in mechanical engineering from NC State University in December 2002.

Communications/Visit/Travel

John Kong, the PhD student who is working on the infrared-based diesel exhaust aftertreatment filter temperature measurement, was working at Cummins Technical Center in Fall 2002 semester as a PhD co-cp student. He has further expanded the methods used for infrared temperature measurements of diesel exhaust filters. Albert Shih visited ORNL on Dec. 16.

Publications

B. J. Boothe, A. J. Shih, J. Kong, W. L. Roberts, "Goniometric Characteristics of Optical Fibers for Temperature Measurement in Diesel Engine Exhaust Filters," *Measurement Science and Technology*. (submitted)

J. Qu, A. J. Shih, R.O. Scattergood, and J. Luo, "Abrasive Micro-Blasting of Surface Layers of Electrical Discharge Machined WC-Co Composite," Journal of Materials Processing Technology. (submitted)

J. Kong, A.J. Shih, R.O. Scattergood, T.M. Yonushonis, D.J. Gust, M.B. Grant, and S.B. McSpadden (2003) "Cost-Effective Form Grinding of Zirconia using Silicon Carbide Wheels and Ceramic Grinding Temperature Measurement," *2003 NSF Design, Service and Manufacturing Grantees and Research Conference*, Birmingham, Alabama, Jan. 6-9, 2003.

References

[1] Nubling R K and Harrington J A 1997 Optical properties of single-crystal sapphire fibers *Applied Optics* **36** 5934-40.

[2] International Standard 2001 CEI IEC 60793-1-43 Part 1-43: Measurements methods and test procedures – numerical aperture *International Electrotechnical Commission*, Geneva.

[3] B. J. Boothe, A. J. Shih, J. Kong, W. L. Roberts, "Goniometric Characteristics of Optical Fibers for Temperature Measurement in Diesel Engine Exhaust Filters," *Measurement Science and Technology*. (submitted)

Advanced Cast Austenitic Stainless Steels For High Temperature Components

P. J. Maziasz, R. W. Swindeman, and N. D. Evans
Oak Ridge National Laboratory
and
M. J Pollard
Caterpillar, Inc.

Objective/Scope

The objective of this new CRADA project is commercial scale up of the new modified cast austenitic stainless steels developed by Caterpillar and ORNL as cost-effective high-performance alternatives to SiMo ductile cast iron. SiMo cast iron is the standard material for most diesel engine exhaust manifold and turbocharger housing components. Cast austenitic stainless steels like CN12 can withstand prolonged exposure at temperatures of 750°C or above and are much stronger than SiMo cast iron above 550-600°C. The new modified CN12 and modified CF8C steels have better aging resistance and ductility after creep. This suggests they would also have better fatigue and thermal fatigue resistance, and therefore be resistant to cracking during the severe thermal cycling that exhaust components experience. This project will provide the more comprehensive properties data needed by designers to qualify these new alloys and to design optimized components for trial component production. This new advanced diesel engine CRADA (Cooperative Research and Development Agreement) project (ORNL02-0658) began on July 21,2002, and will last at least three years. More detailed information on this project must be requested directly from Caterpillar, Inc.

Technical Highlights, 1st Quarter, FY2003

Background

Advanced large diesel engine must have higher fuel efficiency as well as reduced exhaust emissions, without sacrificing durability and reliability. Therefore, exhaust manifold and turbocharger-housing materials must withstand temperatures ranging from 70 to 750°C or higher in a normal duty cycle that includes prolonged, steady high-temperature exposure as well as more rapid and severe thermal cycling. New technology to reduce emissions and heavier duty cycles will push temperatures in these critical components even higher. Current exhaust components are made from SiMo ductile cast iron, and higher engine temperatures would push such materials well beyond their current strength and corrosion limits. The previous CRADA produced systematic data comparing cast CN12 stainless steel and SiMo cast iron for such diesel exhaust component applications. The data demonstrated a clear tensile strength advantage of standard CN12 steel above 550-600°C, and even larger advantages in creep strength and fatigue life above 700°C. The previous CRADA project also developed new modified CN12 and modified CF8C steels with better creep strength, and significantly better aging resistance and thermal fatigue resistance than standard CN12. The purpose of this new CRADA project is commercial scale up of these new modified stainless steel heats, and development of the systematic and thorough database required by designers to optimize component design, and to qualify them for trial component production.

Approach

Prior work on lab-scale (15 lb induction melts with argon cover gas) heats of modified CN12 and modified CF8C and screening tests (aging, tensile, creep) at 800-850°C at ORNL provided a composition of each alloy for commercial scale up. High-temperature fatigue testing at Caterpillar Technical Center has identified a significant advantage of the modified CN12 steel. Two commercial stainless steel foundries have produced 500 lb heats of the modified CN12 and modified CF8C steels for testing and evaluation.

Technical Progress

Creep tests continued this quarter at 850°C and 35 MPa, which show that the modified CF8C (over 23,000 h) has similar or better rupture strength than standard CN12 (over 13,000 h) steel (Fig. 1).

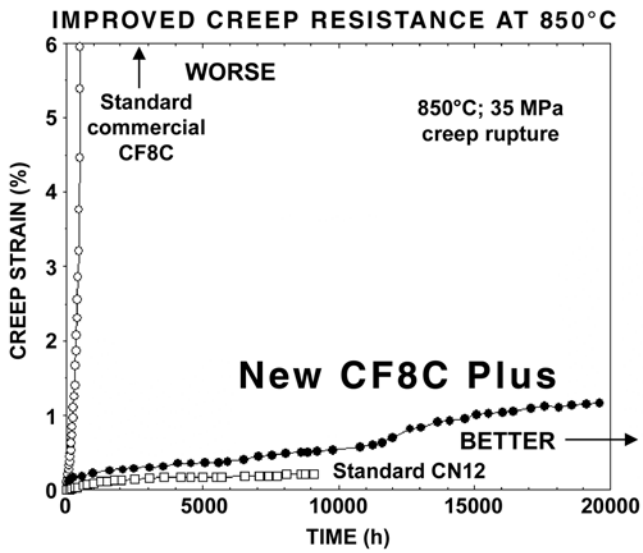

Figure 1 – Creep testing at ORNL of standard, commercial CF8C and CN12 stainless steels, and a lab-scale heat of modified CF8C steel (CF8C Plus) at 850°C and 35 MPa in air.

Tensile, fatigue testing, and thermal fatigue testing continued this quarter at Caterpillar. Tensile results show that the modified CF8C (CF8C Plus) is about as strong as the standard and modified CN12 steels, but still has high ductility similar to the standard CF8C steel (Fig. 2). The good combination of strength and ductility at both higher and lower temperatures is a good indication that the thermal fatigue resistance of the CF8C Plus should also be very good. Aging of tensile/fatigue specimens for 1,000 and 10, 000 h at 700-850°C began at ORNL this quarter. Microstructural analysis of aged or creep-tested specimens of the new modified CN12 and modified CF8C steels continued this quarter.

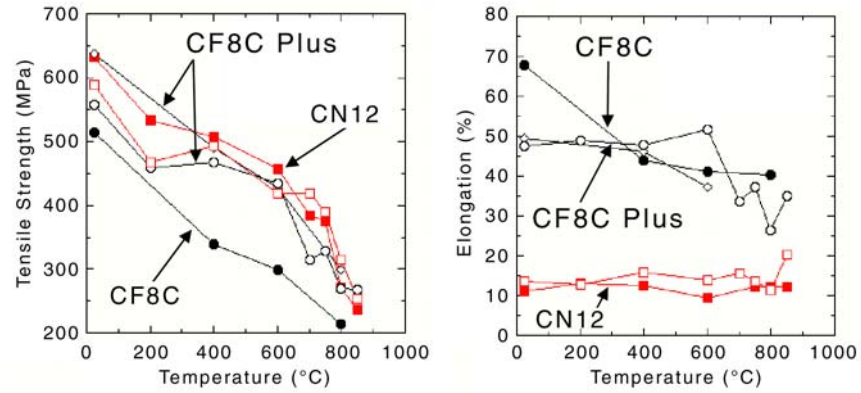

Figure 2 – Tensile properties measured by Caterpillar for the commercial scale-up heats of the new modified CN12 and CF8C stainless steels at room temperature to 850°C in air.

Communications/Visits/Travel

Detailed team communications between ORNL and Caterpillar occur regularly, at least once or twice a week. The new 3 year CRADA began on July 21, 2002, when the previous CRADA ended.

An invention disclosure and patent application on cast austenitic stainless alloys with improved performance were completed by Caterpillar and filed with the U.S. Patent Office in December 2000. It is entitled "Heat and Corrosion Resistant Cast Stainless Steels With Improved High Temperature Strength and Ductility," by P. J. Maziasz (ORNL), T. McGreevy (U. of Bradley/CAT), M. J. Pollard (CAT), C. W. Siebenaler (CAT), and R. W. Swindeman (ORNL). This quarter, two separate new patent applications were developed, one on the modified CF8C steel and the other on the modified CN12 steel.

Status of Milestones

Formal milestones were imbedded in the previous CRADA and in the new CRADA, which is part of the DOE/OFCVT Heavy Vehicle Propulsion Materials Program, but a task in the ORNL FWP. However, all milestones have been achieved or are significantly ahead of schedule.

Publications/Presentations

A final ORNL report for CRADA ORNL99-0533 was prepared last quarter, and was submitted for approval from Caterpillar for unrestricted release, entitled "Development of Low-Cost Austenitic Stainless Gas-Turbine and Diesel Engine Components With Enhanced High-Temperature Reliability," P. J. Maziasz and R. W. Swindeman, ORNL, P. F. Browning, Solar Turbines, Inc., and M. E. Frary, M. J. Pollard, C. W. Siebenaler, and T. E. McGreevy, Caterpillar Inc.

"Overview of Selection, Performance, and Development of Austenitic Stainless Steels for High-Temperature Applications," by P. J. Maziasz and R. W. Swindeman was present as a keynote talk during the Plenary Session of the ASM Stainless Steel and Specialty Materials Conference, held October 7-9, 2002, in Columbus, OH.

“Modified Stainless Steel Alloys for High Temperature Engine Components,” by M. E. Frary, M. J. Pollard, P. J. Maziasz, and R. W. Swindeman, was presented at the ASM Stainless Steel and Specialty Materials Conference, held October 7-9, 2002 in Columbus, OH.

Development Of TiAl/Ti_3Al Nanocomposite for Advanced Diesel Engine Applications

Luke Hsiung
Lawrence Livermore National Laboratory

Objective/Scope

The objective of this effort is to design and fabricate in-situ TiAl/Ti_3Al nanolaminate composites for advanced Diesel engine applications. The primary goals of this projects are (1) to exploit advanced thermomechanical processing techniques to fabricate in-situ TiAl/Ti_3Al laminate composites with the size of lamella width down to submicron or nanometer length-scales, (2) to experimentally verify microstructural stability and mechanical properties (room-temperature ductility and strength, and elevated-temperature creep resistance) of the refined lamellar alloys, and (3) to investigate the fundamental interrelationships among processing, microstructures, alloying additions, and mechanical properties of the laminate composites so as to achieve the desired properties and performance of the alloys for high-temperature structural applications.

Technical Highlights

Two-phase [TiAl (γ-$L1_0$) and Ti_3Al (α_2-DO19)] lamellar TiAl alloys have recently attracted a great attention because of their low density (ρ = 3.9 g/cc), high specific strength, adequate oxidation resistance, and good combination of ambient-temperature and elevated-temperature mechanical properties, which are of interest for engineering applications such as Diesel engine components. Through alloy design and microstructural optimization, significant progress has been made to improve both room-temperature ductility/toughness and high-temperature creep resistance of the alloys. The result of a preliminary effort has revealed that the alloys fabricated by hot extrusion of gas-atomized TiAl powder at 1400°C can form a refined lamellar microstructure (the width of γ lamellae varies between 100 nm and 350 nm, and the width of α_2 lamellae varies between 10 nm and 50 nm) in association with interlocking colony boundaries through a shear-assisted eutectoid transformation induced by hot-extrusion process as shown in Figs. 1 (a) and (b).

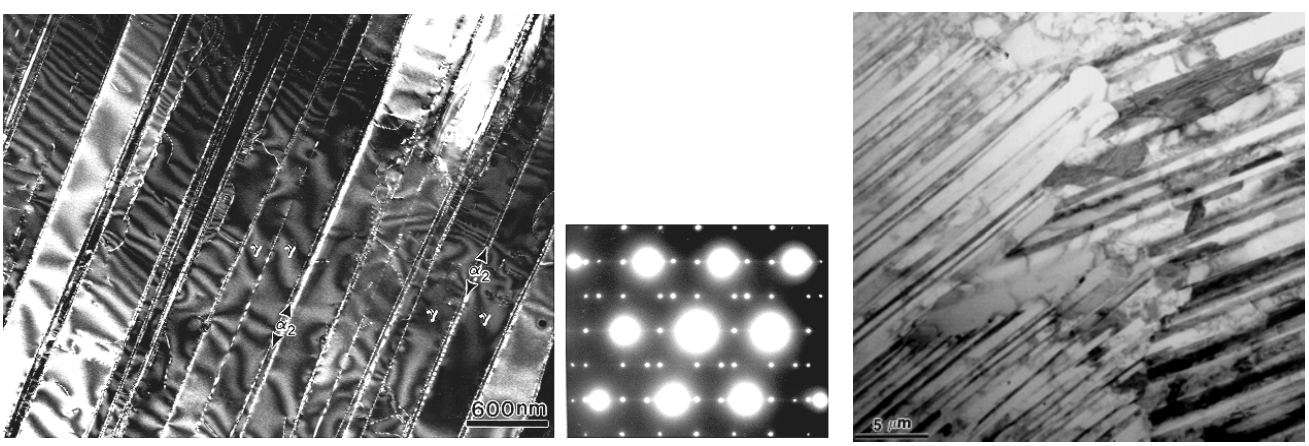

(a) (b)

Fig. 1. (a) A dark-field TEM image showing a typical lamellar microstructure observed from Ti-47Al-2Cr-2Nb extruded at 1400 ^{o}C, and an SAD pattern generated from the domain in (a) showing the phase relationships between γ and α_2, $\mathbf{Z} = [011]_\gamma \parallel [01\bar{1}0]_{\alpha 2}$; (b) A bright-field TEM image showing a interwoven colony boundary in the lamellar TiAl alloy.

The hot-extruded lamellar alloys provide a better combination of room temperature and high-temperature mechanical properties than those of lamellar TiAl alloys fabricated by conventional ingot

metallurgy. Accordingly, there is of great interest to further refine lamellar spacing of the alloys to submicron or nanometer length-scales to develop TiAl nanolaminate composites for engineering applications. A recent report of the formation of nanoscale lamellae (with lamellar spacing in the order of 5 to 10 nm) within a water-quenched TiAl alloy by Hono et al. revealed the feasibility of materializing the idea of fabricating TiAl nanophase composites. However, in parallel to make an effort for developing TiAl nanolaminate composites, there is a need to understand if further refinement of the lamellar microstructures would lead to adverse effects on high-temperature creep properties. A preliminary investigation of creep behavior of a refined lamellar Ti-47Al-2Cr-2Nb (at.%) revealed that there existed two distinct creep regimes as shown in Fig. 2, where a nearly linear creep behavior [i.e. steady-state creep rate = $k\sigma^n$, where σ is applied creep stress and $n \approx 1$] was observed in low-stress (*LS*) regime (i.e. $\sigma < 300$ MPa at 760°C), and power-law break down ($n > 6$) was observed in high-stress (*HS*) regime (i.e. $\sigma > 300$ MPa at 760°C).

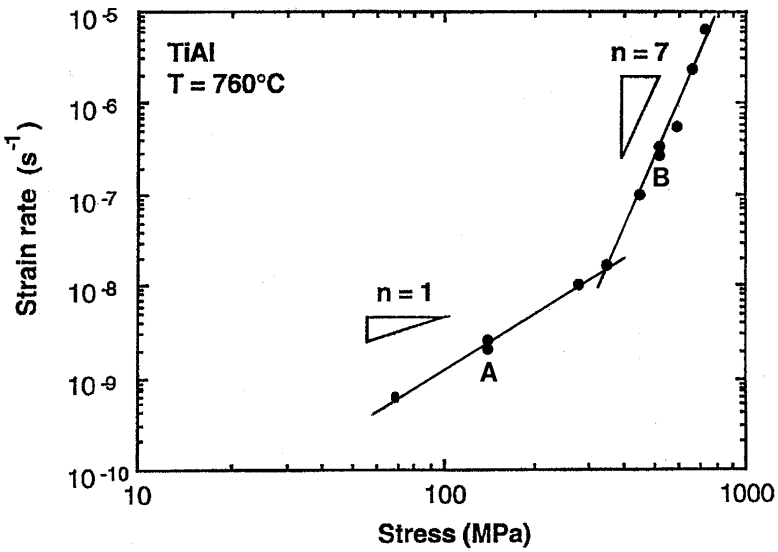

Fig. 2. Steady-state creep rate plotted as a function of applied stress at 760 °C showing that there existed two distinct creep regimes, i.e. low stress (*LS*) and high stress (*HS*) regimes.

TEM investigation of deformation substructures within creep-deformed specimens has revealed the occurrence of interface sliding in *LS* regime and deformation twinning in *HS* regime as shown in Figs. 3 (a) and (b), which has led us to propose that interface sliding associated with viscous glide of pre-existing interfacial dislocations is the predominant creep mechanism in *LS* regime, and interface-activated deformation twinning in γ lamellae is the predominant creep mechanism in *HS* regime. Furthermore, it is also suggested that the solute atoms segregated at lamellar interfaces can act as short-range barriers to drag the motion of interfacial dislocation arrays during interface sliding. It is also anticipated that more effective barriers to impede the interface sliding can be obtained by interfacial precipitation resulting from the solute segregation. It is accordingly suggested that while further refining of lamellar spacing may increase creep resistance of lamellar TiAl in *HS* regime by restraining *LD* motion within constituent lamellae and impeding *ID* motion by impinging *LD* and *DT* onto lamellar interfaces, it can cause an adverse effect on the creep resistance of lamellar TiAl in *LS* regime. The creep resistance of refined lamellar TiAl in *LS* regime may be promoted by reducing the mobility of interfacial dislocations by the segregation of low-diffusivity solutes such as Ta and W to impede the motion of interfacial dislocations. Although more rigorous investigations are needed for the effects of solute segregation at lamellar interfaces to the creep resistance of lamellar TiAl at *LS* regime, a preliminary result demonstrating the promotion of creep resistance of lamellar TiAl by the addition of Ta, W, and B is shown in Fig. 4 (a). As can be seen clearly that steady state creep rates significantly

decrease as a result of the solute additions of Ta, W, and B. Figure 4 (b) shows a preliminary result of TEM examination of the Ti-47Al-2Cr-1Nb-0.8Ta-0.2W-0.15B (at.%) alloy sample creep-deformed at 70 MPa. It reveals the formation of TiB_2-type boride particles at α_2/γ interfaces, but it is interesting to note that no such boride particles were found at γ/γ interfaces. This suggests that solute segregation phenomenon is more pronounced at α_2/γ interfaces than at γ/γ interface. Detail microanalysis of solute segregation at different lamellar interfaces is currently underway in order to facilitate the effort of developing advanced TiAl nanophase composites for high-temperature applications through the alloying modification of lamellar interfaces.

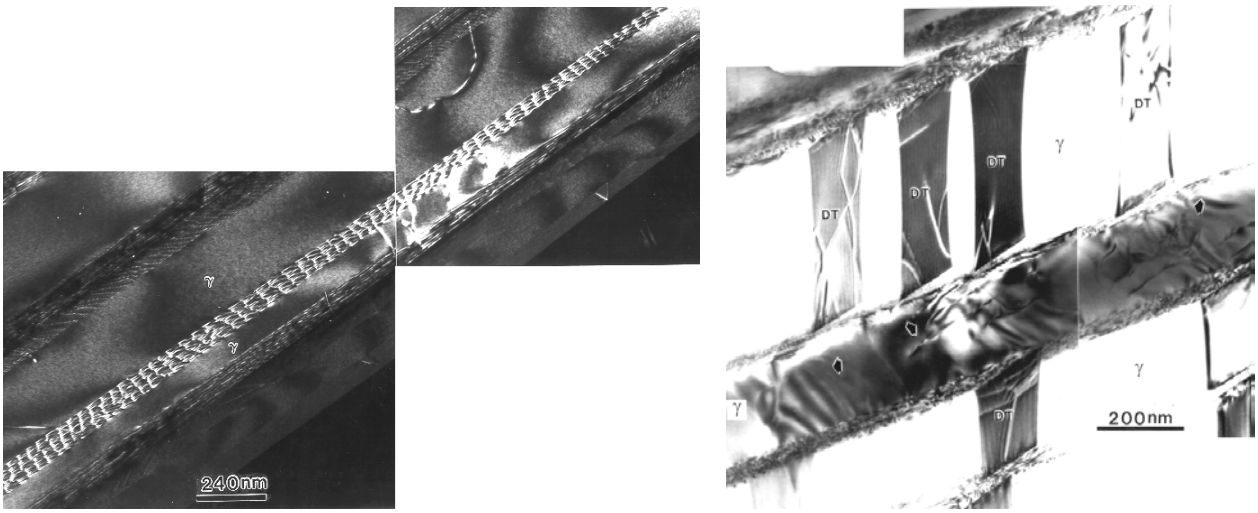

(a) (b)

Fig. 3. A TEM image showing the zigzag motion of interfacial dislocation array observed within a specimen creep deformed at *LS* regime (760 °C, 136 MPa); (b) A bright-field TEM image showing the formation of ($\bar{1}$ 11) type deformation twins (*DT*) within a specimen creep deformed at 760 °C, 518 MPa.

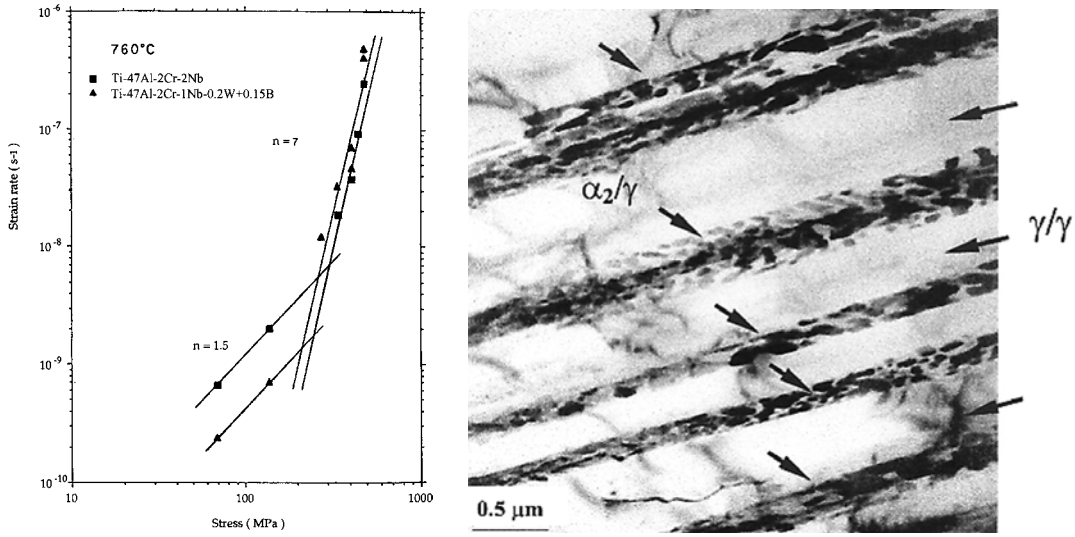

(a) (b)

Fig. 4. (a) Creep data show the effects of alloying modification to the creep resistance of refined lamellar TiAl alloys in *LS* regime at 760 °C; (b) Bright-field TEM images showing the formation of TiB_2-type boride particles at α_2/γ interfaces within a Ti-47Al-2Cr-1Nb-0.8Ta-0.2W-0.15B alloy sample creep-deformed at 760 °C, 70 MPa. Notice that no precipitation was found in γ/γ interfaces which appeared as faint contrasts in (b).

Future Plans

1. Continue to search an effective thermo-mechanical route to fabricate TiAl/Ti_3Al laminate composites of nanometer length-scales (≤ 100 nm).
2. Continue TEM characterization and microanalysis to measure the extent of solute segregation at α_2/γ and γ/γ lamellar interfaces.
3. Collaboration with Brown University (Professor Clyde Briant) on theoretical modeling of solute segregation at lamellar interfaces.
4. Continue creep tests to investigate the creep resistance and microstructural stability of the laminate composites at elevated temperatures up to 850 °C.
5. Conduct in-situ TEM experiment to record a direct observation of interface sliding.

Travel

MRS Fall Meeting, Boston, MA (12/1 – 12/5, 2002).

Status of FY 2002 Milestones

1. Collaboration with ORNL (Dr. C.T. Liu) to fabricate in-situ TiAl/Ti_3Al composite from cast Ti-46.5Al-3Nb-1.0W-0.1B (at. %) alloy using the hot extrusion process.
2. Characterize the effect of alloying modification on creep resistance of the composite material.

Publications

1. L.M. Hsiung, T.G. Nieh, B.W. Choi, J. Wadsworth, "Interfacial Dislocations and Deformation Twinning in Fully Lamellar TiAl," *Materials Science and Engineering A*, **329-331** (2002), 637-643.
2. L. M. Hsiung and T. G. Nieh, "Microstructures and Properties of Powder Metallurgy TiAl Alloys," accepted to publish in *Materials Science and Engineering A*, in press.
3. L. M. Hsiung, "Interfacial Control of Creep Deformation in Ultrafine Lamellar TiAl," submitted to publish in Proceedings of MRS Fall Meeting, *Applications of Nanomaterials for Structural Applications*, 12/1 – 12/5, 2002.

Synthesis of Powders for Titanium Carbide/Nickel Aluminide Cermets

Alan W. Weimer, PI, Michelle Zeles, and Christopher Gump,
University of Colorado

Objective/Scope

The purpose of this research is to find a cheap, efficient way to produce titanium carbide and nickel aluminide cermets. ORNL is interested in this cermet for possible use in diesel engine parts due to its resistance to wear and its high melting temperature. Recently, all the research has been on a small scale reacting approximately two grams of precursor in a large cup capacity Thermogravimetric Analyzer (TGA). These experiments have successfully produced a submicron nickel aluminide (NiAl), titanium carbide (TiC), and their cermet powder. The process used to create the cermet is a modified SHS process called Thermally Ameliorated Rapid Powder Synthesis (TARPS). The next step is to scale up the TARPS process to produce larger quantities of powder for evaluation. A new batch graphite reactor was designed to run approximately fifty grams of reactant (fifteen times more than that what the TGA can produce).

Technical Highlights

This new reactor will be placed inside of a horizontal tube furnace that is capable of reaching temperatures up to 1700°C. The reactor will be composed of high purity graphite and hold approximately fifty grams of starting material (fifteen times more material that the TGA). Inert gas (Argon or Nitrogen) will flow through the enclosed reactor with a perforated plate inside the front of the vessel to insure the dispersion of the gas throughout the reactants. The attached Figures 1-4 show the specifications and design of the reactor.

The process for producing TiC and the cermet is very similar to the process used in the small-scale TGA setup. To produce TiC, titania and carbon pellets are fabricated in order for the titania and carbon to be in proximity close enough to react with each other. The titania and carbon black powders are milled together in a 3 to 1 molar ratio. Small amounts of corn and wheat starch are added (5% by mass) to the milled mixture. This dry powder mixture is then mixed with water. The starch and water act as a binder for the mixture and create paste that is then run through the extruder to form the pellets. These pellets are dried in the new reactor at around 300°C for four hours to drive off the water and calcine the starches. Afterwards, the temperature is increased to 1500°C for carbothermal reduction of the TiO_2 to produce TiC. The TiC product will then be used as the seed material to synthesize the cermet. Nickel and aluminum powders are mixed with TiC using a ball mill and then placed in the reactor vessel and heated to a temperature of 700°C. The exothermic reaction occurs. The scaled-up product powder should be identical to the product obtained from the smaller exploratory TGA experiments.

The reactor design (Figures 1 to 4) was submitted to four companies to cost. The length of the reactor changed slightly (from four to four and a half inches) from the original design. Figures 5-7 are photographs of the new graphite reactor. This reactor will be placed inside a horizontal furnace capable of reaching temperatures up to 1700°C.

Future Plans

1. Produce submicron TiC from titanium dioxide/carbon precursor pellets
2. Produce submicron cermet TiC/nickel aluminide powders
3. Analyze the above produced powders (XRD, SEM, TEM, PSD, SA, LECO C and O)
4. Synthesize TiC and the TiC/nickel aluminide cermet using the aerosol flow reactor

Travel

2002 AIChE Annual Meeting in Indianapolis, IN – presented by Christopher Gump

Status of FY 2002 Milestones

1. Submicron nickel aluminides were produced by adding diluent to the reactants using the TARPS method (March 2002)
2. TiC was made from titanium dioxide and carbon pellets (June 2002)
3. TiC and NiAl cermet was made with mixtures of varying TiC mass percents (from 1-40%) (Completed September 2002)
4. Graphite reactor design done and sent out for bid (October 2002)

Publications

Three papers are in the process of being written about each of the following: nickel aluminide, titanium carbide, and their cermet

Figure 1 - Overall view of the reactor

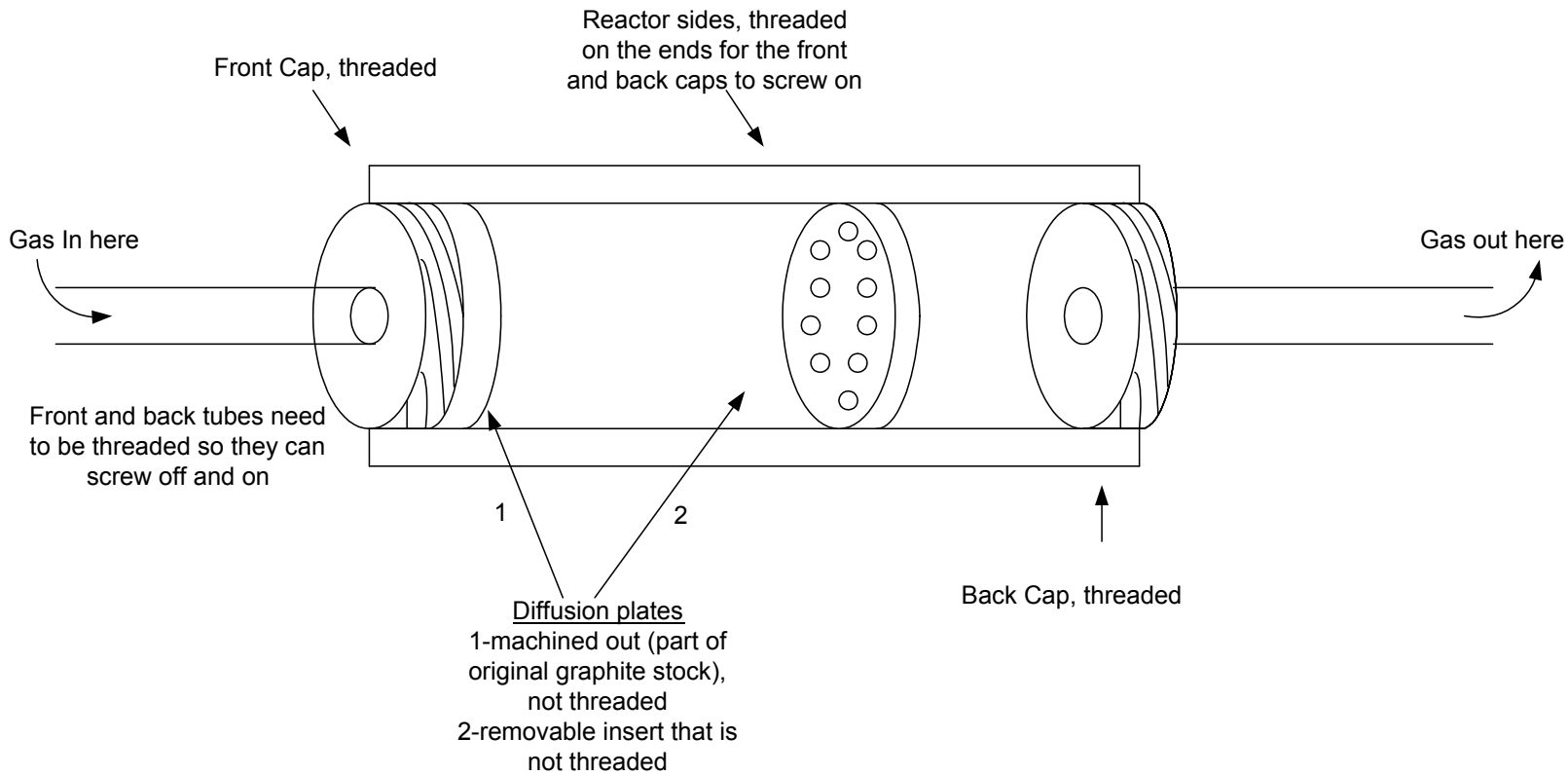

This reactor must be made out of high or ultra high purity graphite. The temperatures it will be subjected is anywhere from 300 deg C to 1500 deg C. This reactor needs to fit inside a horizontal tube furnace with a hot zone of 3 inches in length. The inner diameter of the tube furnace is 2 inches and the reactor fits inside it.

Figure 2 - Front and side view of the reactor with specifications

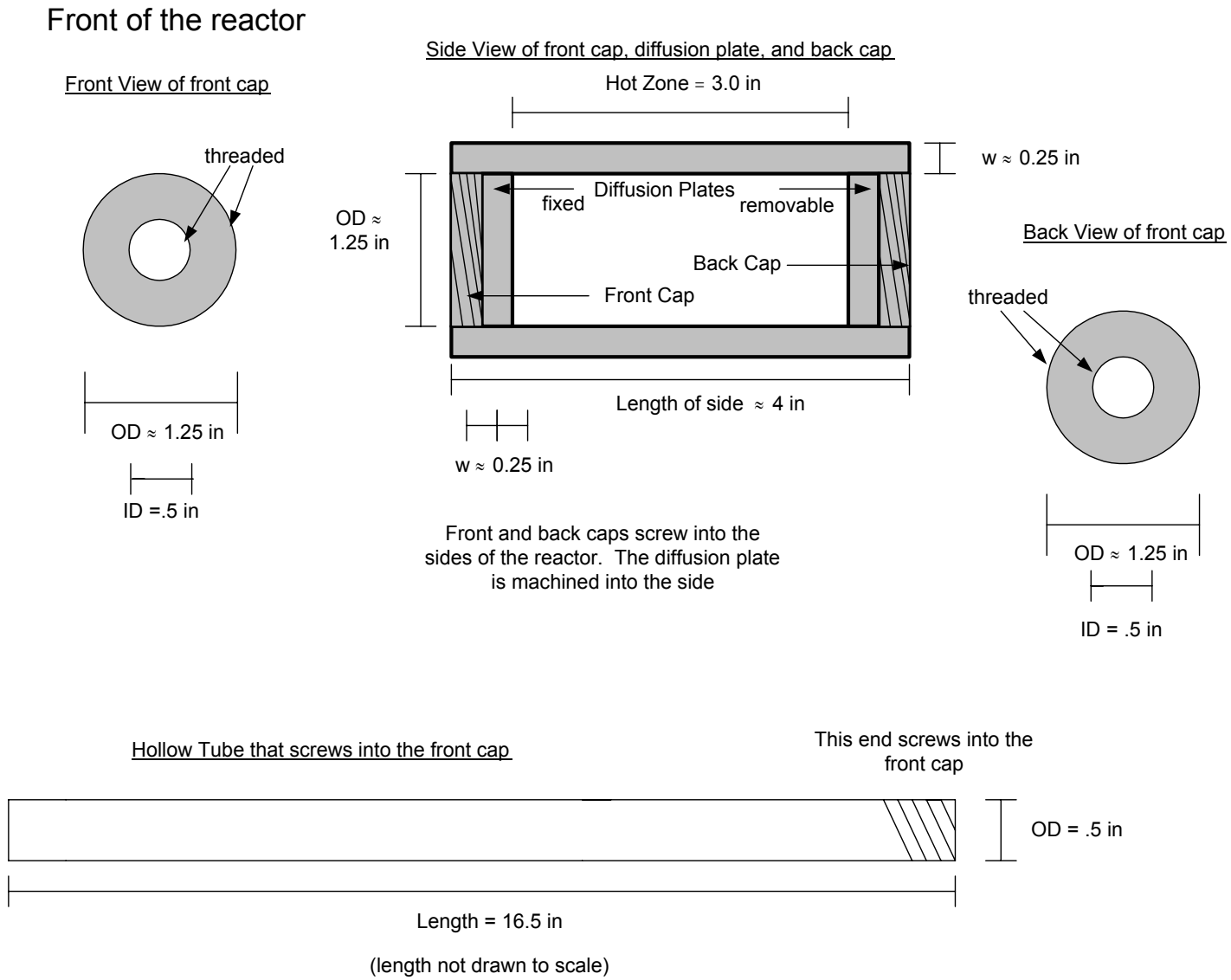

Figure 3 – View of the diffusion plate with information on the purpose of the each plate

Diffusion Plate

Front View of the diffusion plate

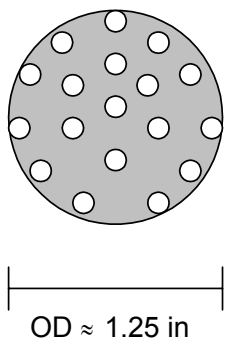

Side View of the diffusion plate

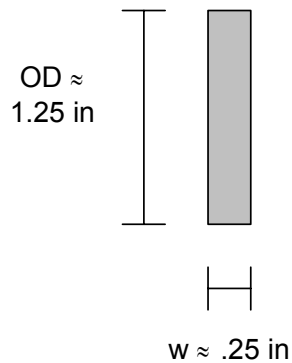

Holes NOT drawn to scale. They must be very small to let the gas (argon) diffuse through but not the specimen. The gas needs to be spread throughout the tube. The holes should be 1/32 inch if possible and there should be about 20 individual holes

These two plates serve two different purposes and the plates look the same but are slightly different. The first plate is next to the front cap and must be machined into the reactor (connected to the sides). The point for this is so the incoming gas is dispersed evenly throughout the reactor and doesn't escape around the side of the plate. The second plate is in front of the back cap. The job of the second plate is to keep all product in the reactor and not escape into the out gas. The second plate is removable so that samples can be put into the reactor and the plate will stand between the samples and the back cap.

Figure 4 – The back view of the reactor

Back of the Reactor

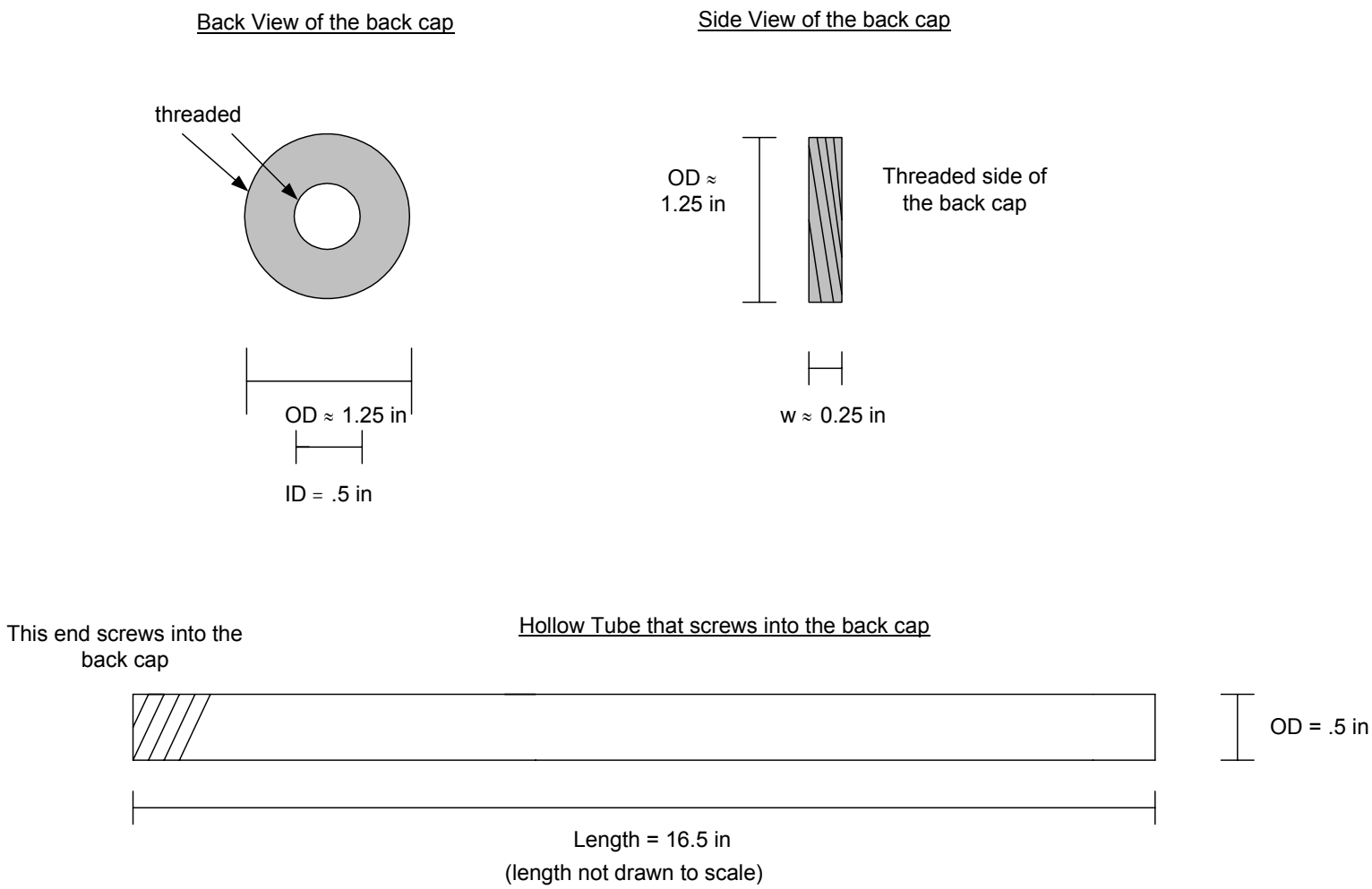

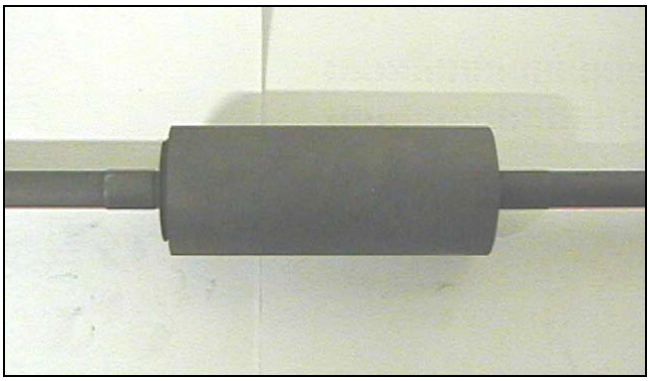

Figure 5- The reactor put together with all the parts.

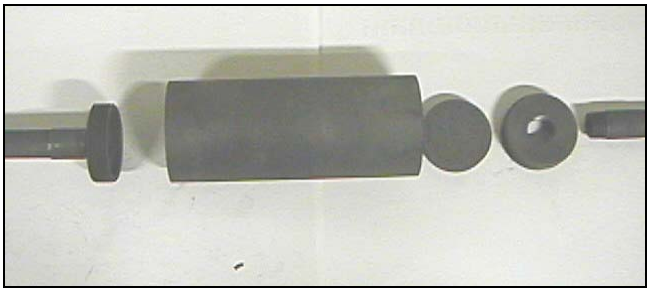

Figure 6- The layout of the reactor with the pieces shown in the order they attach.

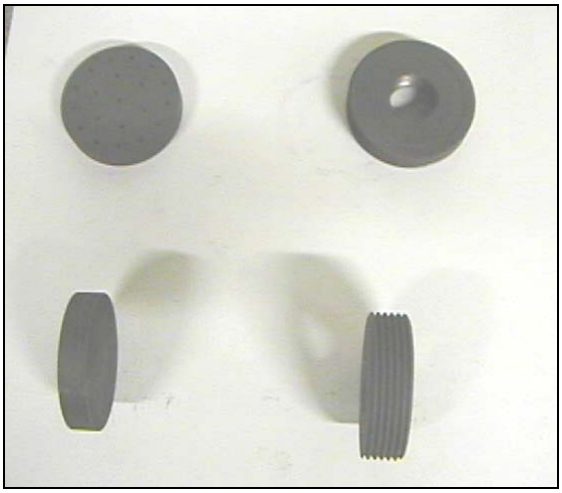

Figure 7- On the left, the dispersion plate with a front view and a side view (notice the inlet gas holes). On the right, the front and/or back cap with a front view and side view (notice the threads to screw the cap into the reactor).

Laser Surface Texturing Of Lubricated Ceramic Parts

Peter J. Blau and Jun Qu
Oak Ridge National Laboratory

Objective/Scope

The objective of this effort is to evaluate the frictional benefits of laser dimple patterns on the lubrication of ceramic surfaces. This project is part of a joint Argonne National Laboratory/ ORNL analysis of the benefits of a laser surface texturing (LST) process developed by Prof. Itzhak Etsion, Surface Technologies, Ltd., Israel. That process uses a computer-controlled laser to produce a pattern of shallow, rounded dimples on bearing surfaces. Based on calculations, preliminary tests, and limited field trials, the developer claims that LST enhances the ability of a lubricated surface to establish a load-bearing hydrodynamic film that decreases friction relative to a non-dimpled surface. The ORNL portion of this joint effort is focused on two aspects of LST: (1) conducting reciprocating tests of ceramic surfaces using lubricating fluids with various viscosities, and (2) determining the microstructural changes that are associated with the LST process.

Technical Highlights

Effects of LST on the Friction of Lubricated Silicon Carbide in Oscillating Motion. As previously reported, experiments were performed to investigate the effects of LST on the frictional response of transformation-toughened zirconia (TTZ). Effects of applied load and frequency of oscillation were observed for oscillatory sliding of TTZ on ground silicon nitride. The current work continues to investigate these effects, but using LST and non-LST pins of Hexaloy SA (a commercial grade silicon carbide supplied to us by Norton-St. Gobain) sliding on ground Hexaloy SA tiles. In the last quarterly report, a different friction testing system had been used in an attempt to improve pin-on-flat alignment, but no apparent difference in the friction coefficient between LST and non-LST SiC was observed. This time, the original set-up and testing conditions, used for the TTZ work, was used for the SiC specimens.

Distilled water and a simple paraffinic mineral oil were used as lubricants. Tests were conducted using the Plint TE-77 machine with a stroke length of 10 mm. First, 3-mm-wide flat surfaces were ground lengthwise on round Hexaloy SA pins. Some pins were kept as-ground (designated as here as "Non-LST"), and others were sent to Israel for LST. In contrast to the TTZ prepared earlier by Surface Technologies Ltd, the current lot of post-LST pin specimens had apparently been further finished after LST. They were received in a smoother condition than the batch of LST TTZ, with most of the rims associated with the laser-dimpling process, having been polished away. Traces of the original grinding marks of the flat areas on the ORNL-ground pins had also been removed.

Figure 1 summarizes the effects of load and frequency of oscillation on the friction coefficients for LST SiC rubbing on SiC under both water and mineral oil lubrication. The following can be concluded:

(1) Compared with water, mineral oil reduced the friction coefficient of LST SiC by approximately 0.15 – 0.18 over the range of testing conditions.

(2) The friction coefficient tended to decrease with applied load for the lowest frequency of oscillation (2 Hz). For water lubrication at the two higher frequencies, the friction coefficient tended to increase with increasing load, with 5 and 10 Hz data being quite similar. For mineral oil lubrication, the friction coefficient tended to remain approximately level as the load increased, and there was no significant difference between results obtained at 5 and 10 Hz.

(3) The effect of oscillating frequency on average friction coefficient was negligible at the highest applied loads with both water and mineral oil lubrication.

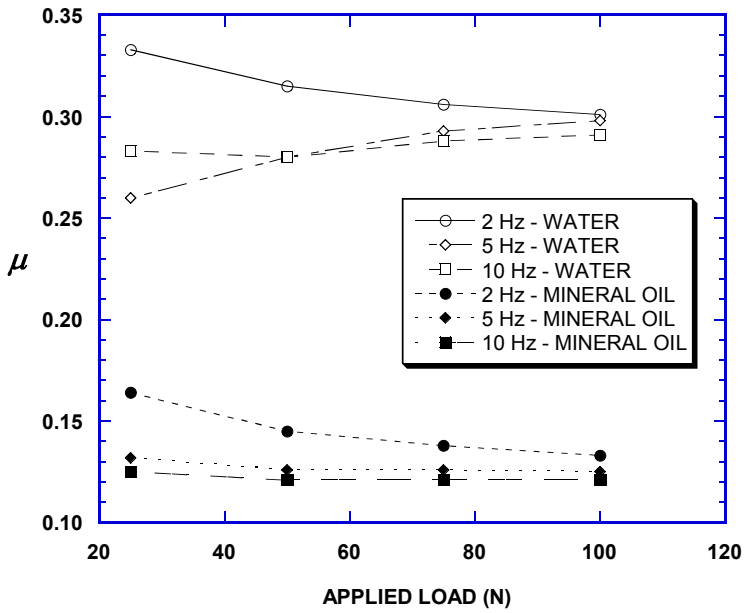

Figure 1. Effect of lubricant type, load, and oscillating frequency on the average friction coefficient of LST SiC sliding on SiC. Each point represents the average of approximately 8 sec of data, with a minimum of 800 data per value.

A similar series of tests was also conducted on mineral oil-lubricated SiC that had not been LST. Results are shown in Figure 2. Similarly to the results presented in Fig. 2 of the last quarterly report, but obtained using a different testing machine, results for 2 Hz showed that the friction coefficient for LST and non-LST SiC specimens were similar. On the other hand, the higher frequency (10Hz) data obtained in recent tests showed that the non-LST couple actually had lower average friction than the LST couple.

To determine the reason for this unexpected result, the digital friction force data were analyzed on a stroke-by-stroke basis rather than on an averaging basis. There were subtle differences in the friction force versus time profiles for LST and non-LST couples. The non-linear change in friction as the slider accelerated, decelerated, and changed direction during oscillation biased the average friction force data differently in non-LST and LST pairs. Thus, the average values do not distinguish between the regimes of boundary and mixed-film lubrication that occur during

different portions of the oscillating stroke. The details of this analysis will be reported in more detail in subsequent publications.

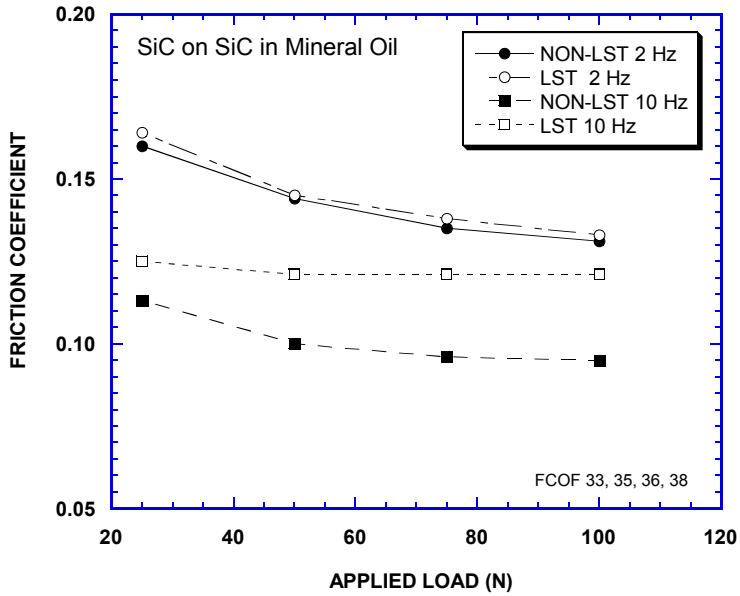

Figure 2. Friction coefficient for LST and Non-LST SiC in mineral oil for two frequencies and four loads.

Future Plans

(1) Analyze stroke-by-stroke behavior of LST and non-LST SiC specimens.
(2) Continue to characterize LST microstructural damage to both TTZ and SiC.

Travel

None.

FY 2003 Milestones

1) Complete studies on the effects of LST on the frictional behavior and microstructural changes produced on ceramic bearing surfaces. Submit final report. (09/03)

Publications

None this period.

Standards For Reliability Testing Of Heavy Vehicle Propulsion Materials

Stephen Hsu, William Luecke, and Lew Ives
National Institute of Standards and Technology

Objective/Scope

The objective of this project is to develop international standard test methods for assessing the reliability of ceramic components used in diesel engines and other heavy vehicle propulsion systems. Silicon nitride ceramics offer a unique combination of light-weight, high-temperature strength, and wear resistance. These properties make them attractive as roller lifters, valve inserts, and injectors for diesel engines. Their use allows longer durability. Reliability and cost-effectiveness are critical issues in implementing ceramics in the valve train of diesel engines. Ceramic valve train components are subjected to demanding conditions that include high contact loading, elevated temperatures, and corrosive environments. To ensure a reliable service life, standard test methods are needed to evaluate the performance of potential ceramics in highly loaded rolling and sliding contacts. This project will develop test methods for evaluating the contact damage behavior of ceramics under rolling and sliding conditions that simulate the cam roller followers, valves and valve seats. In support of this goal we will pursue four research thrusts: 1) fundamental understanding between microstructure and performance, 2) basic mechanisms of contact damage, 3) effect of machining damage on contact reliability, and 4) development of international standards for assessing contact damage.

Technical Highlights

IEA Annex III Activities

Activities under the IEA Annex III, approved by the Executive Committee in July 2002 include various forms of contact damage testing and evaluations relevant to the implementation of advanced materials in engines. These include rolling contact fatigue, sliding and fretting wear, fretting fatigue, and other mechanical performance phenomena that control the reliability of contacts in advanced engines. Materials under consideration may include structural ceramics, composites, and nanostructured friction/wear coatings.

Two Subtasks were initiated under this new annex. The objective of Subtask 1 (Technical Information Exchange) is to achieve a balanced exchange of technical information between the participating countries on contact reliability of ceramics and coatings. The Subtask activities may include (a) Exchange of reports, studies, and software packages as agreed upon in advance by the Executive Committee on an annual basis; (b) Joint technical meetings; (c) Reciprocal invitations to workshops and conferences; and (d) Reciprocal visits to research facilities.

The objective of Subtask 2 (Rolling Contact Fatigue Testing) is to compare the currently employed test methods used for evaluating rolling contact fatigue of advanced ceramics to develop a uniform, internationally agreed-upon testing protocol. Four test configurations are currently in popular use. These include 3-ball-on-rod (mostly used in the U.S.), cylinder-on-cylinder (mostly used in Europe), 4-ball (primarily used for lubrication analysis), and the thrust bearing (mainly used for bearing life testing). Each test configuration has unique attributes.

However, no attempt has been made to compare and correlate the data generated by these test configurations. Many issues require particular attention: defining ‘failure”, understanding the method by which “failure” is detected, distinguishing wear from fatigue, specifying parameters for surface finish, evaluating possible influences from machining damage, and incorporating microslip and sliding into models.

Recent Events

Dr. Said Jahanmir left NIST on Nov. 1, 2002. The project was assumed by Dr. Stephen Hsu who spent considerable time reviewing the project. Dr. William Lucke was also reassigned to the Metallurgy Division but still will spend time to work on the project. Dr. Lew Ives, an experienced tribologist joined the project recently. Dr. Jerry Chuang, a well-known finite element modeler, will also participate in the project in developing a model to predict contact damage.

More technical details will be reported next quarter.

Travel

Dr. Said Jahanmir attended the ASME Tribology Conference in Cancun, Mexico, and organized the Contact Fatigue Symposium on Oct. 29, 2002.

Status of FY 2003 Milestones

1) Completed a symposium among the participating countries on IEA activities on Oct. 29, 2002, during the ASME Tribology Conference in Cancun, Mexico.

Publications

None

Implementing Agreement For A Programme Of Research And Development On Advanced Materials For Transportation Applications

M. K. Ferber
Oak Ridge National Laboratory

Objective/Scope

The International Energy Agency (IEA) was formed via an international treaty of oil consuming countries in response to the energy crisis of the 1970s. A major objective of the IEA is to promote secure energy supplies on reasonable and equitable terms. The governing board of the IEA, which is composed of energy officials from each member country, regularly reviews the world energy situation. To facilitate this activity, each member country provides energy experts who serve temporary staff assignments at IEA headquarters. These staff or secretariat support the governing board by collecting and analyzing energy data, making projections in energy usage, and undertaking studies on specialized energy topics. The governing board is also assisted by several standing groups, one being the committee on energy research and technology (CERT), which encourages international cooperation on energy technology. Implementing agreements (IAs) are the legal instruments used to define the general scope of the collaborative projects. There are currently 40 active implementing agreements covering research topics such as advanced fuel cells, coal combustion science, district heating and cooling, enhanced oil recovery, fluidised bed conversion, fusion materials, solar heating and cooling, pulp and paper, hydropower, heat pumping technologies, hybrid and electric vehicles, high temperature super conductivity, wind turbines, and high temperature materials. A complete listing can be found at the IEA website, www.iea.org.

This progress report summarizes recent activities in the implementing agreement entitled, "Implementing Agreement For A Programme Of Research And Development On Advanced Materials For Transportation Applications." This implementing agreement currently consists of one active annex entitled," Annex II: Co-Operative Program on Ceramics for Advanced Engines and Other Conservation Applications". The motivation for this IA is the development of new and improved ceramic materials, brittle material design methods, and life prediction methodology. The objective of Annex II is coordinated R&D on advanced ceramics leading to standardized methods for testing and characterization.

The Executive Committee for the IA on Advanced Materials is also exploring the possibility of adding new efforts (Annex III and Annex IV). Annex III focuses on the characterization of contact damage (fatigue) while Annex IV deals with materials for hydrogen storage.

Technical Highlights

A fax vote was taken by the Executive Committee to address the following issues:

1. Agreement to the validity of this written procedure (faxvote) as an Executive Committee decision (all Contracting Parties to vote; unanimous decision needed).

2. Approval of the minutes from the executive committee meeting held in Italy in 2002.

3. Approval to invite United Kingdom to participate in our Implementing Agreement. Roger Morrell of the NPL Materials Centre, National Physical Laboratory has expressed an interest in participating in Annex III.

All three issues were approved.

Status of Milestones
All milestones are on track.

Communications/Visits/Travel
None.

Publications
None.

References
None

Mechanical Property Test Development

George Quinn
NIST

Objective/Scope

This task is to develop mechanical test method standards in support of the Propulsion Systems Materials Program. Test method development should meet the needs of the DOE engine community but should also consider the general USA structural ceramics community as well as foreign laboratories and companies. Draft recommendations for practices or procedures shall be developed based upon the needs identified above and circulated within the DOE engine community for review and modification. Round robins will be conducted as necessary. Procedures will be standardized by ASTM and/or ISO.

Technical Highlights

1. General

The emphasis this period was on writing four manuscripts on machining damage in sintered reaction bonded silicon nitride. This culminated several years of work on this topic and the task is now completed. Major accomplishment of this work include:

a. Techniques to recognize machining crack damage on fracture surfaces have been made much easier. This new know how has been transferred to the general community via a series of publications and revisions to the ASTM fractography standard C 1322.
b. The nature of the machining damage is now much better understood. New damage maps for machining damage in silicon nitride have been constructed. Simplified versions will be sent to key machine shops to help them understand the nature of machining cracks from grinding.

Final statistical analysis of the Standard Reference Material 2831, Vickers Hardness of Ceramics and Hardmetals data is underway. SRM 2831 is a tungsten carbide (12% cobalt) disk that has been polished and indented with master Vickers indentations at NIST. This SRM will support the ASTM standards C 1327 for Hardness of Ceramics and E 384 for Microhardness of Materials, as well as the new (2000) ISO standard 14705 and the new European CEN standard EN 843-4. There also has been progress on revisions and updates to several ASTM that were developed earlier in this program.

2. Fracture Toughness

a. ISO FDIS 18756, Fracture Toughness by the SCF method

The final draft international standard (FDIS) is being polished. The last 5-month international ballot concluded in October 2002 and only minor editorial comments were received.

3. Flexural Strength of Advanced Ceramics – Rectangular Specimens

a. ASTM C 1161 Room Temperature Flexural Strength Revisions

No activity. Project completed. Major revisions to this standard were made in 2001 – early 2002.

b. ISO 14704 Room Temperature Flexural Strength

There was no activity since the standard is complete. Nevertheless, we have learned that the Korean delegation has proposed a new VAMAS round robin to investigate the effect of room temperature humidity upon apparent flexural strength at room temperature. They are evidently not satisfied with the solutions in the ISO document, which state that if environmental effects are suspected or are of concern, the user may test specimens at faster than normal rates, or alternatively, may use an inert atmosphere. The Koreans are mot convinced that dry nitrogen gas or silicone oils are adequate to ensure inert conditions. This VAMAS project will run in 2003 if the VAMAS Technical Working Area #3 members approve it. Kristin Breder of Norton Advanced Ceramics is the TWA 3 chairwoman. We do not plan to participate at this time since we are satisfied with the current solutions to deal with environmental effects and we are shorthanded. We will stay abreast of developments.

c. ASTM C 1211, Elevated Temperature Flexural Strength Revisions

This standard, which is the elevated temperature version of C1161, was due for an overhaul in 2002. The ballot for twenty separate revisions closed out on September 10th, 2002. Most of the revisions were minor and editorial. Some were clarifications on whether flexure data can be used for design. Some were revisions to definitions such as inert flexural strength. Some were meant to bring C 1211 into conformance with the revised room temperature standard C 1161 and also the ISO versions. Several negatives were received. The principal voters were Jon Salem, Mike Jenkins and Vic Tennery. All the feedback was reviewed at the November ASTM Committee C-28 meeting in Miami. After about 1 hour of discussion, satisfactory solutions were found for all input received. No further ballots are needed. At some point, the proof of the revised C 1211 will have to be carefully reviewed in early 2003. This seemingly trivial step has been problematic in the past due to problems at ASTM.

d. ISO 17565, Elevated Temperature Flexural Strength

This document overdue for its 5-month enquiry stage ballot phase as a FDIS, "Final Draft International Standard." We will contact the secretariat to find out what is the source of the delay.

4. Fractography

a. ASTM Standard C 1322, Fractographic Analysis of Advanced Ceramics

The second set of seven revisions was balloted in July – September 2002. The second set included eight groups of new or revised definitions. All revisions were approved in November 2002. Jon Salem withdrew a negative ballot on the term "crack". Hopefully the ASTM editor will approve an editorial revisions to this term to change it from "a volume distributed flaw ……" to "a volume or surface" distributed flaw …." At some point in early 2003, we expect to receive a proof copy of this document and once the changes are incorporated the new document will be ASTM C 1322-03, where the "03" denotes the year 2003.

In the meantime, the first set of major revisions which were adopted in early 2002, were incorporated into a proof version of C 1322-02. The revisions included numerous illustrations of machining damage cracks and a whole new table of fracture mirror constants. Unfortunately, there were severe problems with the ASTM proof copy of the document. We spent a lot of time cleaning up the proof copy and working with the ASTM editor. This was a real nuisance. Some sections were incorrect and some sections duplicated. The layout was dreadful in some instances, with text being separated from accompanying figures by as much as 5 pages. Many of the figures were rendered very badly. The latter problem was traced to a faulty filter setting in one of the ASTM computer's Adobe Acrobat software packages. Fortunately, the original .tif and .jpeg images were fine and the problem has been resolved.

b. New NIST Guide to Practice for Fractographic Analysis

Although the ASTM Standard Practice for Fractographic Characterization of Fracture Origins has been on the books for six years now, NIST management felt that there was still a need for a separate user-friendly "Guide to Best Practice" for fractographic analysis. Work will commence on this topic in FY 2003.

5. Flexural Strength Testing of Cylindrical Ceramic Specimens

The NIST Ceramic Machining Consortium program was completed in December 2001. Follow on analysis and intensive fractographic examination of hundreds of Ceradyne sintered reaction bonded silicon nitride (SRBSN) specimens continued until the end of May 2002. A major

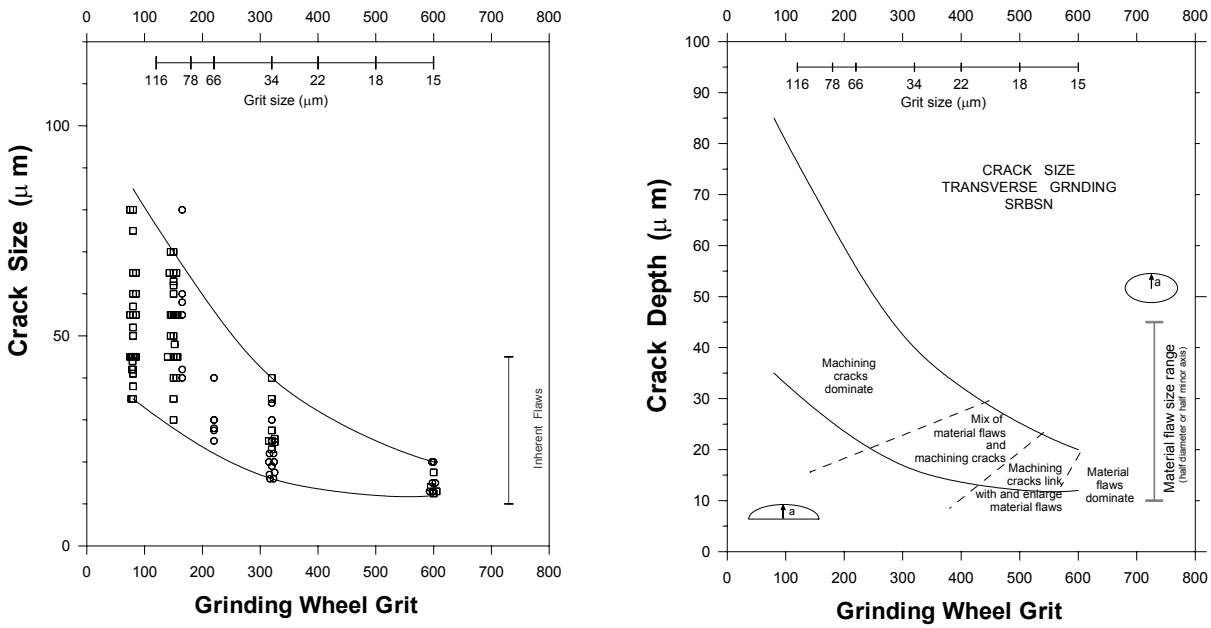

(a) (b)

Figure 1. Depth of parallel machining cracks in transversely ground sintered reaction bonded silicon nitride rods and bars. (a) shows that the size of the machining cracks varied by up to a factor of two within a batch of identically prepared specimens. (b) shows that the materials inherent flaws became dominant for specimens ground with 600 grit or inner wheels. Between 320 and 600 grit, machining flaws mixed with or competed with the inherent flaws for dominance. Wheels coarser than 320 grit formed machining cracks that dominated strength.

NIST Special Publication on the findings was completed in November 2002. It is now being reviewed. A short condensed article was written for Ceramic Engineering and Science Proceedings and will be presented at the Engineering Science Division meeting of the American Ceramic Society in Cocoa Beach in January 2003. Two major journal articles were prepared and submitted to Machining Since and Technology in December and January 2003. Preprints have been sent to key parties in the USA. **Figure 1** shows one of the principal findings from the study: Strength limiting machining cracks vary in size by as much as a factor of two from specimen to specimen for a group of specimens ground under identical conditions, irrespective of shop or wheel grit size. We also learned that a single severe grit in a diamond wheel may control performance. A simple machining cracks damage map for sintered reaction bonded silicon nitride is shown in **Figure 2**. Another stunning finding was that silicon nitrides with enhanced fracture toughness actually develop deeper machining cracks that less tough nitrides, when ground under identical conditions.

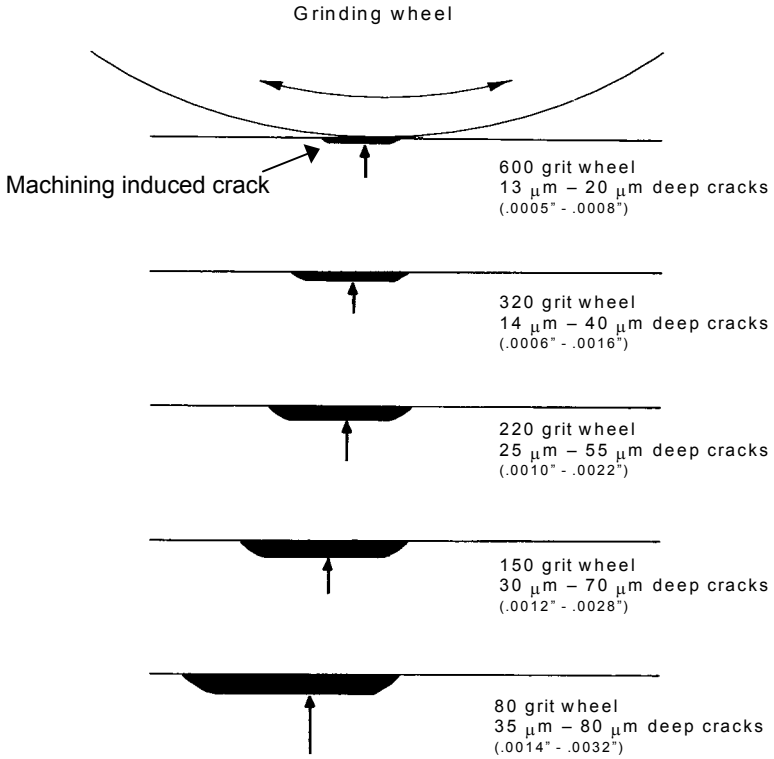

Figure 2. The depth of machining cracks created by surface grinding SRBSN silicon nitride primarily depends upon the wheel grit size of the grinding wheel.

In addition to writing the four manuscripts, we finished up evaluating the fracture toughness of Dow toughened sintered silicon nitride from the size of machining cracks that we measured in two sets of 30 bend bars transversely-ground by 150 and 80 grit wheels. We also measured the size of machining cracks in Eaton reaction bonded silicon nitride. **Table 1** shows some of the characterization data. These other silicon nitrides had also been used in the NIST Ceramic Machining Consortium program. Much less effort was spent on the fractographic analysis of machining cracks in these two materials, but they provided fascinating contrasts to the Ceradyne Sintered reaction bonded silicon nitride. Machining cracks were smaller than normal in the weak, low toughness Eaton RBSN, but were larger than normal in the strong, enhanced toughness Dow SSN! One would expect that the toughened silicon nitride would have retarded machining crack formation, and thus would have had the smallest machining cracks for a given grinding condition, but this was not the case. These seemingly paradoxical results are explained in the new manuscripts.

Table 1.

Property data for four silicon nitrides for comparison.

Material	Density (g/cm^3)	Grain size (μm) width X length	Elastic Modulus (GPa)	Hardness, (GPa)‡	Fracture toughness (MPa√m)†
SRBSN Ceradyne Ceralloy 147-31N	3.21 *	0.5 to 3. X up to 10. long	310 – 320 *	HK(2) 13.3 ± 0.2 HK(1) 13.7 ± 0.2 HV(5) 15.4 * HV(1) 15.0 ± 0.3 HV(.3) 17.6 *	5.8 ± - * 5.41 ± .54 29 machining cracks 5.58 ± 0.24 SCF 5.59 ± 0.22 SEPB 5.28 ± 0.17 CN *
SSN Dow	3.20	0.3 - 1.3 X up to 10. long	306	HK(2) 12.7 ± 0.2 HK(1) 13.0 ± 0.2 HV(5) - HV(1) 14.5 ± 0.3	6.8 ± - * 7.25 ± 0.38 28 machining cracks 7.18 ± 0.31 30 machining cracks 6.75 ± .29 SCF
RBSN Eaton	2.36	0.5 – 1. X 1. – 2.	200	HK(2) 4.6 ± 0.3 HK(1) 5.0 ± 0.3 HV(5) - HV(1) 5.2 ± 0.4	2.5 ± - IS (Ref. Xu et al.)
HPSN Norton NC 132	3.22 – 3.26	< 3.	315 – 320	HK(2) 14.3 ± 0.3 HK(1) 15.0 ± 0.2 HV(5) 15.4 ± 1.3 HV(1) 17.3 ± 0.5	4.57 ± 0.11 SCF, SEPB, CN, SRM 2100

* Manufacturer's data

‡ HV denotes Vickers hardness. HK denotes Knoop hardness. In accordance with the notation scheme in ASTM standards C 1326 and C 1327, the number in parenthesis is the indentation load (kgf).

† Test method: SCF surface crack in flexure; CN chevron notched beam; SEPB, single-edge precracked beam; IS, indentation strength

\- Not available or reported.

One other aspect of this program will continue a little longer. We have collaborated with the Professor Rodel at the Technical University Darmstadt in Germany to measure R-curves for the Ceradyne SRBSN. Preliminary data indicates this toughened silicon nitride (≈5.6 MPa√m on the plateau) does indeed have a rising R-curve, but that the initial toughness may be as low as 1.6 or 2.0 MPa√m. We are somewhat puzzled by these results, since analysis of the machining cracks produced fracture toughness estimates in the mid 5's and they did not show very much evidence of stable cracks extension (5 – 15 μm at the most). Evidently the fracture resistance may start quite low, but increases rapidly to near plateau levels during the crack pop in during the machining process. These issues will be studied further and we will try to reconcile the R-curve experiments with the observed strength test data.

6. New Standard Reference Material SRM 2831 for Vickers Hardness

During the last quarterly period, we finished the preparation of the long overdue SRM 2831, Vickers Hardness of Ceramics and Hardmetals. One hundred and eight tungsten carbide disks were prepared, indented, and measured. Ninety-six were accepted for distribution by the NIST Reference Materials Office. The disks are finished and ready, but the Statistical Engineering Division is in the process of reviewing the data collected in order to prepare the uncertainty estimates for the certificate. This should not be too difficult, since we did this once before with the SRM 2830 Knoop Hardness Reference disks material which have been available since late 1996. SRM 2831 should be available in a matter of 2-3 months.

Table 2 shows the three Standard Reference Materials, which support several of the standards developed in this program. Regrettably, the market for these SRM's has been soft. Department of Energy contractors and researchers are encouraged to inquire further about these SRM's which are valuable tools to verify proper instrument operation. The SRM's are also valuable aiding product compliance with specifications.

To complete our data base, we also measured Vickers and Knoop hardness as a function of load. Hardness decreases with load in accordance with the well-known indentation size effect. **Figure 3** shows the trends for NC 132 hot pressed silicon nitride and also NBD 200. The Knoop and Vickers trends are similar, but the exact hardnesses do vary. This underscores how important it is that people who report hardness, explicitly state how it was done and at what indentation load.

In 2003, the two ASTM hardness standards, C 1326 for Knoop and C 1327 for Vickers are due for review. We prepared a short list of minor revisions for the committee to consider.

Table 2. Reference Materials

SRM	Specifics	Availability	Images
#2100 Fracture Toughness of Ceramics K_{Ic}	(5) silicon nitride bend specimens with certified fracture toughness values: 4.57 MPa√m. Any method may be used.	Immediate $355	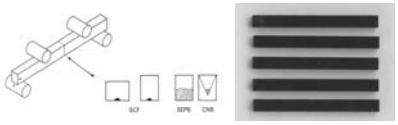
#2830 Knoop Hardness of Ceramics HK2	(1) hot-isopressed (NBD-200) silicon nitride disks with 5 NIST 19.6 N (2 kgf) indentations HK ~ 14.0 GPa; 1,400 kgf/mm^2	Immediate $581	
#2831 Vickers Hardness of Ceramics and Hardmetals HV1	(1) hot-isopressed tungsten carbide disk (12% cobalt) with (5) NIST 9.8 N (1 kgf) indentations. HV ~ 15.0 GPa; 1500 kgf/mm^2	Estimated Mar. 2003 Estimated $450	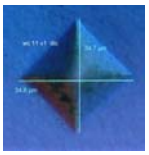

For more information about these SRM's, or any of the NIST power size standards, contact:

http://ts.nist.gov/ts/htdocs/230/232/232.htm

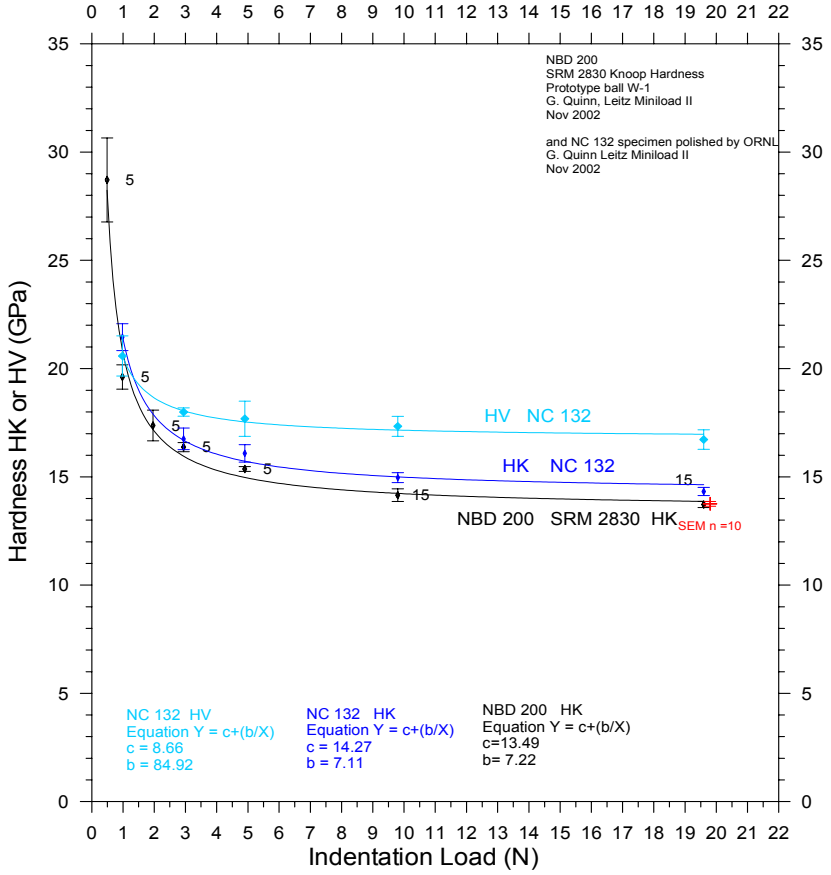

Figure 3. Hardness versus load for two silicon nitrides. The trend of decreasing hardness with indentation load is the "indentation size effect." Most diagonal length readings were made with a conventional microhardness machine optical microscope, but a few readings for the SRM 2830 NBD 200 reference block disk were made by a calibrated scanning electron microscope. The optical and SEM readings concurred for the 19.6 N (2 kgf) indentations.

7. Other

None

<u>Status of Milestones</u>

412146 Ballot major revisions to ASTM C 1161 flexural strength September 2001,
Completed , October 2002✓

412147 Prepare ballot revisions for ASTM C 1322, Fractographic Analysis April 2002,
Completed, January 2002✓

412148 Prepare follow on specimen machining revisions to ASTM C 1161 April 2002
flexural strength if needed **Completed, April 2002✓**

412149 Prepare ballot-ready first ASTM draft of cylindrical rod flexure April 2002
strength test **Delayed**

412150 Prepare paper on effect of machining on strength of SRBSN rods. May 2002
Completed Nov. 2002 ✓

412151 Prepare review paper on flexural testing of cylindrical rods. October 2002
Delayed by completion of SRM 2831, HV

Communications/Visits/Travel

Short articles about the major revisions to the fractography standard C 1322, were sent to several major trade journals. A selection of fragments of previously tested silicon nitride Standard Reference Material 2100, fracture toughness specimens were sent to Jon Salem at NASA-Glenn. He will use the fragments to run some miniature chevron notched beam experiments. The goal is to verify that miniature (3 x 4 x 20+ mm) chevron notched beam specimens tested on 10 x 20 mm fixtures will produce the correct results. If so, the ASTM standard for fracture toughness will be expanded to include the miniature specimen. The standard already allows miniature Surface Crack in Flexure (SCF) and Single-edged Precracked Beam SEPB) specimens.

Mr. Quinn attended the ASTM C28 advance Ceramic meeting in Miami in November whereupon he conducted much of the business pertaining to the standards cited above. The Committee decided to reorganize itself at the meeting. New subcommittees that are application oriented will be formed. From its inception in 1986, the committee had been organized into subcommittees that had focused on generic properties such as mechanical test methods, or powder characterization procedures, design and nondestructive testing.

Collaborations with Technical University Darmstadt are underway to reconcile R-curve data they have generated on the SRBSN with our strength, fracture toughness, and fractography findings.

Publications and Presentations

1. G. D. Quinn, J. J. Swab, and M. J. Motyka, "Fracture Toughness of a Toughened Silicon Nitride by ASTM C 1421," accepted by J. Am. Ceram. Soc., 2002.
2. G. D. Quinn, "Weibull Strength Scaling for Standardized Rectangular Flexure Specimens," accepted J. Am. Ceram. Soc., July 2002.
3. G. D. Quinn, "Weibull Effective Volumes and Surfaces for Cylindrical Rods Loaded in Flexure," accepted by J. Am. Ceram. Soc., 2002.
4. G. D. Quinn, L. K, Ives, and S. Jahanmir, "On the Fractographic Analysis of Machining Cracks in Ground Ceramics: A Case Study on Silicon Nitride," NIST SP, 2003.
5. G. D. Quinn, L. K, Ives, and S. Jahanmir, "Machining Damage Cracks: How to Find and Characterize Them by Fractography, " to be publ. Ceram. Eng. Sci Proc., Vol. 24, Issue 3 or 4, 2003.
6. G. D. Quinn, L. K, Ives, and S. Jahanmir, "On the Nature of Machining Cracks in Ground Ceramics: Part I: SRBSN Strengths and Fractographic Analysis," subm to Machining Science and Technology, Dec. 2002.

7. G. D. Quinn, L. K, Ives, and S. Jahanmir, "On the Nature of Machining Cracks in Ground Ceramics: Part II: Comparison to Other Silicon Nitrides and Damage Maps subm to Machining Science and Technology, Jan. 2003.